UNIVERSITY OF BIRMINGHAM

Tribological interactions of the finger pad and tactile displays.

by

Brygida Maria Dzidek, M.Sc.Eng.

A thesis submitted to
University of Birmingham
for the degree of
DOCTOR OF PHILOSOPHY

School of Chemical Engineering
University of Birmingham

March 2017

Abstract

This thesis summarise the results of an investigation of the tribological interactions of the human finger pad with different surfaces and tactile displays. In the wide range of analyses of the mechanical properties of the finger pad, an attempt has been made to explain the nature of the interactions based on critical material parameters and experimental data. The experimental data are presented together with detailed modelling of the **contact mechanics** of the finger pad compressed against a smooth flat surface. Based on the model and the experimental data, it was possible to account of the loading behaviour of a finger pad and derive the Young's modulus of the fingerprint ridges. The frictional measurements of a finger pad against smooth flat surfaces are consistent with an occlusion mechanism that is governed by first order kinetics. In contrast, measurements against a rough surface demonstrated that the friction is unaffected by occlusion since Coulombic slip was exhibited. The thesis includes an investigation of critical parameters such as the **contact area**. It has been shown that four characteristic length scales, rather than just two as previously assumed, are required to describe the contact mechanics of the finger pad. In addition, there are two characteristic times respectively associated with the growth rates of junctions formed by the finger pad ridges and of the real area of contact. These length and time scales are important in understanding how the Archardian-Hertzian transition drives both the large increase of friction and the reduction of the areal load index during persisting finger contacts with impermeable surfaces. Established and novel models were evaluated with statistically meaningful experiments for phenomena such as lateral displacement, electrostatic forces and squeeze-film that have **advanced applications**.

“If I have seen further it is only by standing on the shoulders of giants.”

Issac Newton rephrased after Bernard of Chartres, 1676

Acknowledgments

First and foremost, I want to thank my supervisors Professor Mike Adams and Professor Zhibing Zhang. It has been an honour to be their Ph.D. student. I appreciate all their contributions of time, ideas and constant attention that make my research productive and stimulating.

I specially acknowledge Dr Simon Johnson. I cannot find the suitable words to appreciate his professional help and support during my experiments, data analysis and papers reviews. Together with Professor Adams, thanks to their knowledge, patience and attention to the details that made my research work valuable and possible to reach the highest standards.

Being given a chance, to become a member of the international, interdisciplinary project, it contributed immensely to my personal and professional development. The group has been a source of friendships as well as good advice and collaboration. I would like to thank to all the Supervisors, Industrial Partners and Research Fellows as well as Kathleen Hynes (project manager) for your hard work and commitment.

Lastly, I would like to thank my all family for all their love and encouragement. For my parents, who raised me with a love of science and supported me in all my pursuits.

Thank you.

List of publications:

Published work:

Dzidek, B.M., Adams, M.J., Andrews, J.W., Zhang, Z. and Johnson, S.A., 2017. Contact mechanics of the human finger pad under compressive loads. Journal of The Royal Society Interface, 14(127), p.20160935.

Bochereau. S., Dzidek B.M., Adams M.J., Hayward V., 2017, Characterizing and imaging gross and real finger contacts under dynamic loading., IEEE Transaction of Haptics.

Sednaoui, T., Vezzoli, E., Dzidek, B.M., Lemaire-Semail, B., Chappaz, C. and Adams, M., 2017. Friction Reduction Through Ultrasonic Vibration Part 2: Experimental Evaluation of Intermittent Contact and Squeeze Film Levitation. IEEE Transactions on Haptics.

Dzidek, B., Bochereau, S., Johnson, S., Hayward, V. and Adams, M., 2016, April. Frictional dynamics of finger pads are governed by four length-scales and two time-scales. In Haptics Symposium (HAPTICS), 2016 IEEE (pp. 161-166). IEEE.

Sednaoui, T., Vezzoli, E., Dzidek, B., Lemaire-Semail, B., Chappaz, C. and Adams, M., 2015, June. Experimental evaluation of friction reduction in ultrasonic devices. In World Haptics Conference (WHC), 2015 IEEE (pp. 37-42). IEEE.

Vezzoli, E., Dzidek, B., Sednaoui, T., Giraud, F., Adams, M. and Lemaire-Semail, B., 2015, June. Role of fingerprint mechanics and non-Coulombic friction in ultrasonic devices. In World Haptics Conference (WHC), 2015 IEEE (pp. 43-48). IEEE.

Dzidek, B.M., Adams, M., Zhang, Z., Johnson, S., Bochereau, S. and Hayward, V., 2014, June. Role of occlusion in non-Coulombic slip of the finger pad. In International Conference on Human Haptic Sensing and Touch Enabled Computer Applications (pp. 109-116). Springer Berlin Heidelberg.

In preparation:

- ✓ Dzidek B.M., Bochereau S., Johnson S.A., Hayward V., Adams M.J., *"Why do pens have rubbery grips"*, PNAS, 2017

List of Contents

Introduction

Since the late 70s technological revolution, every year new tactile devices have been introduced. The hardware and software engineers are facing increasingly demanding market drives that attempt to meet high consumer expectations. Touch screens have become much more than just a transparent glass interface. Enhanced optical and mechanical properties are chasing functionality and fashion demands. Every year the marketing of mobile phones and tablets etc. is expanding, fulfilling new applications and a constant desire for improvements including those associated with the functionality of touch screens.

A new class of the touch screens will be able to enhance the user experience by the introduction of integrated haptic feedback. Through direct contact with the screen, each user will have the opportunity to experience illusions of textures and shapes. Tactile devices having haptic feedback depend on contact with the skin (the *stratum corneum* of human finger pads), moreover its complex structure, properties and large range of behaviour across different users is an obstacle for further development. What is the common tactile response between all of us? Are we able to reproduce artificial self-adapting tactile illusions? We are uncertain, nevertheless the answer must be in the significant similarities within mechanical contacts that lead to perceptual constancy across individuals.

The ITN project, (PROTOTOUCH) was established to support this high-technology evolution of touch screens with haptic feedback. The aim was to make substantial progress by bringing together experts in a wide range of disciplines such as hardware developers, computer modellers, tribologists, and specialists in artificial intelligence and neuroscience equipment. Bringing together researchers form several correlated disciplines allowed communication and collaboration within a common interest. The results of these

collaborations that involved the author, are presented in chapters of this thesis as refereed published papers.

The main chapters create the consequent flow of the theoretical work, based on existing mechanical models, followed by focussed analysis of selected problems and concluded with application analysis (Figure 1). Each sub-chapter presented in the thesis comprises the research associated with the understanding of fundamental problems of the tribological interactions of finger pads and tactile devices, and to expand knowledge and contribute to the development of the next generations of haptic interfaces.

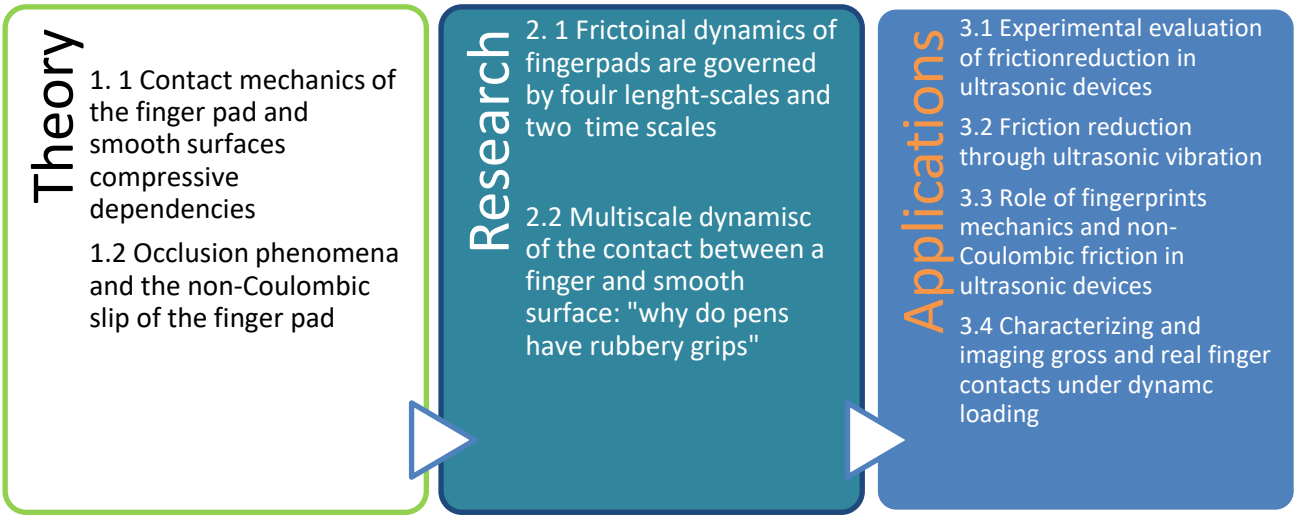

Figure 1 Research evolution included in the chapters.

The first part of **chapter one** is a paper reviewing previous knowledge of the contact mechanics of the finger pad and smooth surface compressive dependencies. The application of a linear elastic model of the finger pad that is homogeneous and isotropic but is constrained by the distal phalanx was found to be consistent with the loading behaviour and the gross and nominal contact areas of the fingerprint ridges. However, clearly it was not possible to determine accurately the sub-surface stress field with this approach since the

structure of finger pad involves two outer layers of skin comprising the *epidermis* and *dermis* and an inner region of biphasic fat and water in addition to the *distal phalanx*.

The finger pad is strongly viscoelastic and hence its compressive behaviour is rate dependent but the data reported here correspond to times that are long compared to the longest relaxation time. Consequently, it was possible to assume steady state conditions. However, it was shown in previous work that it is possible to separate the strain and strain rate dependence of the contact mechanics, which is a viable strategy for deriving analytical solutions of contact.

In summary it has been shown, that the current model provides a mechanistically based understanding for the observed load dependence of the friction of a finger pad against a smooth surface. However, it was limited to the fully-occluded state where it is reasonable to assume that the fingerprint ridges make complete contact with the surface due to the plasticisation induced by the excretion of moisture as sweat. However, in these states the model may be used to calculate the gross contact area.

The second part of the **chapter one** is a paper that describes the author's early friction experiments. A brief and conclusive analysis is presented of the relationship between occlusion phenomena and the non-Coulombic slip of the finger pad. The results demonstrate that the frictional force is a power law function of the normal load, with an index between 2/3 and 1. For smooth impermeable surfaces, occlusion of moisture excreted by the sweat glands may cause up to an order of magnitude increase in the coefficient of friction. This is a result of a transition from glassy to the rubbery state of the *stratum corneum* due to the plasticising action of the moisture in sweat. The data are consistent with a first order kinetics approximation for the growth in the friction with a characteristic time of ~ 20 s. The temporal

evolution of the contact area of a finger pad is critical during tactile interactions, whether for gripping or discriminating surfaces.

Texture appreciation and shape discrimination also rely on frictional dynamics since they can be expected to depend on the microscopic features of finger pads. **Chapter two** integrates the analysis and discussion for the most important, yet frequently underestimated, parameter of the interface mechanics i.e. the contact area. The contact of the finger pad was imaged using a high-resolution optical method to delineate the characteristic length and time scales. It was observed that the contact of the ridges was not continuous but that small junctions were formed, which were associated at a small length scale to a newly defined contact area i.e. the area of the junctions. Moreover, the findings demonstrated that the growth of the contact area results from a two-step mechanism, with some correlation between the steps.

We take for granted the ability of grasping and texture recognition, where the grip and touch abilities are mediated through the finger pads. While a detailed knowledge of the bio-tribology of fingertips is fundamental to studies of gripping behaviour and discriminative touch, this knowledge has gained additional importance with the recent advent of tactile displays that depend on the modulation of fingertip friction to operate. **Chapter two** presents the first direct, *in-vivo*, contact area evolution. The influence of parameters such as the normal load and moisture content were investigated.

The observed contact evolutions during interactions is also a tribute to the abilities of the human nervous system, despite the extensive variations in detailed contact mechanics through time during finger contact with objects. One of the most important implications of the fully-understood contact area evolution is the design of touch screens with haptic feedback that rely on the modulation of friction to provide computer-controlled sensations.

Chapter three is a compilation of four papers describing experiments were designed that would provide data to evaluate various models of tactile displays. Measurements were conducted within the project collaborations that involved the most advanced technologies applied within the new generation of devices.

The first two sub-chapters are the proceedings of the experimental evaluation of intermittent contact and squeeze film levitation of the finger pad. Analysed data were consistent with the previous finite element model (developed in part 1 of this publication) and also the data superposition scheme derived in this work. The proposed ratchet mechanism was a satisfactorily explanation for the friction modulation of ultrasonic displays. It shown that the friction modulation depends on the exploration velocity and is independent of the applied normal force. Based on the work, it was not possible to quantify the relative contribution of squeeze film levitation, what makes this research so innovative and outstanding compared with similar studies. Data reduction using an exponential function of a dimensionless group showed a reasonable description of the experimental data, provided that the intermittent contact is sufficiently well developed.

The following sub-chapter is a description of the role of fingerprint mechanics and non-Coulombic friction in ultrasonic devices. An experimental evaluation of the previously described models was conducted. Ultrasonic vibrations were used to modulate the friction of a finger pad sliding on a surface. This modulation could modify the user perception of the flat screen and induce the perception of textured materials on future tactile devices. Simple models of the contact mechanics described in the work were useful in order to establish key principles for formulating models that are more complex. The non-linear viscoelastic behaviour of the finger pad was particularly relevant since it controls the gross temporal response. It was concluded that ultrasonic frequencies are essential for ensuring that the

finger pad is sufficiently stiff to cause periodic contact separation for the out-of-plane vibrations.

The final part of the chapter three is the evaluation of a new instrument intended to study finger pad contacts under tangential dynamic loading. The innovative setup could be characterized by imaging the gross and real finger pad contacts under dynamic loading. The paper is reports the extensive variety of possible experiments as well as a first data analysis. As a preliminary example of the type of phenomenon that was identified with this apparatus, it was shown that traction in the range from 10 to 1000 Hz tends to decrease faster with excitation frequency for dry fingers compared with those that are moist.

Chapter One

Part 1: Contact mechanics of the human finger pad under compressive loads.

Brygida Dzidek[1], Michael J. Adams[1], James W. Andrews[1], Zhibing Zhang[1], Simon A. Johnson[2]

[1] School of Chemical Engineering, The University of Birmingham, Birmingham B15 2TT, UK

[2] Unilever R&D Port Sunlight, Bebington, Wirral, CH63 3JW, UK

Authors' contributions

BD and MJA designed and coordinated the study and drafted the manuscript; BD and SAJ performed the experiments and conducted the data analysis; JWA and ZZ participated in the statistical analysis and contact modelling. All authors made substantial contributions to the critical revision of the submitted manuscript.

Author Queries

Journal: Journal of the Royal Society Interface

Manuscript: rsif20160935

Due to the publisher's copyright restriction, the full-text article is redacted from the online version. Please refer to Dzidek, B.M., Adams, M.J., Andrews, J.W., Zhang, Z. and Johnson, S.A., 2017. Contact mechanics of the human finger pad under compressive loads. Journal of The Royal Society Interface, 14(127), p.20160935.

INTERFACE

rsif.royalsocietypublishing.org

Research

Cite this article: Dzidek BM, Adams MJ, Andrews JW, Zhang Z, Johnson SA. 2017 Contact mechanics of the human finger pad under compressive loads. *J. R. Soc. Interface* 20160935.
http://dx.doi.org/10.1098/rsif.2016.0935

Received: 18 November 2016
Accepted: 13 January 2017

Subject Category:
Life Sciences–Physics interface

Subject Areas:
biomechanics, biophysics, biomaterials

Keywords:
tribology, friction, touch, fingerprint, skin

Author for correspondence:
Michael J. Adams
e-mail: m.j.adams@bham.ac.uk

Electronic supplementary material is available online at rs.figshare.com.

THE ROYAL SOCIETY PUBLISHING

Contact mechanics of the human finger pad under compressive loads

Brygida M. Dzidek[1], Michael J. Adams[1], James W. Andrews[1], Zhibing Zhang[1] and Simon A. Johnson[2]

[1]School of Chemical Engineering, University of Birmingham, Birmingham B15 2TT, UK
[2]Unilever R&D Port Sunlight, Bebington, Wirral CH63 3JW, UK

SAJ, 0000-0001-6621-7622

The coefficient of friction of most solid objects is independent of the applied normal force because of surface roughness. This behaviour is observed for a finger pad except at long contact times (greater than 10 s) against smooth impermeable surfaces such as glass when the coefficient increases with decreasing normal force by about a factor of five for the load range investigated here. This is clearly an advantage for some precision manipulation and grip tasks. Such normal force dependence is characteristic of smooth curved elastic bodies. It has been argued that the occlusion of moisture in the form of sweat plasticises the surface topographical features and their increased compliance allows flattening under an applied normal force, so that the surfaces of the fingerprint ridges are effectively smooth. While the normal force dependence of the friction is consistent with the theory of elastic frictional contacts, the gross deformation behaviour is not and, for commonly reported values of the Young modulus of *stratum corneum*, the deformation of the ridges should be negligible compared with the gross deformation of the finger pad even when fully occluded. This paper describes the development of a contact mechanics model that resolves these inconsistencies and is validated against experimental data.

Chapter One

Part 2: Role of occlusion in non-Coulombic slip of the finger pad.

Brygida Dzidek[1], Michael Adams[1], Zhibing Zhang[1], Simon Johnson[2], Séréna Bochereau[3], and Vincent Hayward[3]

[1] School of Chemical Engineering, University of Birmingham, Birmingham B15 2TT, UK.

[2] Unilever R&D Port Sunlight, Bebington, Wirral CH63 3JW, UK.

[3] Sorbonne Universités, UPMC Univ Paris 06, UMR 7222, ISIR, F-75005, Paris, France.

Authors' contributions

BD and MJA designed and coordinated the study and drafted the manuscript; BD and SAJ performed the experiments and conducted the data analysis; SB and VH participated in the statistical analysis. All authors made substantial contributions to the critical revision of the submitted manuscript.

Draft. Final version in
Haptics: Neuroscience, Devices, Modeling, and Applications, Part-I, Auvray, M. and Duriez, C. (Eds). pp. 109-116

Role of occlusion in non-Coulombic slip of the finger pad

Brygida Dzidek[1], Michael Adams[1*], Zhibing Zhang[1], Simon Johnson[2], Séréna Bochereau[3], and Vincent Hayward[3]

[1]School of Chemical Engineering, University of Birmingham, Birmingham B15 2TT, UK.
m.j.adams@bham.ac.uk
[2]Unilever R&D Port Sunlight, Bebington, Wirral CH63 3JW, UK.
simon.johnson@unilever.com
[3]Sorbonne Universités, UPMC Univ Paris 06, UMR 7222, ISIR, F-75005, Paris, France.
hayward@cim.mcgill.ca

Abstract. Understanding how fingers slip on surfaces is essential for elucidating the mechanisms of haptic perception. This paper describes an investigation of the relationship between occlusion and the non-Coulombic slip of the finger pad, which results in the frictional force being a power law function of the normal load, with an index n; Coulombic slip corresponds to $n = 1$. For smooth impermeable surfaces, occlusion of moisture excreted by the sweat glands may cause up to an order of magnitude increase in the coefficient of friction with a characteristic time of ~ 20 s. This arises because the moisture plasticises the asperities on the finger print ridges resulting in an increase in their compliance and hence an increase in the contact area. Under such steady state sliding conditions a finger pad behaves like a Hertzian contact decorated with the valleys between the finger print ridges, which only act to reduce the true but not the nominal contact area. In the limit, at long occlusion times (~ 50 s), it can be shown that the power law index tends to a value in the range $2/3 \leq n \leq 1$. In contrast, measurements against a rough surface demonstrate that the friction is not affected by occlusion and that a finger pad exhibits Coulombic slip.

Keywords: Finger pad, Friction, Coulombic slip, Occlusion, Skin hydration

1 Introduction

Over a century ago, Katz [1] showed that a finger often oscillates when it slides on most surfaces. These rapid fluctuations are often attributed to irregularities on the surfaces in contact. However, surface irregularities alone are frequently unable to explain the observed fluctuations since they can also arise from simple relaxation oscillations or from more complex phenomena such as, *inter alia*, Schallamach waves. Understanding of the sliding event can assist in explaining the factors that govern the oscillatory mechanisms perceived by the finger through vibrotaction. Such insights would be very valuable since the fluctuations play a determinant role in the perception of textures [2], in motor behaviour [3] and in most instances of haptic behaviour in humans [4]. The fluctuations are a dynamic system response that depends

on the tribological properties of the finger pad, and the compliance of the finger in addition to any frictional force measurement device. Evaluating the quasi-static tribological properties in isolation is fundamental to understanding the system dynamics. This is possible when there is continuous sliding, which may occur for some surfaces under particular combinations of normal load and sliding velocity, however the results have proven to be surprisingly complicated. For example, there is evidence that, contrary to classic contact mechanics theory [5], two different coefficients of friction contribute to the net friction. Since they influence the dynamics of contacts, this multiplies the possible stick-slip evolutions of the contact area. In fact, Terekhov and Hayward [6] found that a cutaneous contact evolves differently if the dynamic friction is greater than the static value: the stuck surface area can diminish as the tangential load increases until reaching a *minimal adhesion surface area* where it vanishes abruptly.

The complexity of the tribological properties was also exemplied by the extraordinary experiments of Cartmill [7] who showed that the frictional force, F, of the fingers of small clawless primates such as squirrels depends on a fractional power of the normal load, termed the load index, n, thus $F = kW^n$, where W is the normal load and k is sometimes termed the friction factor. This non-linear frictional behaviour, corresponding to *non-Coulombic slip* ($n < 1$), is also seen for the human finger pad [8] and has been argued to be important in explaining the force modulations arising from tactile interactions with rough surfaces [9]. An intuitive explanation for the occurrence of the decaying harmonics is the distribution and nature of the multiple micro features on the surfaces in contact with the finger [10]. These asperities have arbitrary shapes, and varying sizes and heights, making the signal complex. The sum of the areas of all the contact spots constitutes the real (true) area of contact, A [5]. When two such surfaces (the finger and the counter surface) move relative to each other tangentially under load, the adhesion between the asperities creates the frictional force. This adhesion mechanism relates the frictional force to A by $F = \tau A$ where τ is the interfacial shear strength associated with the rupture of the intermolecular junctions e.g. van der Waals attractive potentials. In the case of organic polymeric materials, such as the *stratum corneum,* τ is a linear function of the mean contact pressure, $p = W/A$, such that $\tau = \tau_0 + \alpha p$ where τ_0 is the intrinsic shear strength and α is a pressure coefficient [11]. The finger pad is topographically rough at the length scales of the finger print ridges and their associated asperities. It is well established that A for any multiple asperity contact is proportional to the normal load, i.e. $A = cW$ where c is a material constant [5]. Thus the adhesion mechanism yields $F = (c\tau_0 + \alpha)W$. Since the terms in brackets are material constants, a multiple asperity contact should be *Coulombic*, i.e. $F = \mu W$ where μ is the coefficient of friction. Thus Cartmill's results [7] would not have been anticipated on the basis of classic contact mechanics given the topographical features of a finger pad.

Actually, the value of μ at a given normal load depends on several variables such as the hydration state of the finger, its displacement, and the sliding time [4]. In particular, skin moisture dramatically affects the contact dynamics during the evolution from sticking to slipping. There is up to an order of magnitude increase in μ during sustained sliding against smooth impermeable surfaces because the asperities on the

finger print ridges are plasticised by the occlusion of the excreted moisture from the sweat pores that heavily populate these ridges. This process may be described by first order kinetics with a characteristic time of ~ 20 s [12]. Moreover, excess hydration reduces the tendency of the contact to slip, regardless of the variations of the coefficient of friction [13]. In such cases, different parts of the skin can be in a stick or slip state at the same time.

In the current paper, we investigate the evolution of k and n as a function of the sliding time for smooth and rough surfaces with different hydrophobicities. These parameters are sensitive measures of the prevailing contact mechanics and will thus provide insights about the influence of moisture occlusion. A particular aim is to identify the mechanism that leads to the load dependence of μ. The work involved measurements of the friction as a function of the normal load for a range of occlusion times from first contact until steady state. They were conducted under passive touch conditions at a constant velocity.

2 Experimental

The counter surfaces (75 x 25 mm) were an optically flat glass plate (hydrophilic), a sheet of smooth polypropylene (PP) (hydrophobic), and PP that had been roughened with 240p grade "wet and dry" abrasive paper. The surface textures were evaluated using a profilometer (Sensofar S neox 3D Optical Profiler). The glass and smooth PP had mean Rq values of 2 nm and 50 nm respectively, while that for the rough PP was 6 µm.

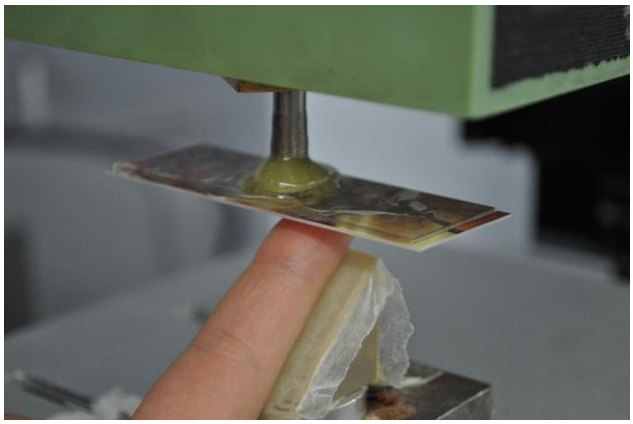

Fig. 1. Photograph of the tribometer configuration used to measure finger pad friction.

The friction measurements were carried out using a Tabor-Eldredge tribometer, which consisted of a balanced beam with a bearing as its fulcrum [12]. The tangential force at one end was measured by two flexible, strain-gauged, cantilever steel beams to which the counter surface was attached via a rigid beam spacer assembly. The left

hand index finger of a healthy female volunteer (26 yr) was supported by a sloping platform assembly (Fig.1), which could be raised to bring the finger into contact with the counter surface. The finger was initially washed with soap, rinsed, dried and allowed to equilibrate for a minimum of 10 min. Normal loads in the range 0.02 to 2.0 N were applied by placing weights on the tangential force transducer, directly above the contact region. Motorised actuation allowed a reciprocating motion of ~ 45 mm to be applied at a constant velocity of 24 mm/s for ~ 4 min. Between each load being applied, the finger pad was allowed to equilibrate with the ambient environment (21°C and 55% RH) for about 1 min and the finger pad wiped with a tissue immediately prior to each measurement.

3 Results

In the case of the smooth surfaces, the frictional force increased asymptotically with occlusion time to an approximately steady state value. The values of k and n, as a function of the occlusion time, *t*, which were obtained from the best fits of data to the power law equation ($F = kW^n$) at specific occlusion times, are shown in Fig. 2 together with the best fits to the following first order kinetics equations:

$$= \ _{\infty} + (\ n_0 - \ n_{\infty}\ ) \exp\ (-t/\lambda) \quad (1)$$

$$k = k_{\infty} + (\ k_0 - \ k_{\infty}\ ) \exp\ (-t/\ \lambda) \quad (2)$$

where the subscripts 0 and ∞ refer to the time at first contact and at steady state, and λ is a characteristic time. The values of the parameters are given in Table 1 and those for *k* increase with time and are relatively similar for the two smooth surfaces, which is consistent with the trends in μ obtained previously for a different subject at a single normal load of 0.2 N [12]. The characteristic times are also similar being 24 and 16 s for glass and PP at the same sliding velocity of 24 mm/s compared with 18 and 16 s in the current work. The values of n for both nominally smooth surfaces decrease from about unity to ~ 0.63 and ~ 0.80 for glass and PP.

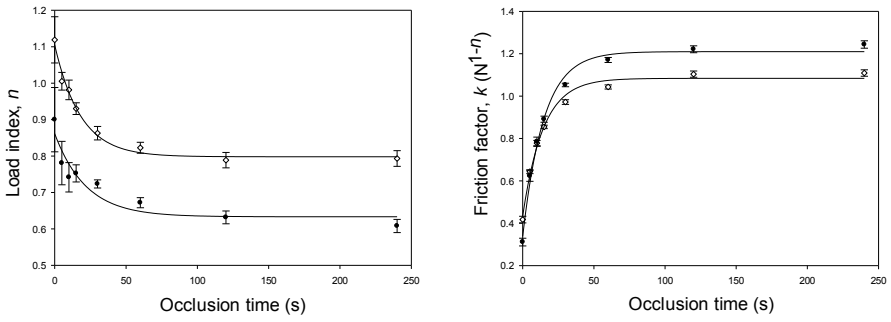

Fig. 2. The parameters n and k as a function of occlusion time for smooth PP (◊) and glass (●). The lines in the left and right hand figures are the best fits to equations (1) and (2) respectively. The error bars represent the standard error of the mean.

Table 1. Parameter values for glass and PP corresponding to equations (1) and (2).

	$_0$	$_\infty$	k_0 (N^{1-n})	k_∞ (N^{1-n})	λ (s)
Glass	0.86±0.03	0.63±0.02	0.34±0.03	1.21±0.02	18±5
PP	1.10±0.01	0.80±0.01	0.43±0.03	1.08±0.02	16±3
Rough PP	0.98±0.01	0.98±0.01	0.53±0.001	0.53±0.001	

The frictional force was relatively independent of the occlusion time for the rough PP; the load index was found to be close to unity (0.98) and the value of k is 0.53 $N^{0.02}$, which is initially greater than that for the smooth surfaces but is less at steady state.

4 Discussion

It might be expected that the load index should be unity at first contact even for the nominally smooth surfaces since the *stratum corneum* will be in a near-glassy state [4] and thus the asperities on the finger print ridges will be relatively non-deformable. Consequently, a multiple asperity contact should be formed with a contribution from the counter surface depending on the extent of the surface roughness. The simplest model of such contacts was proposed by Archard [14] who considered a Hertzian sphere with spherically capped Hertzian asperities on which such asperities of smaller radii were located, and so on. He showed that n tends from 2/3 to unity in the limit. Essentially he demonstrated that the mean asperity contact pressure is constant since the value on existing asperities increases with load but new contacts experience a small pressure. Consequently, τ should be independent of the load.

Asperities reduce the real area of contact and hence the coefficient of friction should decrease with increasing roughness of the counter surface. This is the case here for the values of $\mu\,(= k/W^{1-n})$ at steady state sliding, particularly at small normal loads, but those for glass and smooth PP asymptotically reduce to a similar value at large normal loads that is about a factor of two greater than that for the rough PP. That these values and those of the characteristic times are similar within experimental error suggests that under these sliding conditions the formation of thin water films is not a significant factor, despite the glass being hydrophilic and the PP being hydrophobic. For triangular ridged hard surfaces it has been observed that the friction of the finger pad was relatively independent of the roughness in the range of Rq values studied here [15]. However, the sliding time was not controlled in this work, which is clearly a factor at small loads for the nominally smooth surfaces. The lack of sensitivity to the sliding time observed in the current study for rough PP suggests that for rough surfaces there is sufficient interstitial voidage between the asperity valleys for moisture to diffuse readily and thus eliminate the effects of occlusion. Alternatively, the plasticisation of the asperities on the finger print ridges and resulting in-

crease in compliance is not sufficient to change significantly the extent to which they conform to those on the PP.

To understand the origin of n being less than unity for smooth surfaces at steady state occlusion, it is necessary to assume that the loading of the finger pad is Hertzian [5] at the length scale of the gross curvature. This is consistent with the measured parabolic pressure profile [16] and the variation of A with load [8] for the range of normal loads invesitigated here. Hertzian contact assumes linear elastic deformation and it arguable that more complex material models, e.g. viscoelastic or hyperelastic [17], would be more appropriate but Hertzian contact provides a useful first order interpretation of the data. The frictional force for such a contact, assuming that the adhesion mechanism applies, is given by the following expression [18]:

$$F = \pi\tau_0[3R(1-\nu^2)/4E]^{2/3}W^{2/3} + \alpha W \quad (3)$$

where E, R and ν are the Young's modulus, mean radius and Poisson's ratio of the finger pad. It may be approximated by a power law in W such that the load index is in the range $2/3 \geq n \geq 1$ depending on the relative values of the load coefficients in equation (3) [18]. Thus, for example, in the case of an elastomeric Hertzian contact, α = 0 and thus n = 2/3 [11], which was the case considered by Archard [14]. The values of n observed here are consistent with the gross contact area of individual finger print ridges being independent of load due to the much greater gross compliance of the finger pad. Given the approximately trapezoidal cross-section of the finger print ridges, a reasonable model of the finger pad is a smooth Hertzian spherical cap with triangular valleys between the finger print ridges. Thus the friction may be described by equation (3) after accounting for the ratio of the real and nominal areas of contact, ξ:

$$F = \pi\xi\tau_0[3R(1-\nu^2)/4E]^{2/3}W^{2/3} + \alpha W \quad (4)$$

That the value of n_∞ is slightly less than 0.67 for the glass and the initial value for PP is greater than unity reflects either the approximate nature of the model or experimental uncertainties. The complexity of the finger pad contact, such as a tendency to roll during the application of the tangential force, is likely to be a contributory factor. However, it has been observed that the contact area decreases under the action of a tangential load before any slip is initiated [13]. Thus if the rate of increase of the residual area with normal load was less than expected from the Hertz equation then a value of $n < 2/3$ is theoretically possible. In terms of the Archard model, as the extent of occlusion increases from first contact, the smallest asperities will be preferentially flattened because of their greater contact pressure and thus the value of n will decrease. The steady state occlusion time is surprisingly long (~50 s) and will reflect the physiological factors involved and the possibility of some moisture being lost due to deposition on the counter surface or interface diffusional loss through the contact.

The steady state values of n increase with the roughness of the surfaces studied. For glass, the initial value is < 1, which suggests that the moisture content of the unoccluded *stratum corneum* is sufficient to cause significant deformation of the asper-

ities on the finger print ridges. However, the initial value for smooth, like the rough PP is ~ 1, which shows that the asperities on even relatively smooth surfaces have a considerable influence on unoccluded *stratum corneum*. This is consistent with the steady state value of > 2/3, which indicates that even fully occluded *stratum corneum* is extremely sensitive to small topographical features. The important point is that this load index is greater than that for glass rather than being > 2/3, since it is theoretically possible for a smooth Hertzian contact to exhibit a value > 2/3 depending on the relative values of the coefficients in equation (4) as mentioned previously.

5 Conclusion

In the current work, the quasi-static component of the kinetic friction as a function of the occlusion time has been monitored. The friction factor and load index are instrumental in defining the relationship between the friction coefficient and the load exerted by the finger. For smooth surfaces, the occlusion time dependent load index provides a sensitive measure of the transition from a multiple asperity Coulombic contact to one that is non-Coulombic due to the finger print ridges developing an intimate contact with the counter surface. Rough surfaces appear to be indifferent to occlusion as evidenced by the insensitivity of the coefficient of friction to the sliding time. The results represent an important precursor to understanding the much more complex dynamic behavior elicited by the finger pad in haptic contacts such as vibrotaction. Moreover, it should provide a basis for elucidating the complex evolution of a finger pad contact when tangentially loaded. For example, whether or not the initial reduction of the contact area is due to a peeling mechanism prior to true slip. This phenomenon may play an important role in our ability to detect slip, which is crucial in grip function. Finally, the current work was limited to one subject and three surfaces but a recent larger study has concluded that occlusion has a major effect on the variability in μ for different subjects [19].

6 Acknowledgements

This work was funded by the FP7 Marie Curie Initial Training Network PROTOTOUCH, grant agreement No. 317100.

7 References

1. Krueger, L.E.: Tactual Perception in Historical Perspective: David Katz's World of Touch. Tactual Perception; A Sourcebook 1–55, Cambridge University Press (1982)
2. Bensmaia, S.J., Hollins, M., Washburn, S.: Vibrotactile Adaptation Impairs Discrimination of Fine, but not Coarse Textures. Somatosensory Motor Res. 18, 253–262 (2001)

3. Wiertlewski, M., Endo, S., Wing, A.M., Hayward, V.: Slip-Induced Vibration Influences the Grip Reflex: A Pilot Study. Proceedings of the 2013 World Haptics Conference, 627–632 (2013)
4. Adams, M.J., Johnson, S.A., Lefèvre, P., Lévesque, V., Hayward, V., André, T., Thonnard, J.L.: Finger Pad Friction and its Role in Grip and Touch. J. R. Soc. Interf. 10, 20120467 (2013)
5. Johnson, K.L.: Contact Mechanics, Cambridge University Press (1987)
6. Terekhov, A., Hayward, V.: Minimal Adhesion Surface area in Tangentially Loaded Digital Contacts. J. Biomech. 44, 2508–2510 (2011)
7. Cartmill, M.: The Volar Skin of Primates: Its Frictional Characteristics and Their Functional Significance. Am. J. Phys. Anthrop. 50, 497–509 (1979)
8. Warman, P.H., Ennos, A.R.: Fingerprints are Unlikely to Increase the Friction of Primate Fingerpads. J. Exp. Biol. 212, 2016–2022 (2009)
9. Wandersman, E., Candelier, R., Debrégeas, G., Prevost, A.: Texture-induced Modulations of Friction Force: The Fingerprint Effect. Phys. Rev. Lett. 107, 164301 (2011)
10. Wiertlewski, M., Hudin, C., Hayward, V.: On the 1/f Noise and Non-Integer Harmonic Decay of the Interaction of a Finger Sliding on Flat and Sinusoidal Surfaces. Proceedings of the 2011 World Haptics Conference, 25–30 (2011)
11. Briscoe, B.J., Arvanitaki, A., Adams, M.J., Johnson, S.A.: The Friction and Adhesion of Elastomers. Trib. Ser. 9, 661–672 (2001)
12. Pasumarty, S.M., Johnson, S.A., Watson, S.A., Adams, M.J.: Friction of the Human Finger Pad: Influence of Moisture, Occlusion and Velocity. Trib. Lett. 44, 117–137 (2011)
13. Andre, T., Levesque, V., Hayward, V., Lefevre, P., Thonnard, J.L.: Effect of Skin Hydration on the Dynamics of Fingertip Gripping Contact. J. R. Soc. Interf. 6, 1574–1583 (2011)
14. Archard, J.F.: Elastic Deformation and the Laws of Friction. Proc. R. Soc. Lond. A, Math. Phys. Sci. 243, 190–205 (1957)
15. Tomlinson, S.E., Carré, M.J., Lewis, R., Franklin, S.E.: Human Finger Contact with Small, Triangular Ridged Surfaces. Wear 271, 2346–2353 (2011)
16. Pawluk, D.T., Howe, R.D.: Dynamic Contact of the Human Fingerpad Against a Flat Surface. ASME J. Biomech. Eng. 121, 605–610 (1999)
17. Lin, D.C., Shreiber, D.I., Dimitriadis, E.K., Horkay, F.: Spherical Indentation of Soft Matter Beyond the Hertzian Regime: Numerical and Experimental Validation of Hyperelastic Models. Biomech. Model. Mechanobiol. 8, 345–358 (2009)
18. Adams, M.J., McKeown, R., Whall, A.: A Micromechanical Model of the Confined Uniaxial Compression of an Assembly of Elastically Deforming Spherical Particles. J. Phys. D: Appl. Phys. 30, 912–920 (1997)
19. Derler, S., Rossi, R.M., Rotaru, G.M.: Understanding the Variation of Friction Coefficients of Human Skin as a Function of Skin Hydration and Interfacial Water Films. Proc. Inst. Mech. Eng. Pt. J: J. Eng. Trib., in press (2014)

Chapter Two

Part 1: Frictional dynamics of finger pads are governed by four length-scales and two time-scales.

Brygida Dzidek[1], Simon Johnson[2], Séréna Bochereau[3], Vincent Hayward[3], Michael Adams[1]

[1] School of Chemical Engineering, University of Birmingham, Birmingham B15 2TT, UK.

[2] Unilever R&D Port Sunlight, Bebington, Wirral CH63 3JW, UK.

[3] Sorbonne Universités, UPMC Univ Paris 06, UMR 7222, ISIR, F-75005, Paris, France.

Authors' contributions

BD and MJA designed and coordinated the study and drafted the manuscript; BD, SAJ and SB performed the experiments and conducted the data analysis; MJA and VH participated in the statistical analysis. All authors made substantial contributions to the critical revision of the submitted manuscript.

In press, Haptics Symposium , Philadelphia USA, 2016

Frictional dynamics of finger pads are governed by four length-scales and two time-scales*

Brygida Dzidek, Séréna Bochereau, Simon Johnson, Vincent Hayward and Michael Adams

***Abstract*—The evolution of the contact area of a finger pad against a surface is critical during tactile interaction, whether for gripping or discriminating surfaces. The contact area made by a finger pad is commonly considered at two distinct length scales corresponding to the gross area, A_{gross}, and to the smaller ridge area, A_{ridge}, that excludes the interstitial spaces between the ridges. Here, these quantities were obtained from high-resolution imaging of contacts during loading and stress relaxation. While A_{gross} rapidly reaches an ultimate value, the contact made by the ridges is initially formed from unconnected junctions with a total contact area, A_{junct}, which continues to increase for several seconds during the holding period. Thus, the contact area grows in a two-step process where the number of junctions made by the ridges first increases, followed by a growth of their size and connectivity. Immediately after contact the *stratum corneum* is in a glassy state and the individual junctions form a multiple asperity contact. At longer contact times, the asperities soften owing to the occlusion of moisture excreted from the sweat pores in the ridges. Thus, the real area of contact, A_{real}, which drives the creation of friction, grows with time at a relatively slow rate. It is concluded that multi-asperity dynamic contact models should be preferred compared with static models in order to describe the physics of finger pad contact mechanics and friction.**

I. Introduction

Grip and touch are mediated through finger pads. While a detailed knowledge of the biotribology of fingertips is fundamental to studies of gripping behaviour and discriminative touch, this knowledge has gained additional importance with the recent advent of tactile displays that depend on the modulation of fingertip friction to operate.

The finger pad is a complex mechanical structure that is adapted to interact with a large range of materials under varied loading and environmental conditions. It comprises several layers of different tissues each endowed with particular properties [1]. The outer layer that comes in direct contact with objects, the *stratum corneum*, possesses specific permeation properties rendering the physical chemistry of this material highly sensitive to the presence of water [2]. The fingerprint ridges, furrows, and sweat pores are the visible macroscopic features of this structure. Prior studies have shown that the ridges are far from being smooth but exhibit smaller scale asperities [3].

A detailed understanding of the complexities of fingerprint deformation is necessary to address the mechanisms by which humans discriminate surfaces and grip objects. However, most studies tend to neglect the complexity of the finger pad topography, using instead a bulk approach [4]. As it turns out, we have found in the present study that smaller scale contact mechanics may in fact dominate over gross effects in the finger pad interaction with objects.

There are many sweat pores in the finger print ridges. During sustained contact with an impermeable smooth surface, the secreted moisture softens the ridges by plasticisation thus inducing a glassy-rubbery transition; this occlusion mechanism results in a large increase in the contact area and hence the friction as discussed below [2]. The temporal evolution of friction can be described by an empirical, first-order kinetics relationship,

$$\mu = \mu_\infty + (\mu_0 - \mu_\infty)\exp(-t/\lambda_1), \quad (1)$$

where μ is the coefficient of friction, the subscripts 0 and ∞ refer to the initial and asymptotic values, t is time, and λ_1 is the characteristic time. The increase in friction is surprisingly slow with λ_1 ~ 20 s for optically flat glass. The width, height, and length of each ridge change considerably when stressed in shear or compression [5]. Shearing loads can lead to gross deformation of 100% without damage [6], with small bumps inducing 30% deformation [7]. A water-bed model, [8], could be made to match empirical data under canonical, gross loading conditions.

At a smaller scale, Bhushan [9] applied a multiple asperity contact model proposed earlier by Greenwood & Williamson in [10] for nominally flat elastic bodies. In this model, the sum of the areas of all the individual contacts constitutes the real (true) area of contact. Deformation occurs in the regions of asperity contact, establishing stresses that oppose the applied load. With increasing applied load, the number of asperities and the size of their contact spots increase. Hence, surfaces may be viewed to be composed of features at multiple length scales of roughness that are superimposed on each other [11]. A number of studies have examined the influence of the topography of counter-surfaces on the friction of the finger pad [12]. For regular counter surface textures, it was observed that the coefficient of friction increased with the tip radius and number density of the asperities as would be expected by the resulting increase in the real area of contact [3].

*This work was supported by the FP7 Marie Curie Initial Training Network PROTOTOUCH (grant No. 317100) and by a FP7 European Research Council Advanced Grant (PATCH) to V.H. (No. 247300).

Brygida Dzidek and Michael Adams are with the School of Chemical Engineering, University of Birmingham, Birmingham B15 2TT, UK (e-mail: m.j.adams@bham.ac.uk).

Séréna Bochereau and Vincent Hayward are with Sorbonne Universités, Université Pierre et Marie Curie Paris 06, Unité Mixte de Recherche 7222, Institut des Systèmes Intelligents et de Robotique, 75005 Paris, France (e-mail: vincent.hayward@isir.upmc.fr).

Simon Johnson is with Unilever R&D Port Sunlight, Bebington, Wirral CH63 3JW, UK (e-mail: simon.johnson@unilever.com).

Warman & Ennos [4] examined the effects of fingerprints on friction with a view to explaining their function. They argued that they could improve grip by (a) inducing interlocking on rough counter-surfaces, (b) allowing excess water to escape, (c) acting as part of highly deformable structure to maximise the contact area at small forces and (d) allowing greater normal forces to be applied without damaging the skin. Currently, direct experimental evidence is not available to support these possible mechanisms.

Frictional effects are fundamental during texture discrimination tasks and are directly related to the contact area. The adhesion model of friction [13] is applicable to skin and is such that $F = \tau A_{\text{real}}$ where F, τ, and A_{real} are respectively the frictional force, the interfacial shear strength, and the real contact area [14]. For multiple asperity (rough) junctions, A_{real} is to a first approximation proportional to the normal load, W, hence the friction is Coulombic with $F = \mu W$. For sphere-on-flat (point) or cylinder-on-flat (line) Hertzian junctions, A_{real} is proportional to $W^{2/3}$ or $W^{1/2}$, respectively, so that the frictional force is modelled by $F = kW^n$ where n = 2/3 or 1/2 provided that the dependence of τ on the contact pressure is small; n is termed the *frictional load index* [14]. For contacts of the finger pad, which generally are strongly time-dependent, we observed in the case of an occlusive contact that $n \sim 1$ initially and that it decreased with sliding time to reach a value of ~2/3 [15]. Similarly to (1), the temporal dynamics could be described empirically by a first-order kinetics relationship,

$$n(t) = n_\infty + (n_0 - n_\infty)\exp(-t/\lambda_1). \qquad (2)$$

In the previous literature, two measures of the contact area are generally encountered, namely, the gross value, A_{gross}, which is the total area contained within the overall contact boundary, and the value associated with the ridges, A_{ridge}, which is based on the contact area of the ridges as defined by their gross contact boundaries. In previous works, it is typically assumed that A_{ridge} approximates A_{real}. Warman & Ennos, [4], using ink prints to estimate A_{ridge}, found that the ratio $A_{\text{ridge}}/A_{\text{gross}}$ was ~0.7 but was very sensitive to load. Childs & Henson [16], using an optical method, reported that this ratio was indeed clearly load-dependent with values of 0.12, 0.23, and 0.34 for loads of 0.41, 0.88, and 1.77 N. These results are reasonably consistent with those of Soneda & Nakano [17], who also used an optical method to report that this ratio increased with increasing normal load such that its value was 0.3 at 1.0 N. Moreover, for the fully occluded state at long contact times, it was observed that A_{ridge} increased with load according to the Hertz equations with an areal load index of 2/3. However, the value of A_{gross} was associated with a smaller index of 0.52. It thus appears that A_{ridge} increases faster with the normal load than does A_{gross}, a phenomenon also reported by others [18,19].

In order to estimate the load index of A_{gross} in the fully occluded state, it is reasonable to assume that the fingertip contact can be approximated by an elliptical Hertzian geometry [20]. In addition, the asymptotic areal load index of A_{ridge} in the fully occluded state can be estimated by representing the ridges by Hertzian line contacts. In the initial glassy state, a multiple asperity contact is created because the hard asperities do not deform sufficiently to form a smooth interface. The origin of this asperity persistence has still to be clarified but could involve such factors as the interaction of neighbouring sub-surface stress fields. There are rigorous models of multiple asperity contacts for specific surface topographies, e.g. [21], but the Archard model [22] is conceptually most useful. It considers spherically-capped Hertzian asperities that are such if their number remains constant with increasing load, then $n = 2/3$; but if the number increases with load, then $n \to 1$. One of the aims of the current work was also to understand the contact mechanics consequences of the glassy-rubbery state transition, also known as the Archadian-Hertzian transition, induced by occlusion. To this end, we imaged the fingerprint contact using a high-resolution optical method in order to delineate the characteristic length and time scales of an occluding contact. It was observed that the contact of the ridges was not continuous but that small junctions were formed, which were associated at a small length scale with a newly defined contact area, A_{junct}.

II. Methods

A. Apparatus

The experimental platform used to measure the time evolution of the contact area and the deforming load is shown in Fig. 1. The left index finger of a female volunteer (27 years old) was inclined at 30° with the finger pad facing upwards. A right-angle prism was attached to the loading platform of a universal mechanical testing machine (model no. 5566, Instron, High Wycombe, UK) fitted with a 10 N load transducer. The flat glass prism was pressed down onto the finger pad in order to induce frustrated total internal reflection while the contact area increased with applied load.

Figure 1. Schematic diagram showing the prism-based imaging method. The prism attached to the loading platform was pressed onto the finger pad. The dorsal side of the finger was secured on an angled block by double-sided adhesive tape.

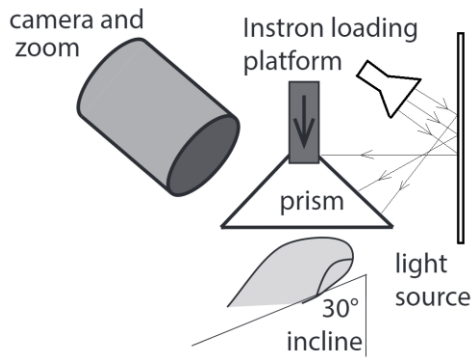

The image resulted in a high-contrast pattern of dark ridges where the light was scattered and a bright background where

the light was completely reflected. The finger pad compression was effected at a rate of 1 mm/s until a load of 2 N was reached. At this point, the prism movement was halted for 10 s before unloading the contact at the same rate. The finger had been washed with commercial soap, rinsed with distilled water and left to dry for 10 min until an equilibrated clean skin state was reached. All measurements were carried out in an environmentally controlled laboratory set to 20°C and 50% relative humidity.

The rear face of the prism was backlit uniformly by reflecting light from a fibre-optic lamp with a diffusely reflecting white surface. The contact was imaged through the front face of the prism using a Nikon D5000 camera with a video resolution of 1280 x 720 pixels at 24 fps and a shutter speed of 1/200 s. The camera was fitted with a macro lens and a small aperture was used to achieve the depth of field necessitated by oblique viewing.

B. Image Analysis

Figure 2. Image of the finger pad at a load of 2 N. The ridges were thicker and darker at the centre, compared to those at the periphery, corresponding to the greater pressure. The zoomed in rectangular area shows the sweat pores as white circular regions.

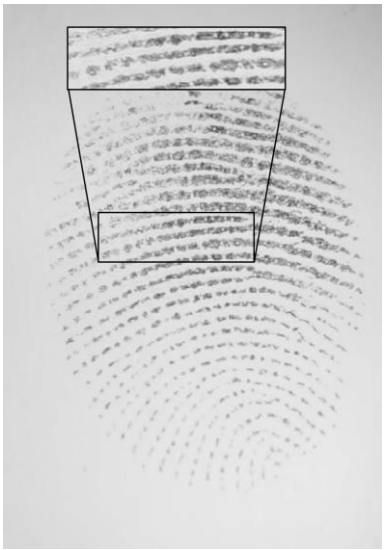

Using the ImageJ software, image analysis was carried out to determine A_{gross}, A_{ridge}, and A_{junct} as a function of the contact duration. Basic grey scale (8-bit) conversion and analysis was applied to 672 frames. The converted images were adjusted to the level of contrast and brightness that allowed for optimal pattern recognition. The values of A_{gross} were determined manually by fitting the peripheral border. To speed up the fitting process, the analysis was performed every 20$^{\text{th}}$ frame during the two second loading period and every 40$^{\text{th}}$ frame during the holding period. The value of A_{ridge} was determined from the value that was enclosed by the gross boundary, which included the spaces between the junctions due to the sweat pores, by interactively setting lower and upper threshold values. Low or uneven connectivity on the periphery was enhanced but remained unconnected. Typical methods were adopted for automatic fingerprint feature extraction [23] and follow a sequence of steps comprising image enhancement, binarisation, thinning, extraction, and post-processing. It was possible to exclude pores and to determine the size and evolution of each feature by segmenting the image into features of interest from the background under each relevant condition by use of a mask function. To estimate A_{junct}, a threshold grey scale value was determined from a histogram of the pixel intensities that allowed the boundaries of the contact junctions to be delineated. The boundary of each junction included sweat pores at the edge of the contact region but it was not possible to automatically exclude those that were internal to the boundaries. It was calculated that the overestimate of the contact area was < 5% since such internal sweat pores represented a relatively small proportion of the total contact area particularly since they were only present in the central region of the finger pad image.

III. RESULTS

An unprocessed image of the finger pad contact is shown in Fig. 2. The darker regions are larger in the central zone of the gross contact. The small white circles within the contact junctions as well as the gaps along the ridges arise from the presence of the sweat pores. The zoomed-in region shows more clearly the disconnected nature of the ridges. Figure 3(a) shows enlarged regions to exemplify the increase in size and connectivity of the junctions over the loading and hold periods. The size and connectivity of these junctions were greater in the central zone compared to the peripheral region. Figures 3(b) and (c) show the contour plots of the fingerprint images at 2 and 11 s from contact onset.

Figure 3. (a) Local binary mask of the junctions over the test period. Contact contour images at (b) the end of the 2 s loading period and (c) at the end of the 11 s hold period.

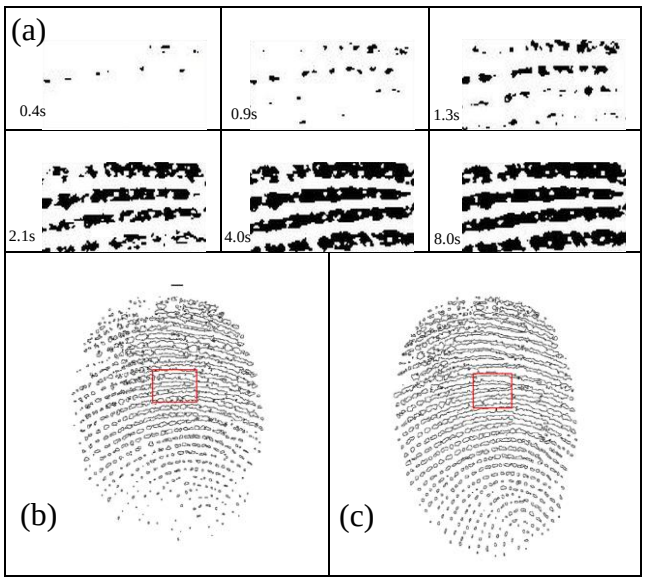

Figure 4 plots the normal force evolution as a function of time, showing and increase during the loading period and stress relaxation during the holding period. The trajectory of A_{gross} as a function of time shows that it reaches a maximum value just after loading and remains constant during the holding period. Figure 4 also includes a plot of the total area of the junctions, A_{junct}. There is a progressive augmentation of this value during the initial phase of the loading period, but A_{junct} continues to grow throughout the entire holding period. In the meantime, A_{ridge} exhibits values that are between the commonly assumed values and those presently observed for A_{junct}. The asymptotic ratio $A_{\text{ridge}}/A_{\text{gross}}$ is about 0.39, which is consistent with the values previously reported [18].

Figure 5 reports the temporal evolution of the number of junctions, N_c. Most were formed during the loading period. The value of N_c decreases only slightly during the holding period because, although there is coalescence of some junctions in the central region, this is compensated by the formation of new junctions in the peripheral region. The junction density, N_c/A_{gross}, first decreases dramatically and then slowly creeps down because the rate of increase of A_{gross} is slightly greater than that of N_c.

Figure 4. Temporal evolution of A_{gross} (Δ), A_{ridge} (□), A_{junct} (○) and load (-) during finger pad compression.

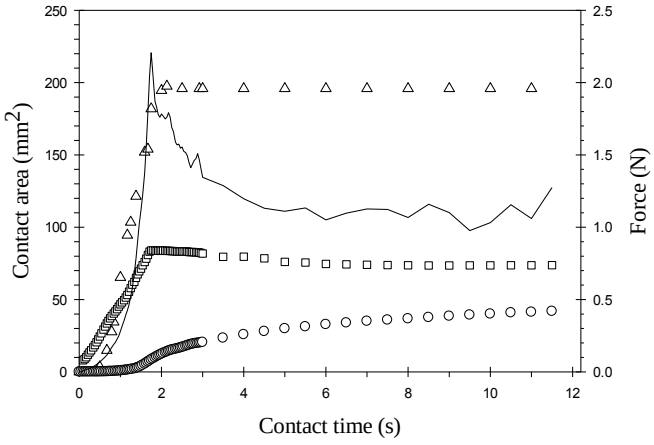

IV. Discussion

The finger print ridges are punctuated by sweat pore openings with trumpet bell profiles. These concavities have a reported average peripheral diameter of 109 μm, and an average separation between them on one ridge of 390 μm [24]. As discussed previously, the frictional load index, n, is about unity at contact onset. Thus, the junctions in the hinterlands between the sweat pores correspond, at short times, to multiple asperity contacts since the *stratum corneum* is in a glassy state. The increase of A_{junct} with load in the initial phase of a contact is thus mostly due to an increase of the number of junctions, N_c, rather than an increase in their size. At longer times, the junctions become plasticised by the transport of moisture from the sweat pores and expand owing to material softening.

A moderate increase in connectivity in the central region where junction growth is greatest can be observed. Plasticisation of the *stratum corneum* by moisture softens the asperities causing existing junctions to progressively form more intimate contacts. Consequently, as A_{gross} grows, the value of n reduces. The existing junctions grow but the peripheral regions of the gross contact become populated by non-plasticised asperities, causing the new contacting asperities to form a multiple-asperity region with n equal to one. At longer time scales, the proportion of peripheral areas exhibiting multiple asperity contacts eventually vanish and thus $n \to 2/3$.

Figure 5. Number of junctions, N_c, as a function of contact time (continuous line) compared with the number density, N_c/A_{gross} (□).

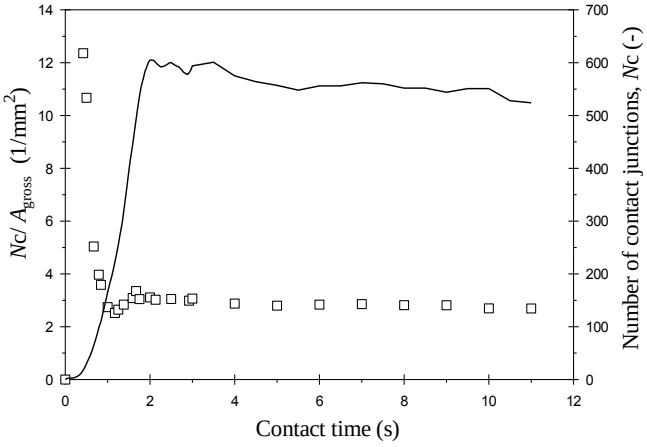

Figure 6 shows how A_{junct} evolves as a function of time. On the basis of (1), the data from the hold period can be fitted with a first order kinetics relationship,

$$A_{\text{junct}} = A_{\text{junct},0} + \left[A_{\text{junct},0} - A_{\text{junct},\infty}\right] \exp\left\{-\frac{(t+t_*)}{\lambda_2}\right\}, \qquad (3)$$

where here t represents the measured time after initial contact. However, the load was not applied instantaneously and it is necessary to add an additional time period, t_* = 1.7 s, that satisfies the boundary condition $A_{\text{junct}} = A_{\text{junct},0} = 0$ at $t + t_* = 0$. The best fit of (3) to the data is shown in Figure 6 corresponding to $A_{\text{junct},\infty} = 50.5 \pm 0.7$ mm^2. Interestingly, λ_2 is 7.1 ± 0.2 s, which is considerably shorter than the value of 18 ± 5 s for λ_1, which is the characteristic time for the increase in friction of the same finger on glass [15]. This result implies that the growth rate of A_{junct} is significantly greater than that of A_{real}. Thus, overcoming asperity persistence is significantly more difficult than the gross deformation of the junctions.

Given that the asymptotic value of A_{gross} is 195.8 mm^2, $\left(A_{\text{junct}}/A_{\text{gross}}\right)_\infty$ = 0.26. Consequently, if it assumed that the asymptotic value of $A_{\text{real}} = A_{\text{junct}}$, then the real area of contact at long occlusion times is about one quarter of the

gross area and will be considerably less at shorter dwell times. It should be emphasised this is a result from limited measurements at a single normal load and for a single subject, but the general behaviour is expected to be applicable irrespective of the loading and subject.

The conventional assumption that $A_{\mathrm{real}} = A_{\mathrm{ridge}}$ has arisen from the use of ink for real contact visualisation or from imaging without sufficient resolution. The present images are consistent with those reported by Childs & Henson [16], but perhaps because of the poor quality of the ink print images, their significance was under-appreciated.

Figure 6. The best fit of Eq. (3) to the measured values of A_{junct} as a function of $(t + t_*)$.

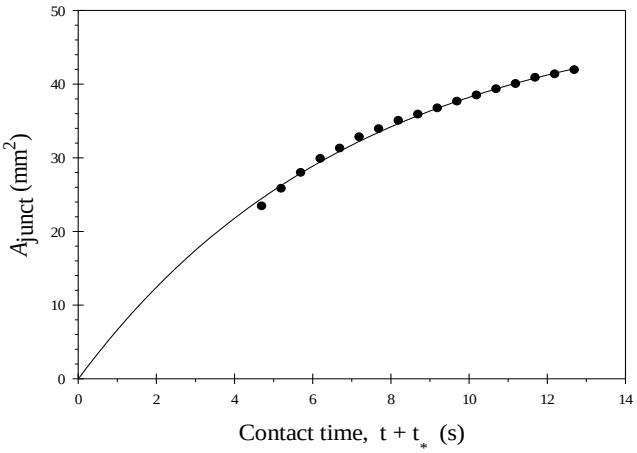

Our results also indicate that friction, driven by the growth dynamics of the real area of contact, may play a determining role in the perception of roughness, slipperiness, and warmth, as recently reviewed in reference [12].

Some tactile displays rely on decreasing friction by ultrasonic vibration of a smooth counter surface [25-27]. It has been shown that the modulation of friction could be explained partially by repeated collisions of the counter-surface with the finger pad [28]. This finding is supported by the fact that at the length scale of the asperities (of the order of microns), exposure to air could lead to drying and de-plasticisation. Consequently, asperity persistence could be an essential contributory factor to friction reduction, thus providing a possible explanatory mechanism for the observed phenomenon.

V. Conclusion

In summary, the present work has shown that four characteristic length scales, rather than just two as previously assumed, are required to describe the contact mechanics of the finger pad; namely those associated with the gross finger geometry, the ridges, the junctions, and the asperities within the junctions. In addition, there are two characteristic times respectively associated with the growth rates of the junctions and of the real contact areas. These length and time scales are important in understanding how the Archardian-Hertzian transition drives both the large increase of friction and the reduction of the areal load index during persisting finger contacts with impermeable surfaces.

It is probable that because of the microscopic length scale of the ridge asperities, de-plasticisation takes place during intermittent contacting caused by ultrasonically vibrating surfaces employed in some tactile displays, enhancing persistence and thus contributing to a reduction in friction.

Moreover, our findings demonstrate that the growth of the contact area results from a two-step mechanism, with some correlation between the steps. The growth of A_{gross} is initially due to the recruitment of ridge apices interacting with the surface during initial loading. The second step is associated with the contributions of peripheral ridges progressively making contact with the counter-surface to form isolated junctions. With increasing load, the number, size, and connectivity of these junctions all grow simultaneously. Initially, *stratum corneum* is in a glassy state so that each junction forms a Coulombic multiple-asperity contact. With the onset of plasticisation due to the trapping of moisture in the junctions, the asperities become softer, but with a characteristic time that is significant longer than that corresponding to junction growth itself.

These findings imply that multiple asperity contact might play a key role in vibration-based tactile stimulation devices. The rendering of tactile sensation could be more realistic if the contact area and pressure distribution of the finger experiencing the device was measured to adapt the stimuli in real time against varying ambient or physiological conditions. Such corrective actions would be feasible since a few seconds are required for full plasticisation and for the formation of intimate contacts.

Texture appreciation and shape discrimination also rely on frictional dynamics since they can be expected to depend on the microscopic features of finger pads. This is because finger pads should be considered as rough surfaces at the small scales at play during short frictional interactions. In the case of an interaction with rough counter surfaces, occlusion is reduced or even absent. For example, with sufficient surface roughness, the coefficient of friction ceases to increase with contact duration [15]. Thus, if we consider a finger sliding over rough surfaces, the rough-rough contacts are likely to influence the spectral content of the vibrations generated by the contact, thus modifying the tactile experience.

Tactile interactions involving relatively short times scales are more easily accomplished if friction is small. However, precision tasks and object gripping *per se* generally require long dwell times and are facilitated by the relatively high friction induced by the plasticisation of the asperities according to the degree of roughness and permeability of the counter-surfaces.

References

[1] M. Geerligs, C. W. J. Oomens, P. A. J. Ackermans, F. P. T. Baaijens and G. W. M. Peters, "Linear shear response of the upper skin layer," *Biorheology*, vol 48, pp. 229–245, 2011.

[2] S. M. Pasumarty, S. A. Johnson, S. A. Watson and M. J. Adams, "Friction of the human finger pad: influence of moisture, occlusion and velocity," *Tribol. Lett.*, vol. 44, no. 2, pp. 117–137, 2011.

[3] J. van Kuilenburg, M. A. Masen and E. van der Heide,"The role of the skin microrelief in the contact behavior of human skin: Contact between the human finger and regular surface textures," *Tribol. Int.*, vol. 65, pp. 81–90, 2013.
[4] P. H. Warman and A. R. Ennos, "Fingerprints are unlikely to increase the friction of primate fingerpads," *J. Exp. Biol.*, vol. 212, no. 13, pp. 2016–2022, 2009.
[5] Q. Wang and V. Hayward, "In vivo biomechanics of the fingerpad skin under local tangential traction," *J. Biomech.*, vol. 40, no. 4, pp. 851–860, 2007.
[6] V. Levesque and V. Hayward, "Experimental evidence of lateral skin strain during tactile exploration," *Proc. Eurohaptics Conf.*, pp. 261–275, 2003.
[7] M. A. Srinivasan "Surface deflection of primate fingertip under line load," *J. Biomech.*, vol. 22, no. 4, pp 343–349, 1989.
[8] M. A. Srinivasan, and K. Dandekar, "An investigation of the mechanics of tactile sense using two-dimensional models of the primate fingertip," *J. Biomech. Eng.*, vol. 118, no. 1, pp. 48–55, 1996.
[9] B. Bhushan, "Contact mechanics of rough surfaces in tribology: multiple asperity contact," *Tribol. Lett.*, vol. 4, pp. 1–35, 1998.
[10] J. A. Greenwood and J. B. P. Williamson, "Contact of nominally flat surfaces," *Proc. Roy. Soc. London A*, vol. 295, pp. 300–319, 1966.
[11] A. Majumbar and B. Bhushan, "Role of fractal geometry in roughness characterization and contact mechanics of rough surfaces," *ASME J. Tribol.*, vol. 112, pp. 205–216, 1990.
[12] J. van Kuilenburg, M. A. Masen and E. van der Heide, "A review of fingerpad contact mechanics and friction and how this affects tactile perception," *Proc. IMechE, Part J*, vol. 229, no.3, pp.243–258, 2013.
[13] F. P. Bowden and D. Tabor, "Friction and Lubrication of Solids," *Oxford University Press*, London, 1954.
[14] M. J. Adams, B. J. Briscoe and S. A. Johnson, "Friction and lubrication of human skin," *Tribol. Lett.*, vol. 26, no. 3, pp. 239–253, 2007.
[15] B. M. Dzidek, M. J. Adams, Z. Zhang, S. Johnson, S. Bochereau, and V. Hayward, "Role of occlusion in non-Coulombic slip of the finger pad," *Haptics: Neuroscience, Devices, Modeling, and Applications*, Springer Berlin Heidelberg, pp. 109–116, 2014.
[16] T. H. C. Childs and B. Henson, "Human tactile perception of screen-printed surfaces: Self-report and contact mechanics experiments," *Proc. IMechE, Part J*, vol. 22, no. 3, pp. 427–441, 2007.
[17] T. Soneda and K. Nakano, "Investigation of vibrotactile sensation of human fingerpads by observation of contact zones," *Tribol. Int.*, vol. 43, no. 1, pp. 210–217, 2010.
[18] X. Liu, Z. Lu, R. Lewis, M. J. Carré and S. J. Matcher, "Feasibility of using optical coherence tomography to study the influence of skin structure on finger friction," *Tribol. Int.*, vol. 63, pp. 34–44, 2013.
[19] S. E. Tomlinson, R. Lewis, M. J. Carre and S.E. Franklin, "Human finger friction in contacts with ridged surfaces," *Wear*, vol. 301, no. 1, pp. 330–337, 2013.
[20] B. M. Dzidek, M. Adams, J. W. Andrews Z. Zhang, S. Johnson, "Contact mechanics of the human finger pad under compressive loads," in preparation, 2016.
[21] K. L. Johnson, "Contact mechanics," *Cambridge University Press*, Cambridge, UK, 1985.
[22] J. F. Archard, "Elastic deformation and the laws of friction," *Proc. Roy. Soc. London A*, vol. 243, no. 1233, pp. 190–205, 1957.
[23] C. Domeniconi, S. Tari, and P. Liang, "Direct gray scale ridge reconstruction in fingerprint images," *IEEE ICASSP*, pp. 2941–2944, 1998.
[24] A. R. Roddy, J. D. Stosz, "Fingerprint features—statistical analysis and system performance estimates," *Proc. IEEE*, vol. 85, no. 9, pp. 1390–1421, 1997.
[25] T. Watanabe and S. Fukui, "A method for controlling tactile sensation of surface roughness using ultrasonic vibration," *IEEE Int. Conf. Robotics and Automation*, vol. 1, pp. 1134–1139, 1995.
[26] M. Biet, F. Giraud, B. Lemaire-Semail, "Squeeze film effect for the design of an ultrasonic tactile plate," *IEEE Trans. Ultrason. Ferroelect. Freq. Control*, vol. 54, no. 12, pp. 2678–2688, 2007.
[27] L. Winfield, J. Glassmire, J. E. Colgate, M. Peshkin, "T-pad: Tactile pattern display through variable friction reduction," *Proc. World Haptics Conf.*, pp. 421–426, 2007.
[28] E. Vezzoli, B. M. Dzidek, T. Sednaoui, F. Giraud, M. J. Adams, B. Lemaire-Semail, "Role of fingerprint mechanics and non-Coulombic friction in ultrasonic devices," *Proc. World Haptics Conf.*, 2015.

Chapter Two

Part 2: Multiscale dynamics of the contact between a finger and a smooth surface.

Brygida Dzidek[1], Simon Johnson[2], Séréna Bochereau[3], Vincent Hayward[3], Michael Adams[1]

[1] School of Chemical Engineering, University of Birmingham, Birmingham B15 2TT, UK.

[2] Unilever R&D Port Sunlight, Bebington, Wirral CH63 3JW, UK.

[3] Sorbonne Universités, UPMC Univ Paris 06, UMR 7222, ISIR, F-75005, Paris, France.

Authors' contributions

BD and MJA designed and coordinated the study and drafted the manuscript; BD, SAJ and SB performed the experiments and conducted the data analysis; MJA and VH participated in the statistical analysis. All authors made substantial contributions to the critical revision of the submitted manuscript.

Why pens have rubbery grips

Brygida Dzidek [*], Séréna Bochereau [†], Simon A. Johnson [‡], Vincent Hayward [†], and Michael J. Adams [*]

[*]School of Engineering, University of Birmingham, Birmingham B15 2TT, UK,[†]Sorbonne Universités, UPMC Univ Paris 06, ISIR, F-75005, Paris, France, and [‡]Unilever R&D Port Sunlight, Bebington, Wirral CH63 3JW, UK

Submitted to Proceedings of the National Academy of Sciences of the United States of America

The process by which human fingers gives rise to stable contacts with smooth, hard objects is surprisingly slow. Using high-resolution imaging we found that, when pressed against glass, the actual contact made by finger pad ridges evolved over time following a first-order kinetics relationship. This evolution was the result of a two-stage coalescence process of microscopic junctions made between the keratin of the *stratum corneum* of the skin and the glass surface. This process was driven by the secretion of moisture from the sweat glands since increased hydration in *stratum corneum* caused it to become softer. Saturation was typically reached within twenty seconds of loading the contact regardless of the initial moisture state of the finger and of the normal force applied. Hence, the gross contact area, frequently used as a benchmark quantity in grip and perceptual studies, is a poor reflection of the actual contact mechanics that take place between human fingers and smooth, impermeable surfaces. In contrast, the formation of a steady state contact area is almost instantaneous if the counter surface is soft relative to keratin in a dry state. It is for this reason that elastomers are commonly employed to coat grip surfaces.

Finger friction | True contact area kinetics | Biotribology | Fingerprints

Abbreviations: PDMS, polydimethylsiloxane; FTIR, frustrated total internal reflection

Introduction

We often take it for granted that our fingers instantly bring about continuous contact when they touch smooth objects. The fingerprint marks remaining on these objects after detachment, however, are the record of a surprisingly slow process. During a period of many seconds, several phenomena take place at different length and time scales that eventually lead to a stable contact state where the flattened apices of the ridges establish a uniform contact with the counter surface. Here we observed that the so-called 'true contact area', which quantifies the amount of material in intimate contact, i.e in atomic proximity [1, 2], varies dynamically over a period of many seconds whilst the apparent, or gross, contact area, by and large, remains unchanged through time.

A knowledge of the evolution of a contact is informative because a true contact area determines the creation of friction, which is so essential to everyday life. Without a large true contact area made by our hands, it would be nearly impossible to lift a glass or to hold onto a handrail in a transport vehicle. Recent tactile display technologies depend crucially on the development of friction between a finger and a glass surface [3, 4]. Some powerful tactile illusions are the direct consequence of the differential frictional properties of surfaces across space [5] and astonishing human perceptual performance in the discrimination of materials can be explained by subtle variations in frictional properties [6]. Thus there is ample motivation for investigating the details of the formation of the true contact area by fingertips in contact with smooth surfaces.

The superficial layer of human finger pads that is in direct contact with objects, termed the *stratum corneum*, is made in a large proportion of keratin (keratinised cells), one of the most abundant structural material in animals. The keratin of the *stratum corneum* is a composite material that comprises a mix of molecules in a crystalline state and those in an amorphous state. The crystalline component is impervious to the effect of water so it can preserve its gross shape. The amorphous component, however, is avid of water and the presence or absence of water profoundly modifies its mechanical properties [7]. Dry *stratum corneum* has an elastic modulus of about 1 GPa but this value can be reduced by approximatively four orders-of-magnitude when it is saturated with water [8]. In the wet state, *stratum corneum* can yield 150% of its original length at almost constant stress, giving it plasticity [9].

The macroscopic geometry of the finger pad, which is characterised by ridges and valleys that compress, decompress, and stretch during interactions with surfaces, undergoes considerable gross deformation even for moderate contact loads [10]. The surface of the ridges exhibit roughly cylindrical cross sections and are separated by valleys [8]. They form loops, whorls, or arch patterns that are unique to each individual. The evolution of the apparent area of contact arising from the deformation of a finger pad has been examined using optical imaging during incipient slip [11], at different force levels [12, 13], at different moisture contents [14] and tangential loads leading to slip [15], under rotation and lateral sliding movements over flat, raised or indented glass surfaces [10], during stick-to-slip transitions in distal, proximal, radial and ulnar directions [16], over complete stick-to-slip epochs [17], and under the effects of oscillating loads [18, 19].

Previous studies considered the area of a finger pad contact macroscopically. A contact was typically described by an apparent, or gross area, and then by excluding the interstitial spaces between the ridges in an effort to better approximate the true contact area. Thus, the total contact area made by the ridges compared to the gross area would quantify their

Significance

Why does gripping a pen, tool or handle feel more secure when it is coated with a rubbery material? The keratin of the outer layer of the skin is stiff and rough at a small scale. When encountering a smooth, stiff, and impermeable surface such as shiny plastic, polished metal or glass, the actual contact area is initially small and hence so is the friction. Because the keratin softens slowly when it is hydrated by the moisture secreted from the sweat pores, it requires many seconds for the contact area to increase to the value reached almost instantaneously with a soft material such as a rubber. This mechanism might also be used by our tactile sense to identify materials and has implications for the design of tactile displays.

Reserved for Publication Footnotes

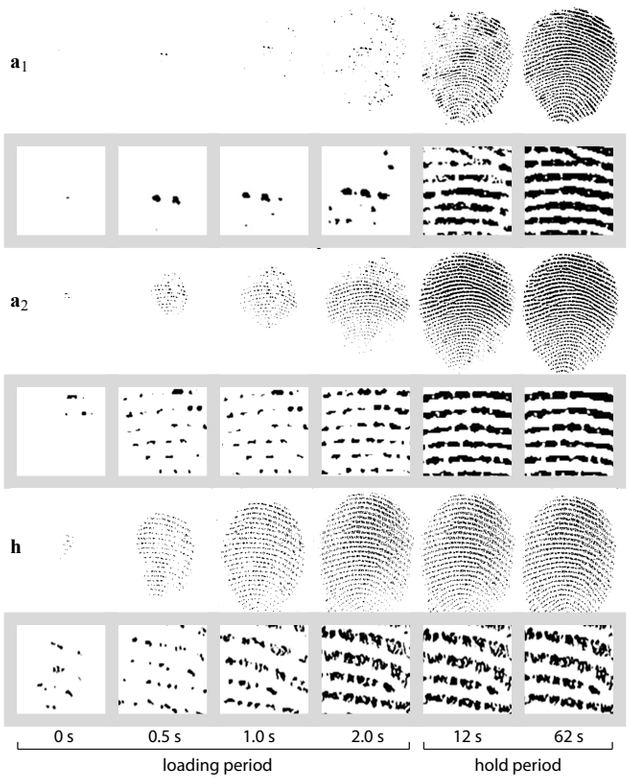

Fig. 1. Temporal evolution of the contact area on a glass surface for participant A corresponding to trials $\mathbf{a}_1$ and $\mathbf{a}_2$ (see Table 1). Each row is associated with framed enlarged image portions depicting the creation, growth, and coalescence of regions of the junction area. The last two rows show the contact evolution on a PDMS surface under similar conditions for participant B; data set **h**.

overall deformation since these two values would coincide if the ridges were completely deformed.

The ridges themselves are far from being smooth and exhibit small-scale topographical features. In a recent study, [20] the effect of these features could be, for the first time, observed directly. They initially yielded few unconnected regions within the ridge contacts. The summed areas of these regions, which were described as junctions, corresponded to a total area denoted, A_{junct}. The total junction contact area was observed to grow for many seconds during the holding period following a loading event, while the gross and ridge areas, A_{gross} and A_{ridge} respectively, remained unchanged [20]. This growth was the result of a two-step coalescence process such that the number of junctions, N, first increased, followed by their expansion that led to a rise in connectivity. It was surmised that this process was the result of an occlusion mechanism such that the *stratum corneum* became gradually plasticised under the action of moisture secreted from the many sweat pores located in the ridges. This phenomenon could explain the first-order growth kinetics exhibited by the coefficient of friction [2].

We investigated this newly discovered phenomenon in greater detail by characterising the influence of the loading forces and the loading rate on its time course. The present study provides a basis for establishing a robust description of the evolution of the contact area for steady pressing conditions associated with everyday interactions involving smooth surfaces. The results are contrasted with the case of a contact of a finger pad with an elastomer. With such a counter surface, the kinetics of contact formation exhibit a drastically different behaviour since its relative softness allows a steady state contact to be reached almost instantaneously.

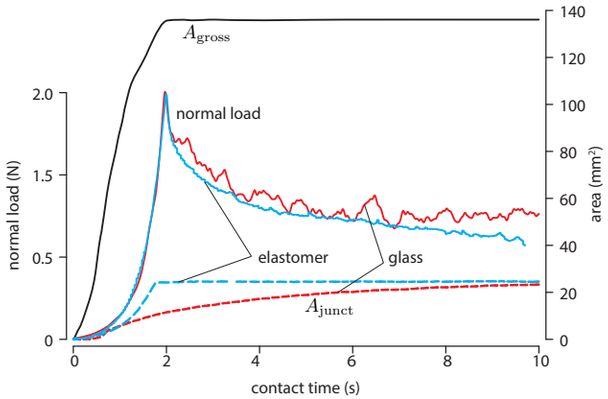

Fig. 2. Typical evolution of the load force, A_{gross} and A_{junct} as a function of contact time for a glass (red) and for an elastomer (blue) counter surface. The evolution of A_{gross} does not depend on the material.

The observed contact evolutions during interactions with solid surfaces is a tribute to the ability of the human nervous system to secure stable grips and to achieve tactile perceptual constancy despite the extensive variations in detailed contact mechanics through time during finger contact with objects. They also have important implications for the design of touch screens with haptic feedback that rely on the modulation of friction to provide computer-controlled sensations.

Results

Fingerprint images for two participants were obtained using the technique of Frustrated Total Internal Reflection (*Methods*). The washed and dried pads of their index fingers were slowly pressed against the face of a prism until reaching a maximum normal loading force. The fingers were then held in a fixed isometric condition for 60 s once the maximum normal load was reached. Testing conditions differed by rate of compression, maximum normal load, counter surface material, and participant. Binary images obtained after enhancement and thresholding (*Methods*) are exemplified in Fig. 1 for different instants after the initial contact. Enlarged image portions more clearly show how the junctions evolved with time. Figures 2 and 3 show the results of an automated image analysis procedure performed at high resolution (*Methods*).

Conditions. There were eight testing conditions labeled from **a** to **h** listed in Table 1. Condition **h** corresponded to the finger of participant B pressing against a sheet of PDMS, a silicone-based transparent elastomer (*Methods*). Trials carried out with a same finger tested twice under the same condition have subscripts 1 and 2. Compression rates were 0.5, 1.0, or 2.0 mm s^{-1} and the maximum normal forces were 1.0 or 2.0 N. The time $t_{\max}$ was the time at which the maximum normal force was reached and A_{E} represented the relative contact area at the end of the hold period computed as A_{junct} normalised by A_{gross}. Fourteen data sets, see Table 1, were successfully acquired with very low likelihood that accidental lateral slips of the finger took place during imaging (*Methods*).

Junction area kinetics. Figure 2 shows the typical evolution of A_{junct} as a function of contact time with glass. During the loading period, the value of A_{gross} increased to a maximum while the value of A_{junct} increased during the loading and the

Table 1. Experimental protocol loading parameters. Subscripts in trial labels indicate repeated conditions. Results show the values of the best fit parameters to first-order kinetics [1]. Missing values indicate the absence of a good fit.

	conditions				results				
trials	rate ($\mathrm{mm\,s^{-1}}$)	load (N)	participant	material	A_0 ($\mathrm{mm^2}$)	A_∞ ($\mathrm{mm^2}$)	λ (s)	$t_{\max}$ (s)	A_E ($t = 60\,\mathrm{s}$)
$\mathbf{a}_1$	1.0	2.0	A	glass	3.7 ± 0.2	39.5 ± 0.2	16.5 ± 0.3	2.2	0.39
$\mathbf{a}_2$	1.0	2.0			20.9 ± 0.6	38.4 ± 0.2	5.5 ± 0.4	2.8	0.35
$\mathbf{b}_1$	1.0	3.0			19.5 ± 0.5	35.5 ± 0.1	3.2 ± 0.2	2.2	0.37
$\mathbf{b}_2$	1.0	3.0			29.5	–	–	2.4	0.39
$\mathbf{c}_1$	2.0	2.0			4.0 ± 0.9	29.3 ± 1.9	27.0 ± 3.1	1.2	0.30
$\mathbf{c}_2$	2.0	2.0			4.3 ± 0.2	30.9 ± 0.2	11.2 ± 0.3	1.0	0.31
$\mathbf{d}_1$	0.5	2.0	B	glass	0.7	–	–	3.4	0.01
$\mathbf{d}_2$	0.5	2.0			1.9	–	–	3.3	0.09
$\mathbf{e}_1$	1.0	2.0			7.4 ± 0.4	26.7 ± 0.4	16.2 ± 1.1	1.4	0.27
$\mathbf{e}_2$	1.0	2.0			15.0 ± 0.6	38.6 ± 0.5	15.6 ± 1.3	1.7	0.37
$\mathbf{f}_1$	1.0	3.0			2.6	–	–	1.7	0.17
$\mathbf{f}_2$	1.0	3.0			9.3 ± 0.4	29.1 ± 0.4	16.0 ± 0.1	1.8	0.25
$\mathbf{g}$	2.0	2.0			8.0 ± 0.7	28.2 ± 0.3	9.5 ± 0.8	0.8	0.28
$\mathbf{h}$	1.0	2.0	B	PDMS	25.0	25.0	< 0.04	2.4	0.38

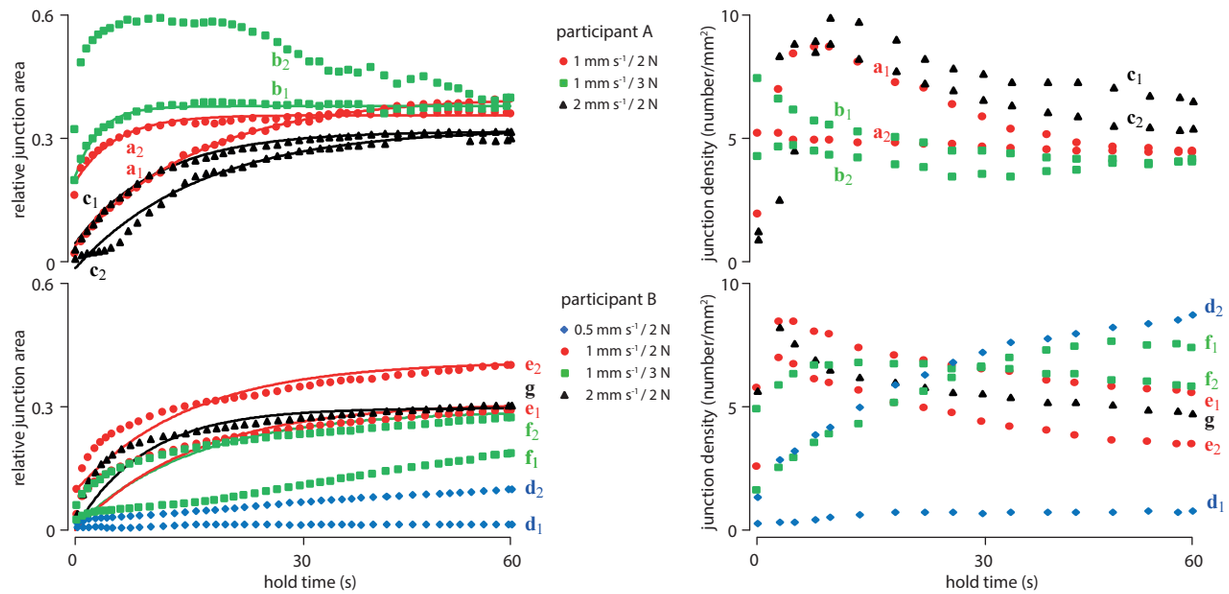

Fig. 3. Evolution of the relative junction area $A_\mathrm{E} = A_\mathrm{junct}/A_\mathrm{gross}$ and of the junction density, N/A_gross, as a function of hold time in contact with glass for participants A and B and for a range of loading rates and applied loads. Solid lines show first-order kinetics best fits.

hold periods. During the hold period at constant compression, the normal force relaxed to less than half its initial value because of the viscoelastic properties of finger tissues [21].

Figure 3 shows the temporal evolution of A_E and of the junction density, N/A_gross, as a function of the hold time, t, for the fourteen trials. With the exception of trials $\mathbf{d}_1$, $\mathbf{d}_2$, $\mathbf{f}_1$, and $\mathbf{b}_2$, A_junct increased relative to A_gross at a decreasing rate such that the data could be adequately described by a first-order kinetics equation,

$$A_\mathrm{junct}(t) = A_\infty + (A_0 - A_\infty)\exp\left(-\frac{t}{\lambda}\right), \qquad [1]$$

where λ is the characteristic time and where the subscripts 0 and ∞ refer to the values of A_junct at times $t = 0$ and $t \to \infty$.

Junction area and junction density kinetics. Fitting the parameters A_∞, A_0, and λ of [1] to the data gave the values indicated in Table 1. The smallest value of the coefficient of determination, R^2, was 0.93. In many cases, the junction density increased to a maximum value during the loading period and then gradually decreases to a stable value. For trials $\mathbf{d}_1$ and $\mathbf{d}_2$, however, the junction density continued to increase during the whole contact period. For the finger pressing against the elastomer surface the evolution of the effective contact area, A_E, was so rapid that the kinetics could not be observed. As a result, A_E closely tracked the evolution of the normal load, reaching its ultimate value once the load ceased to increase.

Discussion

Variability. Despite highly controlled testing conditions, there were very large differences in the evolution of the junction contact area between a fingertip and a hard smooth surface, such as glass. During trial $\mathbf{b}_2$, the normalised contact area, A_E, exhibited a large maximum value 10 s after the onset of the hold period, before decreasing to a steady value. The junction density increased during the loading period and then decreases to a stable value toward the end of the hold period.

For most trials, the evolution of the junction area followed a first-order kinetics relationship, the junction density tended to increase during the loading period and to decrease to a steady value near the end of the hold period. For some trials ($\mathbf{f}_1$, $\mathbf{d}_1$, $\mathbf{d}_2$), however, the effective contact area increased in a manner that could not be described by [**1**].

Role of plasticisation. During the loading period, A_{junct} and N naturally increased. The subsequent behaviour of these values during the hold period, however, depended on other factors than time, chief among them is the extent to which the *stratum corneum* became plasticised. Plasticisation, which is linked to a decrease of the elastic modulus, is caused by hydration and thus depends on pre-existing moisture before contact and on the rate of secretion of sweat from the pores.

For most trials, the reduction in the junction density during the hold period reflected the slow progress of a coalescence process until complete segments became connected. The changes occurred gradually over the hold period which suggests that the coalescence process was governed by the rate of transport of sweat from the pores and by subsequent diffusion into the *stratum corneum* layer. The eventual reduction of the junction contact area for trial $\mathbf{b}_2$ suggests that in this case the finger had a high initial level of hydration followed by evaporation of water within the interstitial ridge valleys.

Trial $\mathbf{d}_1$ is an example of a finger that was very dry, both at the onset of contact and subsequently, as can be seen from the very slow rise in the true contact area and in the junction density. It is nevertheless possible that microscopic junctions actually existed but were too small to be resolved.

Trials $\mathbf{d}_2$ and $\mathbf{f}_1$ corresponded to fingers that were relatively dry but the fact that the contact areas increased with the hold time suggests that the *stratum corneum* was more hydrated than in the case of $\mathbf{d}_1$. Moreover, these trials exhibited a continuous increase in the junction density that must have corresponded to junctions gradually being formed as a result of occlusion, but with insufficient moisture softening for junction coalescence to take place.

In complete contrast, variability was absent for the trials where a finger pressed onto an elastomeric counter surface, regardless of the state of hydration of the finger. This occurence is exemplified by trial **h**. The junction area growth kinetics was so rapid that it could not be resolved by our apparatus.

Contact mechanics. As shown in Fig. 1, throughout the evolution of a finger contact against glass, the width of the junctions and of the ridge apices tended to be greater towards the centre of the contact area than in the periphery. These differences can be understood by applying Hertz theory at two different length scales, one at the scale of the whole finger and the other at the scale of individual ridges [8]. The images of the finger print ridges (see also, Fig. 4a) thus were generally less dense towards the periphery, which is consistent with a decrease of the Hertzian contact pressure. While it is not possible to distinguish between the effects of very narrow gaps and partial contact arising from surface roughness, *in vivo* confocal Raman spectroscopy of skin suggests that it is unlikely that the contacts observed optically involve thin moisture or air films [22].

The sweat pores caused small regions to remain without contact (white regions in Fig. 1). Thus, even for fully connected ridges, A_{true} was always smaller than A_{ridge}.

Tribology. The adhesion model of friction [23, 24], which has been shown to be applicable to the *stratum corneum* [27, 28], states that the frictional force, f_{f}, depends on the product of the interfacial shear strength, τ, and the true area of contact, A_{true}, which is reflected by A_{junct}. The true area of contact measures the amount of intimate, friction-generating contact. Such contacts have transient molecular junctions at the sliding interface.

The frictional force is the work done per unit of sliding distance required to rupture those junctions that transmit stress across the sliding interface and cause sub-surface inelastic deformation to a depth of about 100 nm [25]. For glassy polymers, the interfacial stress, determined by τ, has been related to surface yielding with values of 1 to 10 MPa that are about an order of magnitude smaller than those in the bulk since surface polymer chains have greater freedom to align with the sliding direction [25]. Plasticisation by water of hydrophilic polymers such as nylon is known to cause a reduction in τ in a similar way to that observed for the bulk yield stress [26].

Human fingerprint ridges are decorated with very small-scale surface topographical features that correspond to the asperities of rough surfaces. When compressed, the *stratum corneum* is initially stiff and the deformation of the asperities is limited. The increase in the area of existing junctions or ridges, and the consequent formation of new asperity contacts with increasing applied normal load, w, is the origin of Coulomb's law, $f_{\text{f}} = \mu w$ where μ is the coefficient of friction. With time, the asperities become compliant because of the plasticisation by moisture and A_{true} increases. It is reasonable to believe that the *stratum corneum* behaves like nylon such that, concomitantly, the value of τ decreases as a result of the plasticisation. We can model this process by writing, $f_{\text{f}} = \tau(t)A_{\text{true}} = \tau(t)\phi(t)A_{\text{junct}}(t \to \infty)$, where $A_{\text{junct}}(t \to \infty)$ is the steady state contact area of the junctions, including those that have coalesced to form whole ridge segments. The scalar quantity, $\phi(t)$, varies between zero just before contact and unity at long times, once asperity junctions no longer grow in size and number.

Sliding on impermeable, hard surfaces. We observed previously that the value of μ for a finger pad sliding on a smooth glass surface also increased with the contact time because the increase in A_{true} is greater than the decrease in τ [20]. The value of μ can increase by up to an order of magnitude for small normal loads and its evolution at a constant normal load can be described by a first-order kinetics relationship with a characteristic time of up to 20 s [29]. Thus it is probable that $\phi(t)$ generally exhibits a similar behaviour but a technique able to reliably measure A_{true} for rough surfaces has yet to developed. We also previously reported that with increasing contact time, the friction of a finger pad gradually changes from Coulombic to a nonlinear dependence on a normal load, in a manner that is typical of elastomers, when the asperities are sufficiently compliant to flatten under the applied load [29]. This phenomenon is a direct result of a glassy-rubbery transition of the *stratum corneum* due to the moisture-driven plasticisation. Thus, in the fully occluded state, $A_{\text{true}} \approx A_{\text{junct}}$.

Sliding on soft surfaces. The surprisingly slow formation of a true contact between a finger pad and a hard, smooth, and impermeable surface, such as glass, may be contrasted with the case of a counter surface made of a compliant material, such as a rubber or an elastomer (e.g. PDMS), as further illustrated by the 'true contact' images in Fig. 4a that were acquired with the same finger tested under similar conditions but with a different material. Figure 4b shows the evolution of the coefficient of friction, μ, when a finger pad slid on a smooth elastomeric surface (PDMS: Young's elastic modulus $E = 2.3$ MPa; estimated Young's elastic modulus of keratin: $E \approx 1$ GPa in a dry state) and on a glass surface. For PDMS, the coefficient of friction was nearly constant throughout the contact time, while a first-order kinetic relationship of the form of [**1**] could be successfully fitted in the case of a glass surface.

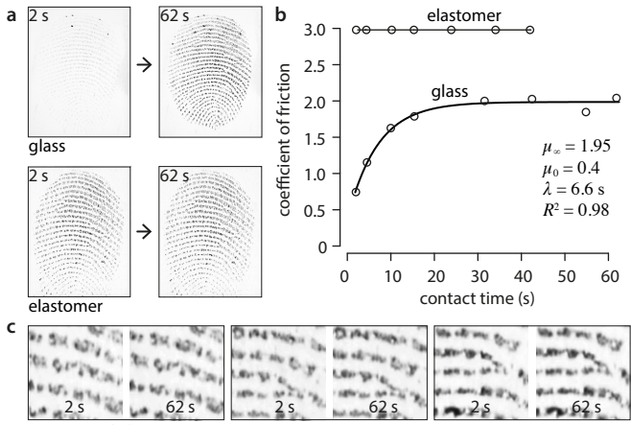

Fig. 4. (**a**) Contrasted kinetics of contact formation for a peak compression of 2 N, showing images at the beginning and end of the subsequent hold period. (**b**) Time course of the evolution of friction for a finger sliding on an elastomeric surface or on a glass surface (fitted to a first-order kinetic relationship) at a velocity of 0.02 m s^{-1} and under a load of 0.2 N.

The greyscale images in Fig. 4a show a few dark spots that may be ascribed to the presence of water droplets. This possibility raises the concern that our analysis of the true contact area may have been be confounded by the occurence of water bridges in interstitial spaces that would cause an overestimation of the true contact area. The presence of water, however, could not explain the increase of the coefficient by a factor five over a period of 20 s as shown by Fig 4b. Moreover, free moisture would be expected to lead to a reduction of the friction.

Implications for the motor and the perceptual functions of touch. The dramatic differences in true contact formation kinetics according to the material properties and to the microtopology of the counter surface has obvious implications for motor behaviour. We intuitively feel that elastic rubbery surfaces, even if they are only thin coatings, provide us with a better grip than hard and smooth surfaces. Conversely, the kinematic and tonic motor behaviour required to explore surfaces is crucially dependent on the nature of these surfaces. Push too hard on a surface made of a compliant material and the finger will become stuck. Conversely, clean glass surfaces will remain slippery within the first ten seconds of contact regardless of their topology, especially in dry ambient conditions. Each of these cases requires fine and flexible motor control strategies for the successful completion of motor or perceptual tasks. The kinetics of true contact formation are also likely to be impacted by the hydrophobicity of the material of the counter surface. In fact, we have recently shown that people can discriminate materials by touch on the sole basis of hydrophobicity differences [6]. We thus can tentatively suggest that the contact formation kinetics divide the tactile world into broad categories of materials: smooth and impermeable surfaces that could be subdivided into those that are hard (glass, glazings, polished metals) or those that are softer than keratin (rubbers, certain polymers); rough surfaces can also be divided into those that are made of relatively hard and soft materials; and porous surfaces (paper, wood, fabrics) that further modify the kinetics of contact formation together with hydrophobicity. For example, it has been observed that for filter paper the friction, and hence A_{true}, reduces with the contact time since the secreted sweat is absorbed, leading to reduction in the compliance of the keratin [2]. It can therefore be argued that each of these factors potentially convey reliable tactile information to the brain pertaining to the nature of the touched objects during tactile exploration.

Implications for tactile displays relying on friction. The modulation of friction by the application of ultrasonic vibration or by electrostatic adhesion is a leading technological option for flat screen haptic displays [30, 31]. They rely on the ability to reduce or augment the overall friction of the screen. The illusion of a ridge [32] may be created by rapidly increasing friction during the exploration by a finger as a result of decreasing the amplitude of vibration or increasing the electrostatic field [3]. The strength and stability of this effect is dependent on the contrast in friction that can be induced, which has critical implications for power requirements [33, 34]. The drastic variations of the evolution of A_{junct} with contact time as was observed here for just two participants in a single day is indicative of the variations that might typically be expected for the corresponding intrinsic friction of touch screens. This variation extends to the increase in μ with time while the data for the glass in Fig. 4b correspond to an increase of about a factor of five. Our findings are indeed consistent with the variations in reported values of the coefficient of friction that are reported in the literature [2, 35, 36]. Thus if the intrinsic friction between a finger pad and screen is small, greater vibrational amplitudes or greater electrostatic voltage swings will be required. Clearly, our findings present a significant challenge to the design of haptic interfaces based on friction modulation in terms of maintaining acceptable fidelity without excessive power requirements.

Materials and Methods

Data Acquisition. The experimental platform used to measure the time evolution of the contact area under an applied normal load is shown schematically Fig. 5a. High contrast images can be obtained directly using the FTIR technique and thus be rendered in a variety of ways other than binary images. An example is shown in Fig. 5b.

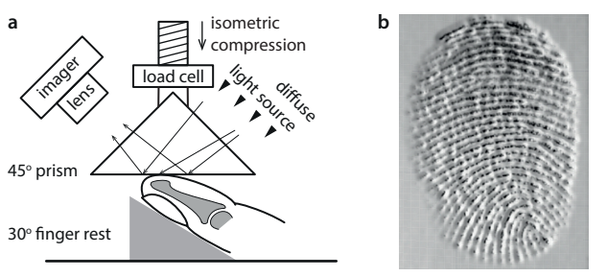

Fig. 5. (**a**) Schematic diagram of the FTIR technique employed to measure the contact area between a finger pad and a glass prism. Light rays are entirely reflected unless there is intimate contact resulting in a dark image against a light background. (**b**) 3D grey-scale rendering of a finger print image.

The left index finger of two female volunteers (27 and 26 years old), who gave informed consent and who are denoted as participants A and B, was inclined at angle of 30° with the finger pad facing upwards. A flat glass prism was pressed down onto the finger pad in order to induce frustrated total internal reflection, while the contact area increased by the applied load. For the elastomer contact studies, a smooth transparent block of PDMS (Sylgard 184) was adhered to the lower rectangular face of the prism. Initially, the fingers were washed with commercial soap, rinsed with distilled water and allowed to dry for 10 min until an equilibrated clean skin state was achieved.

The rear face of the prism was backlit uniformly by reflecting light from a fibre-optic lamp with a diffusely reflecting white surface. The contact was imaged through the front face of the prism using a Nikon D5300 camera with a video resolution of 1920 x 1080 pixels at 25 fps and a shutter speed of 1/160 s. The camera was fitted with a macro lens and a small aperture was used to achieve the depth of field necessitated by oblique viewing. It was fixed to the moving crosshead of the machine and focused on the centre of the lower prism surface.

The images obtained were high-contrast patterns of dark ridges where the light was scattered into a bright background where the light was completely reflected. The compression of the finger pad was conducted at rates of 0.5, 1, and 2 mm s^{-1} until a load of 2 or 3 N was reached (the testing parameters for each participant are listed in Table 1). The prism was attached to a Universal Materials Testing Machine (model no. 5566, ex Instron, UK) via a 10 N transducer. The displacement of the prism was then maintained for 60 s before unloading the contact at the same rate. The compressive force and displacement data were recorded at 500 Hz. To ensure that accidental slip did not take place during imaging, additionally image and force data analysis was performed. Any such slip would have been indicated by abrupt changes in the evolution of the number of junctions and in the normal load. All measurements apart from those associated with Fig. 4a were carried out in a single day and in an environmentally controlled laboratory set to 20°C and 50% relative humidity.

Image processing. Using the ImageJ software [37], image analysis was carried out to determine A_{junct} as a function of the contact duration. Grey scale (8-bit) conversion and analysis was applied. The converted images were adjusted to the level of contrast and brightness that allowed for optimal pattern recognition. Typical methods were adopted for automatic fingerprint feature extraction [38] and followed a sequence of steps comprising: image enhancement, binarisation, thinning, extraction, and post-processing. It was possible to exclude the sweat pores and to determine the size and evolution of each feature by segmenting the image into features of interest from the background under each relevant condition by use of a mask function. To estimate A_{junct} a threshold of the grey scale value was determined from the histogram ($> 75\%$ saturation of the pixel intensities), that allowed the boundaries of the contact junctions to be delineated. The boundary of each junction excluded sweat pores at the edge of the contact region but it was not possible to exclude automatically those that were internal to the boundaries. It was estimated that the overestimation of the contact area was $< 5\%$ since such internal sweat pores represented a relatively small proportion of the total contact area particularly because they were only present in the central region of the fingerprint image.

ACKNOWLEDGMENTS.
This study was funded by the FP7 Marie Curie Initial Training Network PROTOTOUCH, grant agreement No. 317100. It was also supported by the European Research Council (FP7) ERC Advanced Grant (PATCH) to V.H. grant agreement No. 247300.

1. Dyson J & Hirst W (1954) The true contact area between solids. Proc Phys Soc B 67:309–312.
2. Pasumarty SM, Johnson SA, Watson SA, Adams MJ (2011) Friction of the human finger pad: influence of moisture, occlusion and velocity. Tribol Lett 44:117–137.
3. Vezzoli E, Messaoud WB, Amberg M, Giraud F, Lemaire-Semail B, Bueno MA (2015) Physical and perceptual independence of ultrasonic vibration and electrovibration for friction modulation. IEEE Trans Haptics 8:235–239.
4. Wiertlewski M, Friesen RF, Colgate JE (2016) Partial squeeze film levitation modulates fingertip friction. Proc Natl Acad Sci U S A 113:9210–9215.
5. Nakatani M, Howe RD, Tachi S (2011) Surface texture can bias tactile form perception. Exp Brain Res 208:151–156.
6. Gueorguiev D, Bochereau S, Mouraux A, Hayward V, Thonnard JL (2016) Touch uses frictional cues to discriminate flat materials. Sci Rep 6:25553.
7. McKittrick J, Chen PY, Bodde SG, Yang W, Novitskaya EE, Meyers MA (2012) The structure, functions, and mechanical properties of keratin. JOM 64:449–445.
8. Dzidek BM, Adams MJ, Andrews JW, Zhang Z, Johnson SA (2017) Contact mechanics of the human finger pad under compressive loads. J R Soc Interface 14(127):20160935.
9. Wildnauer RH, Bothwell JW, Douglass AB (1971) Stratum corneum biomechanical properties, I. Influence of relative humidity on normal and extracted human stratum corneum. J Invest Dermatol 56:72–78.
10. Lévesque V, Hayward, V (2003) Experimental evidence of lateral skin strain during tactile exploration. EuroHaptics pp 261–275.
11. Tada M, Mochimaru M, Kanade, T (2006) How does a fingertip slip?—visualizing partial slippage for modeling of contact mechanics. EuroHaptics pp 415–420.
12. Warman PH, Ennos AR (2009) Fingerprints are unlikely to increase the friction of primate fingerpads. J Exp Biol 212:2015–2021.
13. Adams MJ, Johnson SA, Lefèvre P, Lévesque V, Hayward V., André T, Thonnard, JL (2013) Finger pad friction and its role in grip and touch. J R Soc Interface 10(80):20120467.
14. André T, Lefèvre P, Thonnard JL (2009) A continuous measure of fingertip friction during precision grip. J Neurosci Methods 179:224–229.
15. André T, Levèsque V, Hayward V, Lefèvre P, Thonnard JL (2011) Effect of skin hydration on the dynamics of fingertip gripping contact. J R Soc Interface 8(64):1574–1583.
16. Delhaye B, Lefèvre P, Thonnard JL (2014) Dynamics of fingertip contact during the onset of tangential slip. J R Soc Interface 11(100):20140698.
17. Terekhov AV, Hayward, V (2011) Minimal adhesion surface area in tangentially loaded digital contacts. J Biomech 44(13):2508–2510.
18. Soneda T, Nakano K (2010) Investigation of vibrotactile sensation of human finger pads by observation of contact zones. Tribol Int 43:210–217.
19. Bochereau S, Dzidek B, Adams MJ, Hayward V (2017) Characterizing and imaging gross and real finger contacts under dynamic loading. IEEE Trans Haptics in press.
20. Dzidek BM, Bochereau S, Johnson SA, Hayward V, Adams MJ (2016) Frictional dynamics of finger pads are governed by four length-scales and two time-scales. Haptics Symposium pp 161–166.
21. Pawluk DTV, Howe RD (1999) Dynamic contact of the human fingerpad against a flat surface. J Biomech Eng 121:605–611.
22. Dąbrowska AK, Adlhart C, Spano F, Rotaru GM, Derler S, Zhai L, Spencer ND, Rossi RM (2016) In vivo confirmation of hydration-induced changes in human-skin thickness, roughness and interaction with the environment. Biointerphases 11:031015.
23. Amuzu JKA, Briscoe BJ, Tabor D (1977) Friction and shear strength of polymers. ASLE Trans 20(4):354–358.
24. Briscoe BJ, Arvanitaki A, Adams MJ, Johnson SA (2001) The friction and adhesion of elastomers. Tribol Series 39:661–672.
25. Briscoe BJ, Smith AC. (1981) Polymer friction and polymer yield: a comparison. Polymer. 22:1587–1589.
26. Cohen SC, Tabor D. (1966) The friction and lubrication of polymers. Proc. Roy. Soc. Lond. A 291: 186–207.
27. Johnson SA, Gorman DM, Adams MJ, Briscoe BJ (1993) The friction and lubrication of human stratum corneum. Tribol Series 25:663–672.
28. Adams MJ, Briscoe BJ, Johnson SA (2007) Friction and lubrication of the human skin. Tribol Lett 26:239–253.
29. Dzidek BM, Adams MJ, Zhang Z, Johnson SA, Bochereau S, Hayward, V (2014) Role of occlusion in non-Coulombic slip of the finger pad. Haptics: Neuroscience, Devices, Modeling, and Applications pp 109-116.
30. Giraud F, Amberg M, Lemaire-Semail B, Casiez G (2012) Design of a transparent tactile stimulator. Symposium on Haptic Interfaces For Virtual Environment And Teleoperator Systems pp 485–489.
31. Meyer D, Peshkin M, Colgate JE (2013) Fingertip friction modulation due to electrostatic attraction. World Haptics Conference pp 43–48.
32. Robles De La Torre G, Hayward V (2001) Force can overcome object geometry in the perception of shape through active touch. Nature 412(6845):445–448.
33. Vezzoli E, Vidrih Z, Giamundo V, Lemaire-Semail B, Giraud F, Rodic T, Peric D, Adams M Friction reduction through ultrasonic vibration part 1: modelling intermittent contact. IEEE Trans Haptics in press.
34. Sednaoui T, Vezzoli E, Dzidek B, Lemaire-Semail B, Chappaz C, Adams M Friction reduction through ultrasonic vibration part 2: experimental evaluation of intermittent contact and squeeze film levitation. IEEE Trans. Haptics in press.
35. Derler S, Rotaru GM (2013) Stick-slip phenomena in the friction of human skin. Wear 301:324–329.
36. Urbakh M, Klafter J, Gourdon D, Israelachvili J (2004) The nonlinear nature of friction. Nature, 430(6999):525-528.
37. https://imagej.net
38. Domeniconi C, Tari S, Liang P (1998) Direct gray scale ridge reconstruction in fingerprint images. IEEE Int. Conf. Acoustics Speech and Signal Processing pp V-2941.

Chapter Three

Part 1: Experimental evaluation of friction reduction in ultrasonic devices.

Thomas Sednaoui[1], Eric Vezzoli[2], Brygida Dzidek[3], Betty Lemaire-Semail[2], Cedrick Chappaz[1], Michael Adams[3]

[1] L2EP-IRCICA and STMicroelectronics, Crolles F38920, France

[2] L2EP-IRCICA Laboratory, University of Lille 1, Lille, France

[3] School of Chemical Engineering, University of Birmingham, Birmingham B15 2TT, UK

Authors' contributions

TS, EV and BD designed and coordinated the study and drafted the manuscript; BD, TS and EV performed the experiments and conducted the data analysis; MJA, BLS and CC participated in the statistical analysis. All authors made substantial contributions to the critical revision of the submitted manuscript.

Experimental Evaluation of Friction Reduction in Ultrasonic Devices

Conference Paper · June 2015

DOI: 10.1109/WHC.2015.7177688

6 authors, including:

Thomas Sednaoui
STMicroelectronics
6 PUBLICATIONS **18** CITATIONS
SEE PROFILE

Eric Vezzoli
GoTouchVR
18 PUBLICATIONS **39** CITATIONS
SEE PROFILE

Brygida Dzidek
University of Birmingham
5 PUBLICATIONS **19** CITATIONS
SEE PROFILE

Michael J Adams
University of Birmingham
58 PUBLICATIONS **1,093** CITATIONS
SEE PROFILE

Experimental Evaluation of Friction Reduction in Ultrasonic Devices

Thomas Sednaoui, Eric Vezzoli, Brigida Dzidek, Betty Lemaire-Semail, *Member, IEEE*, Cedrick Chappaz, and Michael Adams

***Abstract*—Previously proposed models of the ultrasonic lubrication of a finger mediated by flat surfaces are not consistent with the experimental results for vibrational amplitudes greater than a few microns. This paper presents experimental data acquired through a dedicated tribometer and proposes an experimental model of ultrasonic lubrication at high vibrational amplitudes.**

I. Introduction

The last few years have seen the emergence of ubiquitous mobile devices and tactile interfaces. The abundance of these novel interfaces raised the interest in touch based human-machine interactions and the lack of natural touch feedback. The problem was partly responsible for the slow adoption of the technology among consumers. Currently, multiple solutions are being explored to deliver improved haptic feedback on existing mobile platforms such as smartphones or tablets; one such feedback technology, vibrotactile stimulation, is already incorporated on most platforms but provides only a general vibration sensation to the hand and finger of users [1]. To improve upon this, tactile based solutions have been proposed in recent years such as electrovibration [2] and Ultrasonic Lubrication (UL) [3] [4].

The physics underlying electrovibration is well understood [5], but it is not the case for UL mediated by a flat surface. It has been proposed that this technology is able to reduce the perceived coefficient of friction of the user by creating a thin film of air between the finger and plate. The first attempts of modeling haptic UL were made by Watanabe and Fukui in a paper describing the potential usefulness of friction reduction for haptic rendering [6]. The proposed model, which was derived from the Reynolds equations, is based on the squeeze film effect and is thought to be the main contributor to the reduction of friction between a finger and a flat surface.

Since the finger parameters (such as rigidity, roughness and humidity) can be extremely variable between subjects, it is difficult to estimate the actual area of contact between the fingerprint and the surface. This makes any calculation of the squeeze force subject to many simplifications. Moreover, an exhaustive measurement of finger UL has not been conducted in order to validate the proposed model across a range of users and usage parameters.

The current paper demonstrates that the measured friction reduction between a finger pad and a flat surface subjected to ultrasonic vibration does not behave as predicted by the squeeze film effect only. Specifically, the friction reduction phenomenon approaches a lower limit with increasing amplitude of vibration, which is not predicted by the squeeze film model. Moreover, the lower limit corresponds to a coefficient of friction that is too large for persistent acoustic levitation. An experimental model from the measurements is proposed in order to simplify the design of future tactile stimulators.

II. Squeeze Film Model

This section describes succinctly the analytic model of acoustic levitation usually applied to haptic feedback through the squeeze film effect. As previously theorized in [6] and [7], the vibration of a surface under a finger pad of a user generates an ultra-thin film of air (air gap) in the contact region. Figure 1 shows a simplified geometry of the film of air. The film is subject to compression and rarefaction at high frequencies corresponding to the relative displacement of the surfaces.

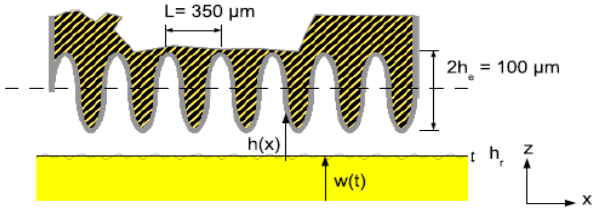

Figure 1: Approximation of the finger pad ridges.

The ridges of the finger pad are approximated by a cosine function and are considered to be rigid, or at least extremely stiff, at these frequencies. With h_{vib} being the amplitude of vibration and h_r the surface roughness, the thickness of the film can then be expressed by:

$$h(x,t) = h_r + h_{vib}[1+\cos(\omega t)] + h_e\left[1+\cos\left(\frac{2\pi}{L}x\right)\right] \quad (1)$$

where the pulsation of the vibrating plate is given by ω. The relationship between the thickness, h , of the air-gap and the pressure, p, can be described by the Reynolds equations [16]:

* This work was funded by the European Union under the FP7 programs FP7-PEOPLE-317100 PROTOTOUCH.

T. Sednaoui and C. Chappaz are with L2EP-IRCICA and STMicroelectronics, Crolles F38920, France (e-mail: thomas.sednaoui@st.com, cedrick.chappaz@st.com).

E. Vezzoli and B. Lemaire-Semail are with L2EP-IRCICA Laboratory, University of Lille 1, Lille, France, 59650 (phone: +33 362531632; e-mail: eric.vezzoli@ed.univ-lille1.fr, betty.semail@polytech-lille.fr).

B. Dzidek and M. Adams are with school of chemical engineering, University of Birmingham, Edgbasto, B152TT, United Kingdom (e-mail: b.m.dzidek@bham.ac.uk, m.j.adams@bham.ac.uk).

$$\frac{\partial}{\partial x}\left(\frac{h^3\rho}{\eta}\frac{\partial p}{\partial x}\right)+\frac{\partial}{\partial y}\left(\frac{h^3\rho}{\eta}\frac{\partial p}{\partial y}\right) = 6U\frac{\partial}{\partial x}(h\rho)+12\frac{\partial}{\partial t}(h\rho) \quad (2)$$

Here ρ and η are respectively the density and the viscosity of the air. The parameter U is the tangential velocity of the surface (exploration velocity of the user finger). A normalized version of (2) is commonly used to describe the squeeze film effect. The new equation introduces the squeeze number Λ and the bearing number σ:

$$\frac{\partial}{\partial X}\left(H^3P\frac{\partial P}{\partial X}\right)+\frac{\partial}{\partial Y}\left(H^3P\frac{\partial P}{\partial Y}\right) = \Lambda\frac{\partial}{\partial X}(HP)+\sigma\frac{\partial}{\partial T}(HP) \quad (3)$$

$$\Lambda=\frac{6\eta U l_0}{h_0^2 p_0} \qquad \sigma=\frac{12\eta\omega_0 l_0^2}{h_0^2 p_0} \quad (4\text{-}5)$$

with $X = x/l_0$, $Y = y/l_0$, $H = h/l_0$, $P = p/p_0$ and $T = \omega_0 t$ t. The parameter l_0 is the active length, h_0 is the mean air gap and p_0 is the ambient pressure. For a haptic device, the finger has a relatively slow velocity compared to the mean out-of-plane velocity of the surface. Thus the velocity of the finger in the x and y directions can be neglected ($U = 0$). We can then simplify (3) by reducing the system to one dimension; (3) becomes:

$$\frac{\partial}{\partial X}\left(H^3P\frac{\partial P}{\partial X}\right)=\sigma\frac{\partial}{\partial T}(HP) \quad (6)$$

This equation is solved in [8] with the assumption of a very large value of σ ($\sigma\to\infty$) by applying the previous mean amplitude equation (1) to this configuration. The resulting differential equation gives the new local pressure of the thin film (see [9] for full solution):

$$P_\infty = p_0\frac{(1+\delta cos(kX))\sqrt{\left(1+\delta cos\left(\frac{k}{2}\right)\right)^2+\frac{3}{2}\varepsilon^2}}{\left(1+\delta cos\left(\frac{k}{2}\right)\right)(1+\varepsilon cos(T)+\delta cos(kX))} \quad (7)$$

with $X=\frac{x}{l_0}$, $T=\omega t$, $\varepsilon=\frac{h_{vib}}{h_0+h_e}$, $\delta=\frac{h_e}{h_0+h_e}$, $k=\frac{2\pi l_0}{L}$

By integrating Equation (7) in time and position, the mean force applied to the fingertip by the squeeze film effect can be determined. F_s is the force applied per unit of length in permanent mode.

$$F_s=\frac{1}{2\Pi}\int_0^{2\pi}\left(\int_{-\frac{1}{2}}^{\frac{1}{2}}(P_\infty-1)dX\right)dT \quad (8)$$

The solution to (6) assumed that $\sigma\to\infty$. Nevertheless it is generally admitted that this condition can be restricted to $\sigma > 10$; this condition is applicable for a vibrational frequency > 25kHz [9] (above the human maximum hearing range).

It is then possible to calculate $\Delta\mu$, which is given by the coefficient of friction under actuation, μ', relative to that at rest, μ_0, viz., at an amplitude of vibration of 0 µm.

$$\Delta\mu=\frac{\mu'}{\mu_0}=1-\frac{(P_\infty-1)}{P_f} \quad (9)$$

The parameters in table 1 are then applied to calculate the relative dynamic friction coefficient, $\Delta\mu$, for the four surface roughnesses of the vibrating plate.

Table 1: Squeeze Film Analytic model parameters

Amplitude of ridges	h_e	50 [µm]
Period of fingertip ridges	L	350 [µm]
Surface Roughness range	h_r	0.2-1.4[µm]
Length of contact	l_0	1 [cm]
Normal force applied	F_f	0.5 [N]
Dynamic Viscosity of air	η	$1.85.10^{-5}$ [Pa.s]
Atmospheric pressure	p_0	0.1 [MPa]

As can be seen in Figure 2, this squeeze film model predicts a reduction to zero of the dynamic friction coefficient when the amplitude of vibration increases.

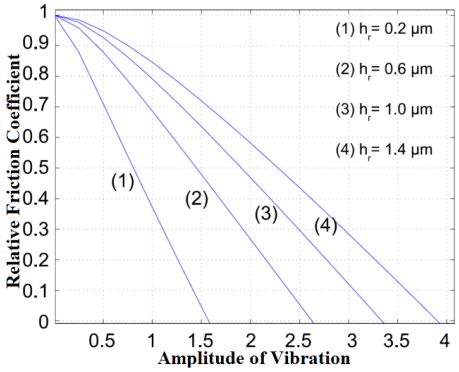

Figure 2: Modeling of the relative friction coefficient for different surface roughnesses.

III. Experimental Setup

This section introduces the two specialized pieces of equipment required for the study. Firstly, a passive touch tribometer and then the ultrasonic friction reduction devices that were specifically developed.

A. Tribometer

In order to control as many parameters as possible in the analysis of UL, a tribometer was designed that was capable of accurately measuring the friction during passive touch. Previous studies of the squeeze film effect have measured the friction between a plate and a finger pad in active touch [10] [11]. In this configuration the user's finger is free and the subject is responsible for both the speed of exploration and the normal force. In order to precisely control these two parameters, instead a passive touch tribometer was designed to measure the friction of the finger pad (Longshore System Engineering, Cornwall, UK). It comprises an arm support to secure the user's hand (sample) in the correct position. A

holder is provided to position the finger at the required angle to the measured surface. The moving part is composed of a 2-axis strain gage sensor attached to the head of a beam supported by a bearing. It can rotate freely and a counterweight can be affixed to balance the mass of the sampled surface. The normal force applied by the measured surface to the finger pad and the probe can be selected by adding a mass on the top of the beam. This possibility was used to experiment with different normal forces in order to determinate the effect on the UL.

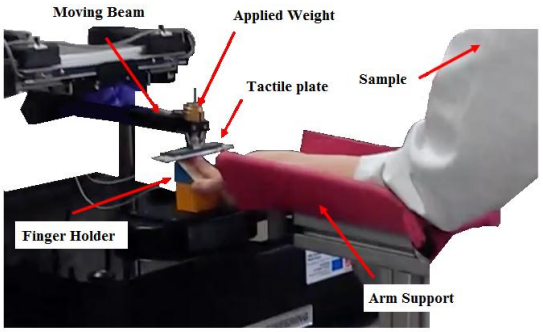

Figure 3: Photograph of the tribometer.

The tangential and normal forces were measured using two strain gauge ADC interfaces with 10 bit precision and a sampling frequency of 70 kHz (DSCSUEASC, Mantracourt). The force measurements were then stored on a Windows computer and re-synchronized and re-sampled using Matlab. Windowing was done to only extract the forces while the finger pad was located in the centre of the moving plate; data from the borders of the plates were removed because the vibrational amplitude decreases toward the external borders of the plate as shown in Figure 4. The first and last half cycles of each test run were removed to prevent any potential artifact when the tribometer accelerated during the changes in direction imposed by the sawtooth displacement profile of the tribometer beam.

B. Tactile Plate

This section describes the UL stimulators created for the study. A specific haptic stimulator was developed in order to obtain the most stable friction reduction. UL is mostly used on large devices with a Lamb wavelength under 10 mm to prevent the user from feeling the reduction of amplitude around nodal lines. For this study, ultrasonic stimulators were designed and fabricated with a mode of vibration seldom used in such devices; this involved having the standing wave (Lamb wave) propagating on the short axis of a rectangular plate. The exploration is done on this axis by the tribometer thus ensuring no crossing of nodal lines in order to induce a stable amplitude across all the exploration range.

Using SALOME-Meca finite element software, the device was simulated such that the first dimension of the short axis was matched with the first resonant mode on this axis. This specific configuration eliminates the possible perturbation to the perceived friction. Multiple haptic devices in this configuration were created to reflect different roughnesses and material properties. Each of these devices incorporates one piezo-ceramic used as a sensor to measure the amplitude of vibration in real time. The devices were pre-calibrated with a vibrometer to extract the specific relationship between the measured voltage (V) and amplitude of vibration (µm).The relationship between the voltage applied to the ceramic transducer and generated amplitude of vibration for the mode selected was calibrated by using an interferometer vibrometer (OV-5000, Polytech, Germany).

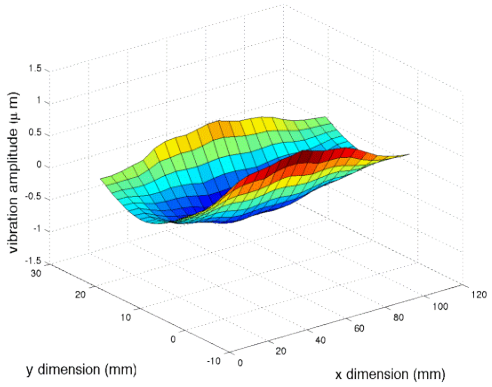

Figure 4: Measured amplitude of vibration of one of the ultrasonic actuator (phase locked).

Two devices of the same dimensions were made of aluminum and glass to further investigate the effects of surface properties on the frictional reduction effect. The voltage to amplitude ratios for the glass and aluminum devices were respectively 0.4146 and 0.2168 µm/V. The longitudinal mode of vibration is the same for the two devices but the resonant frequency is slightly affected by the material properties: 26.7 kHz for the glass and 25.1 kHz for the aluminum device.

IV. Friction Reduction Results

This section describes the results of the experiments done to characterize the frictional reduction evolution when subjected to varying normal force, speed of exploration and amplitude of vibration.

A. Preliminary assessment of the parameters

In order to assess the influence of all main contributing parameters to the UL effect, an initial experimental configuration was designed. This first set of experiment was done sequentially for one subject and finger for all three parameters: normal load, speed of exploration and amplitude of vibration. Every combination of parameters was sampled in a separate session. Three main parameters were measured: 4 normal loads (25, 50, 75 and 100 g), 3 exploration speeds (10, 17 and 25 mm/s) and finally 7 levels of amplitude (driven by an applied voltage from 0 to 120 V). It should be noted that even this first preliminary study is quite long and exhausting for the subject since completing the 3D matrix of friction reduction takes a minimum of 5.5 h. The subject needs to be as static as possible to prevent any artifacts. The protocol itself is straightforward in this case. The finger pad and plate were first cleaned to remove any moisture/grease. The subject then positioned the test arm in the holder. The user's finger was then attached under the probe at 30º to the horizontal (using tape on the second phalange to prevent deformation of the skin). Then the normal load weights were added and the measurements started with the slowest speed

and a null excitation signal. This was repeated for every speed and amplitude voltage at the given load. For each different load the mean value of the voltage was manually measured from the oscilloscope.

The 3D results can be plotted for the friction coefficient as a function of both the speed and the vibrational amplitude. The plots in Figure 5 represent these measures with 25 and 75 g normal force applied. It shows that the friction reduction

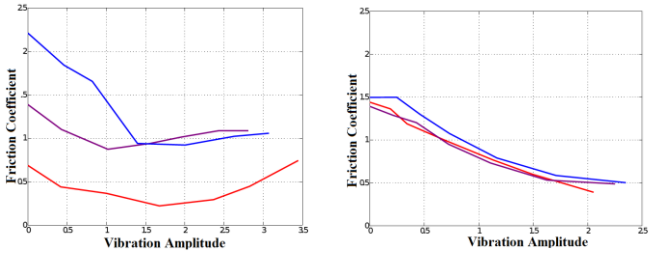

(a) (b)

Figure 5: Dynamic friction coefficient as a function of both the amplitude of vibration and the speed of exploration. (a) and (b) are measured at normal loads of respectively 25 and 75 g. Curves in red, violet and blue have exploration speed of respectively 10, 17 and 25 mm/s.

Figure 5tends toward an asymptotic value as the amplitude of vibration increases. For a normal load of 100 g, a reduction in friction was not observed even at the maximum vibrational amplitude employed in these experiments. The friction increases with increasing speed but it does not affect the observed trends. This seems to validate the simplifications made in equation (6).

B. Fine Amplitude Analysis

The impact of amplitude on the UL was evaluated in a second set of experiments to test multiple subjects with a high resolution on the amplitude of vibration since it is the most critical parameter. The study was limited to four subjects; three male and one female aged between 25 and 30 yr. An exploration speed of 17 mm/s was selected in order to minimize the noise. To obtain more precise amplitude data from the piezo-ceramic sensor, a few changes were made to the equipment. An analog acquisition card (TI) was installed with a small labview program to provide real time measurement of the vibrational amplitude of the haptic probe.

The protocol was slightly different in this study to provide more repeatability and decrease the discomfort of the subject. One of the issues of the previous setup was the difficulty of locating the finger exactly in the same position under the haptic probe. This caused variation in the measured reduction of friction since the vibrational amplitude under the finger pad is slightly different. This issue was corrected by reducing the number of finger repositions. As previously, the user's hand and the probe were cleaned and positioned on the tribometer. Once the finger pad is positioned at the center of the stimulator, the experiment was started and all amplitudes of vibrations were measured in one session. The beam of the tribometer was configured to cycle continuously. The excitation voltage was slowly increased every three cycles (6 displacements in each direction). The half-cycles where the amplitude changed were not considered for the analysis. In order to avoid potential destructive vibrations, the increase in amplitude was limited to 3.5 µm, independently of the tactile plate used, by checking the acquired sensor voltage in accordance with the device specific amplitude ratio. The frictional forces for each half-cycle were averaged locally. The local dynamic friction coefficient was then calculated. Finally, the error propagation of the standard deviation of the dynamic friction coefficient, μ, is calculated using the standard deviation ($\sigma_{F_l}, \sigma_{F_n}$) of the normal and lateral forces (F_l, F_n) as follows:

$$\sigma_\mu = |\mu| \sqrt{\left(\frac{\sigma_{F_l}}{F_l}\right)^2 + \left(\frac{\sigma_{F_n}}{F_n}\right)^2 - \frac{2COV_{F_l F_n}}{F_l F_n}} \quad (10)$$

Figure 6 shows an example of the absolute friction coefficient as a function of the amplitude of vibration of the surface. The applied normal load is 30 g but the resulting normal force is different because it is necessary to subtract the spring effect present in the joint of the arm; this is the reason why the force is only 0.093 N. An exponential decay curve can be fitted to the data with a mean square error of $R^2 > 0.98$ in most cases.

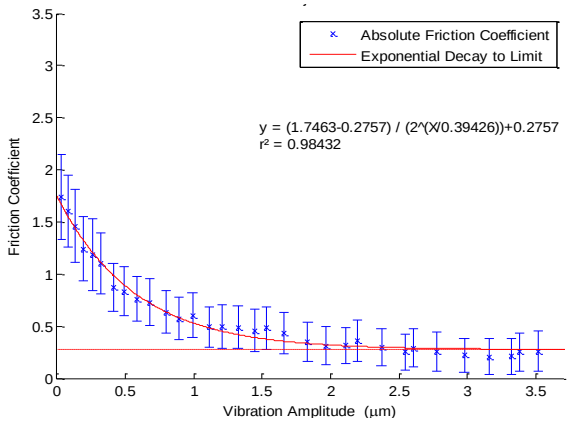

Figure 6: Friction coefficient as a function of vibrational amplitude for a normal force of 0.093 N on aluminum. The data points represent the mean coefficient of friction calculated for three cycles at the same amplitude of vibration. Vertical bars correspond to the propagated standard deviation over stimuli. The red curve shows an exponential decay fit. The dashed line is the limit of the decay fit.

The measured dynamic friction coefficient with an unpowered device (null amplitude of vibration is extremely variable between subjects as shown in Figure 7.

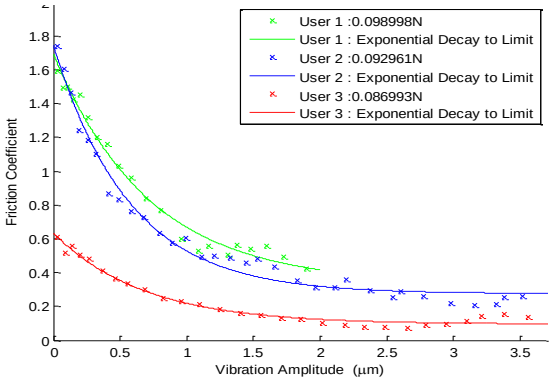

Figure 7: Dynamic friction coefficient as a function of vibrational amplitude for multiple subjects at the same normal load and speed of exploration. The substrate is aluminum. Each color represents a different user.

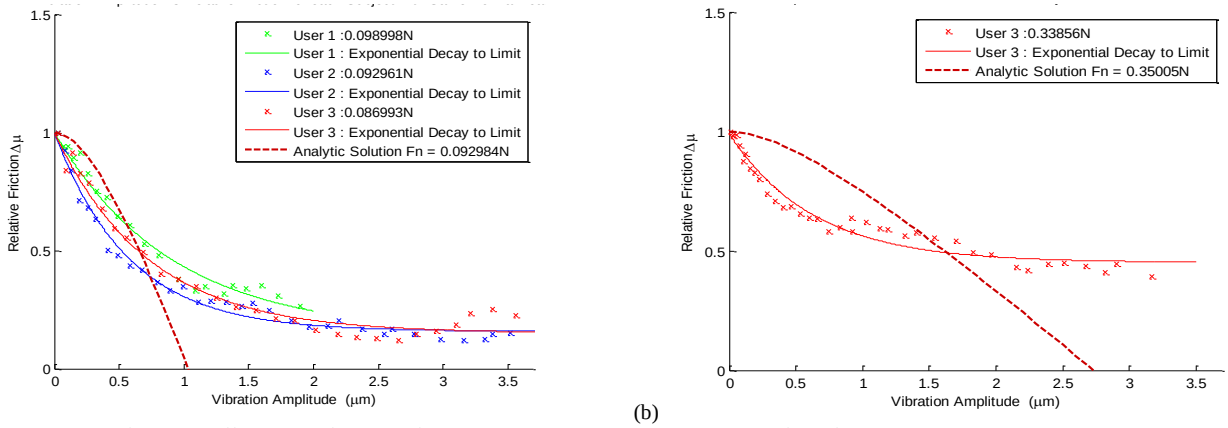

(a) (b)

Figure 8: Relative friction coefficient as a function of vibrational amplitude at the same normal force for three subjects on an aluminum substrate. The normal load is 30 g in case (a) and 75 g in case (b). In both cases the data points represent the mean coefficient of friction calculated over three cycles and divided by the frictional force at rest (amplitude = 0 μm). Each solid line represents the exponential decay fit and the dashed line shows the calculated predicted friction reduction from the analytic squeeze film model at an averaged normal load.

The three measures are done under the same conditions but for different users. The base coefficients of frictions are 0.6, 1.6 and 1.7. It is also to be noted that while the friction reduction tends toward a limit for each curve, this limit is variable between subjects and thus does not seem to depend on the normal load and speed of exploration only.

V. Discussion

This section will compare the measured dynamic coefficients of friction to the model proposed in section II. First the limits of the squeeze film model alone will be highlighted. Then the advantages of the observed behavior for the haptic stimulator will be explored.

A. *Squeeze film model alone is incomplete*

There is a lower limit to the friction reduction as a function of the vibrational amplitude when the amplitude of vibration increases (Figure 6). Due to the large variability of the base dynamic friction coefficient between subjects, it is difficult to directly draw conclusions concerning its evolution. Nevertheless, this phenomenon was observed for all the friction measurement. This seems to contradict an underlying principle of the squeeze film model regarding high amplitudes of vibration. Figure 8 shows an attempt to compare the actual tribological data to the squeeze film analytic model presented in section II. Measuring the overpressure generated in the air-film can be difficult (see [12]) and thus the relative friction coefficient $\Delta\mu = \mu'/\mu_0$ was calculated. The value of $\Delta\mu$ was then compared to the results of equation (9). While for small amplitudes, the model and the experimental data are relatively similar, there is a clear discrepancy between the predicted and observed friction reduction for amplitudes greater than a few micrometers.

The relative coefficient of friction, $\Delta\mu$, tends toward an asymptotic value, $\Delta\mu_1$. In most cases, all three of the subjects had the same value of $\Delta\mu_1$ when the identical normal load and speed were applied. Until now these results were measured on an aluminum substrate but it can be noted that the same pattern is observed on the glass actuator described in section III.B (Figure 9).

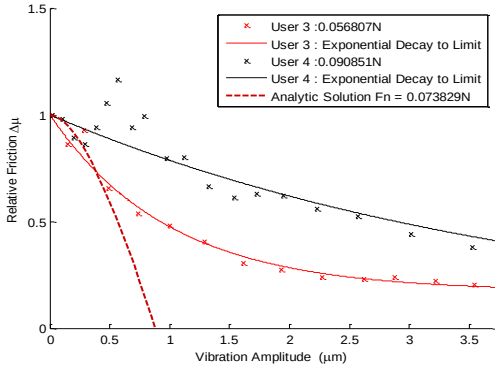

Figure 9: Relative dynamic friction coefficient applied to glass substrate

B. *Experimental Model Design*

The fitting curve applied to each measurement in Figure 8 is an exponential decay to an arbitrary value with the following equation:

$$\Delta\mu(h_r) = \frac{(a-c)}{2^{h_r/b}} + c \qquad (11)$$

The parameter a is the starting friction (with a value of unity when using the relative friction coefficient), b is the half-life and c is the limit of the friction reduction.

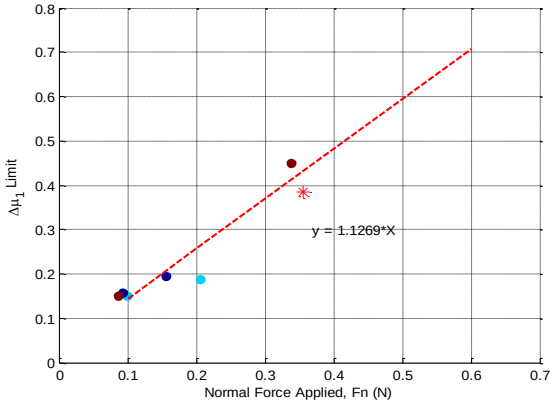

Figure 10: Evolution of the Δμ limit ($\Delta\mu_1$) as a function of the applied normal force (3 subjects). The red line represents a potential trend. Point represented by the Red star is extracted from data of chapter IV.A

The limitations of the current equipment prevented the acquisition of as much data as the other normal loads. However, Figure 10 indicates that $\Delta\mu_1$ increases linearly with the normal force. This trend will need to be verified with improved equipment and a larger number of subjects. Nevertheless, it is possible to propose the following equation to describe the relative dynamic friction reduction mediated by UL:

$$\Delta\mu(h_r) = \frac{1-\Delta\mu_1}{2^{h_r/b}} + \Delta\mu_1 \qquad (12)$$

$$\text{With} \quad \Delta\mu_1 = 1.13F_n$$

The value of the half-time decay b did not correlate with the control parameters of the experiment and so is assumed to be mostly dependent on properties of the fingers. A mean value of $b = 0.6$ µm is representative. The parameters of equation (12) are valid for an aluminum substrate and a speed of exploration of 17 mm/s. This equation while incomplete at this point, fits well with the measurements and provides an improved correlation compared with the squeeze film analytic model.

C. *Impacts on the energy consumption*

The unpredicted phenomenon of the limit of the achievable friction reduction could be useful in the design of new haptic stimulators. Indeed this limit gives an upper bound to the amplitude necessary to achieve maximum friction reduction and thus limits the energetic design constraint for the driver. The dimensions and energy consumption of the piezoceramic driver are especially important considering the level of integration and portability required by the mobile platform industry.

VI. Prospective

A. *Expand the experimental model with larger sample measurement*

Some issues with the protocol prevented acquiring sufficiently repeatable parameters. This is especially true for the positioning of the finger under the haptic stimulator, which can influence greatly the mean amplitude of vibration. To solve this issue, a second set of haptic probes with a larger small axis to reduce the potential misalignment of the finger has been designed. Finally, the acquisition chain will be fully re-implemented to give an order of magnitude increase in the sampling frequency and increase the ADC sampling to 16 bit. The experiments will be conducted with a larger number of users (> 10) in order to build the basis of an experimental model of the ultrasonic friction reduction for a wide range of fingers.

B. *Design of a new analytic model*

The results from this study and the experimental model thus developed will be used in a subsequent study to validate the proposition of an optimized analytic solution of UL based on elastic interaction of the fingerprint ridges [13]. The relatively high lower limit of the coefficient of friction (> 0.1) suggests that, for high amplitudes of vibration, acoustic levitation is not a significant mechanism in the current experiments and that other mechanisms are more important. Once a complete model has been developed, it will provide powerful tools for open-loop control of future UL devices.

VII. Conclusion

The mechanical interaction between a finger pad and a flat ultrasonically vibrating surface has been measured and compared with a squeeze film model of ultrasonic lubrication. Mismatches between the model and measurements were highlighted; specifically the friction does not reduce to zero as predicted and instead tends toward a lower limit when the amplitude of vibration increases above 3 µm. An empirical model based on the friction coefficient measurements was proposed and a general trend of the friction reduction is highlighted.

References

[1] B. M. Schena, "Directional inertial tactile feedback using rotating masses". USA Patent US7182691 B1, 27 February 2007.

[2] D. J. Meyer, . M. A. Peshkin and E. J. Colgate, "Fingertip friction modulation due to electrostatic attraction," in *World Haptics Conference (WHC), 2013*, 2013/4/14.

[3] M. Amberg, F. Giraud, B. Semail, P. Olivo, G. Casiez and N. Roussel, "STIMTAC: a tactile input device with programmable friction," in *Proceedings of the 24th annual ACM symposium adjunct on User interface software and technology*, 2011/10/16.

[4] F. Giraud, M. Amberg, B. Lemaire-Semail and G. Casiez, "Design of a transparent tactile stimulator," *Haptics Symposium (HAPTICS)*, pp. 485-489, 2012/3/5.

[5] E. Vezzoli, M. Amberg, F. Giraud and B. Lemaire-Semail, "Electrovibration modeling analysis," in *9th International Conference, EuroHaptics 2014*, Versaille, 2014.

[6] T. Watanabe and S. Fukui, "A method for controlling tactile sensation of surface roughness using ultrasonic vibration," in *Robotics and Automation, 1995. Proceedings., 1995 IEEE International Conference on*, 1995/5/21.

[7] M. Biet, Conception et contrôle d'actionneurs électro-actifs dédiés à la stimulation tactile, PhD Thesis. Lille 1, 2007/1/1.

[8] C. Winter, Friction feedback actuators using squeeze film effect, PhD thesis. École polytechnique fédérale de Lausanne, 2014.

[9] M. Biet, F. Giraud and B. Lemaire-Semail, "Squeeze film effect for the design of an ultrasonic tactile plate," *Ultrasonics, Ferroelectrics and Frequency Control, IEEE Transactions on*, vol. 54, no. 12, pp. 2678-2688, 2007/12.

[10] L. Winfield, J. Glassmire, . J. E. Colgate and M. Peshkin, "T-PaD: Tactile pattern display through variable friction reduction," in *EuroHaptics Conference, 2007 and Symposium on Haptic Interfaces for Virtual Environment and Teleoperator Systems. World Haptics 2007. Second Joint*, 2007/3/22.

[11] E. Samur, J. E. Colgate and M. A. Peshkin, "Psychophysical evaluation of a variable friction tactile interface," in *IS&T/SPIE Electronic Imaging*, 2009/2/5.

[12] C. Winter and Y. Perriard, "Modeling of the air film pressure for a haptic touch actuator," in *Power Electronics and Applications (EPE 2011), Proceedings of the 2011-14th European Conference on*, 2011/8/30.

[13] E. Vezzoli, D. Brygida, T. Sednaoui, F. Giraud, M. Adams and B. Lemaire-Semail, "Role of fingerprint mechanics and non-Coulombic friction in ultrasonic devices," proposed *World Haptic*, Chicago, 2015.

Chapter Three

Part 2: Friction reduction through ultrasonic vibration part 2: experimental evaluation of intermittent contact and squeeze film levitation.

Thomas Sednaoui[1], Eric Vezzoli[2], Brygida Dzidek[3], Betty Lemaire-Semail[2], Cedrick Chappaz[1], Michael Adams[3]

[1] L2EP-IRCICA and STMicroelectronics, Crolles F38920, France

[2] L2EP-IRCICA Laboratory, University of Lille 1, Lille, France

[3] School of Chemical Engineering, University of Birmingham, Birmingham B15 2TT, UK

Authors' contributions

TS, EV and BD designed and coordinated the study and drafted the manuscript; BD, TS and EV performed the experiments and conducted the data analysis; MJA, BLS and CC participated in the statistical analysis. All authors made substantial contributions to the critical revision of the submitted manuscript.

Friction Reduction Through Ultrasonic Vibration Part 2: Experimental Evaluation of Intermittent Contact and Squeeze Film Levitation

Article *in* IEEE Transactions on Haptics · February 2017

DOI: 10.1109/TOH.2017.2671376

CITATION
1

READS
6

6 authors, including:

Thomas Sednaoui
Go Touch VR
7 PUBLICATIONS **20** CITATIONS
SEE PROFILE

Eric Vezzoli
GoTouchVR
21 PUBLICATIONS **48** CITATIONS
SEE PROFILE

Brygida Dzidek
University of Birmingham
8 PUBLICATIONS **20** CITATIONS
SEE PROFILE

Michael J Adams
University of Birmingham
60 PUBLICATIONS **1,105** CITATIONS
SEE PROFILE

Friction Reduction Through Ultrasonic Vibration Part 2: Experimental Evaluation of Intermittent Contact and Squeeze Film Levitation

Thomas Sednaoui, Eric Vezzoli, Brygida Dzidek, Betty Lemaire-Semail, *Member, IEEE,* Cedrick Chappaz, and Michael Adams

Abstract—In part 1 of the current study of haptic displays, a finite element (FE) model of a finger exploring a plate vibrating out-of-plane at ultrasonic frequencies was developed as well as a spring-frictional slider model. It was concluded that the reduction in friction induced by the vibrations could be ascribed to ratchet mechanism as a result of intermittent contact. The relative reduction in friction calculated using the FE model could be superimposed onto an exponential function of a dimensionless group defined from relevant parameters. The current paper presents measurements of the reduction in friction, involving real and artificial fingertips, as a function of the vibrational amplitude and frequency, the applied normal force and the exploration velocity. The results are reasonably similar to the calculated FE values and also could be superimposed using the exponential function provided that the intermittent contact was sufficiently well developed, which for the frequencies examined correspond to a minimum vibrational amplitude of ~ 1 μm P-P. It was observed that the reduction in friction depends on the exploration velocity and is independent of the applied normal force and ambient air pressure, which is not consistent with the squeeze film mechanism. However, the modelling did not incorporate the influence of air and the effect of ambient pressure was measured under a limited range of conditions, Thus squeeze film levitation may be synergistic with the mechanical interaction.

Index Terms—Tactile devices and display, Tactile stimulator, Squeeze film effect, Ultrasonic devices, Friction modulation.

1 Introduction

The friction of flat screens can be globally modulated by the application of ultrasonic vibration with varying amplitude to create the illusion of a texture [1]. An understanding of the mechanism of friction modulation would greatly facilitate design optimisation and it has been proposed recently that the mechanism involves a combination of squeeze film levitation and intermittent contact [2], [3]. In part 1 of the current work [4], the underlying principles of friction modulation arising from intermittent contact were elucidated by developing numerical models. Here, experimental data involving real and artificial fingertips will be presented in order to validate the modelling. In addition, the results of measurements carried out at reduced ambient pressure will be described, which establish that the contribution of squeeze flow levitation is at least not significant for the particular artificial finger employed in the current work.

- *T. Sednaoui, is with L2EP and ST-Microelectronics, Crolles F38920, France*
  E-mail: thomas.sednaoui@st.com
- *E. Vezzoli, and B. Lemaire-Semail are with Univ. Lille, Centrale Lille, Arts et Metiers ParisTech, HEI, EA 2697 - L2EP - Laboratoire d'Electrotechnique et d'Electronique de Puissance, F-59000 Lille, France*
  E-mail: eric.vezzoli@ed.univ-lille1.fr, betty.semail@polytech-lille.fr
- *C. Chappaz is with HAP2U, CIME NANOTECH, 3, parvis Louis NEEL 38000 Grenoble*
  E-mail: cedrick.chappaz@hap2u.net
- *B.Dzidek, and M. Adams are at the School of Chemical Engineering, University of Birmingham, Edgbaston, B15 2TT, United Kingdom*
  Email: b.m.dzidek@bham.ac.uk, m.j.adams@bham.ac.uk

1.1 Intermittent Contact

Optical measurements have revealed that intermittent contact resulting from ultrasonic vibration may be characterised by the phase shift between the vibrating plate and the skin surface dynamics of the exploring finger pad or probe [3], [4]. That is, for small vibrational amplitudes, contact persists but with increasing amplitude there is a transition regime in which intermittent contact develops with an increasing phase shift. Ultimately, for large amplitudes, the phase shift tends to an asymptotic value corresponding to the intermittent contact being fully developed. Such data were used to calibrate a finite element (FE) of the exploration process [4]. Data interpretation was assisted by the development of a simple elastic model of a finger pad sliding on a vibrating plate at ultrasonic frequencies ($>$ 20 kHz). It was based on a normal and a lateral spring connected to a Coulombic slider of zero mass. While it was not possible to develop an analytical solution, the model enabled the derivation of a dimensionless group, Ψ, that incorporated the governing operating and material parameters:

$$\Psi = \frac{U}{wf\mu_0(1+\nu)} \tag{1}$$

where U is the exploration velocity, w and f are the vibrational amplitude and frequency, μ_0 is the intrinsic coefficient of friction (i.e. without vibration), and ν is the Poisson's ratio of the skin of the exploring finger pad or probe. An implication of Eq. (1) is that the performance of an ultrasonic display is independent of the elastic moduli of the *stratum corneum* and the applied normal force. This was consistent with the results of FE analyses provided that the

intermittent contact is sufficiently well developed; typically this corresponds to vibrational amplitudes greater than $\sim 1\,\mu\mathrm{m}$ P-P. These analyses were carried out for a wide range of the aforementioned parameters and the data could be satisfactorily described by the following function:

$$\mu = \mu_0[1 - \exp(-\Psi/\Psi^*)] \tag{2}$$

where μ is the actual coefficient of friction and Ψ^* is the characteristic value of Ψ. Eq. (2) satisfies the boundary conditions: $\mu = 0$ when $\Psi = 0$ and $\mu = \mu_0$ when $\Psi = \infty$. In part 1, the experimental studies by Dai et al. [2], involving the measurement of intermittent contact of a finger pad at two different vibrational amplitudes using an optical technique, will be extended to a full characterisation of the entire relevant vibrational amplitude range. The data will be employed for calibration and validation of a finite element (FE) model that is developed in order to investigate how intermittent contact would act to reduce the friction. On the basis of the friction reduction mechanism identified by the FE model, a simplified spring-slider model will be developed. It allows a dimensionless group to be identified that incorporates the critical design, operational and user variables that govern the performance of an ultrasonic haptic display. In this work, experimental data will be described showing that a decrease in the ambient pressure does not influence the reduction in friction induced by ultrasonic vibration. This was for a limited set of experimental conditions but it does support the content that the recurrent loss in contact is a contributing mechanism. Furthermore, frictional data for human and artificial fingertips sliding on an ultrasonic plate are reported that are consistent with both the FE and spring-slider models.

1.2 Squeeze Film Effect

The squeeze film effect was first introduced by Watanabe et al. [5] as an explanation for the modification of the roughness perception of an ultrasonic vibrating plate by an exploring finger. A more accurate modelling of the phenomenon was proposed by Biet et al. [6] and Winter [7]. The effect relies on the generation of a thin film of over-pressurised air between a finger pad and the vibrating plate induced by the compression and decompression of the trapped air. The effective normal force, and hence the frictional force, would then be reduced, and the relative coefficient of friction given by:

$$\mu' = 1 - \frac{F_s}{F_n} \tag{3}$$

where F_s is the repulsive force resulting from squeeze film levitation and F_n is the normal force applied by the finger. By applying Reynolds equations, it is possible to define the squeeze number, σ [6]:

$$\sigma = \frac{12\eta w l_0}{h_0^2 p_0} \tag{4}$$

where η is the dynamic viscosity of air, l_0 and h_0 are, respectively, the length of contact and gap between the finger pad and the plate and p_0 is the ambient air pressure. Details of the derivation of Eq. (4) are reported in [6]. It was suggested that a value of $\sigma > 10$ corresponds to the maximum overpressure, p_s, that could be achieved. This approximation allowed an analytical expression for the induced repulsive reaction force to be derived [6]. Similar results were confirmed by more accurate FE analysis [7]:

$$F_s = A p_0 (P_\infty - 1) \tag{5}$$

where A is the gross contact area between the finger pad and the plate, and $P_\infty = p_s/p_0$ is the pressure between the finger pad and the plate induced by the squeeze film for an infinite squeeze number normalized by the ambient pressure. Thus Eq. (5) suggests that the repulsive force is linearly dependent on p_0 given that p_s is not a function of P_∞ for $\sigma > 10$.

2 Experimental Apparatus

2.1 Friction Measurements of Artificial Fingertips

2.1.1 Ultrasonic Probe

Due to the extreme difficulty of performing tribological measurements under controlled conditions for a finger sliding on an ultrasonic device in a reduced pressure environment and the necessity to have a standard evaluation tool, a probe exhibiting frictional modulation similar to that of a human fingertip was developed as shown schematically in Fig. 1(a). It has a silicone elastomeric core with dimensions 16 x 13 x 10 mm, a Young's modulus of 1 MPa and curved edges. The contacting region was covered with a surgical tape having mechanical properties (Young's modulus of $\sim$ 20 MPa) and spatial periodicity similar to that of the fingerprint ridges. To establish that the behaviour of the probe is similar to that of a human finger pad, a tribometer (TRB, CSI, Switzerland), which is shown schematically in Fig. 1(b) was used to record the frictional modulation experienced by the probe sliding on the ultrasonic device at a peak-to-peak amplitude of 2.5 μm, a normal force of 0.5 N and an approximate exploration velocity of 17 mm/s. In addition, the velocity and acceleration of the probe and a finger pad under ultrasonic vibration were measured using the equipment described in part 1 [4] with a vibrational amplitude of 1.35 μm and an applied normal force of 0.25 N.

2.1.2 Low Pressure Friction Measurements

To quantify the influence of the squeeze film mechanism, a special tribometer and a low-pressure chamber were designed in order to investigate the evolution of the frictional modulation as a function of the ambient pressure, Fig. 1(c). The tribometer incorporated a 6-axis force sensor (nano 43, ATI, USA) that provides both lateral and normal force monitoring. The preloading of the axis can be tuned with a magnetic levitation system, and the lateral motion of the probe is actuated by a linear ultrasonic motor (M-663, PI, Germany) coupled with a driver (C-184, PI, Germany).

The vibration device is a glass plate with dimensions 120 x 21 x 2 mm and equipped with three piezoceramic actuators used as a driver and one as a sensor; the resonant frequency is 27.4 kHz with a stable maximum in the center of the plate and it is similar to the plates used in [8]. The pressure system consists of a cylindrical steel chamber with a detachable transparent side as shown schematically in

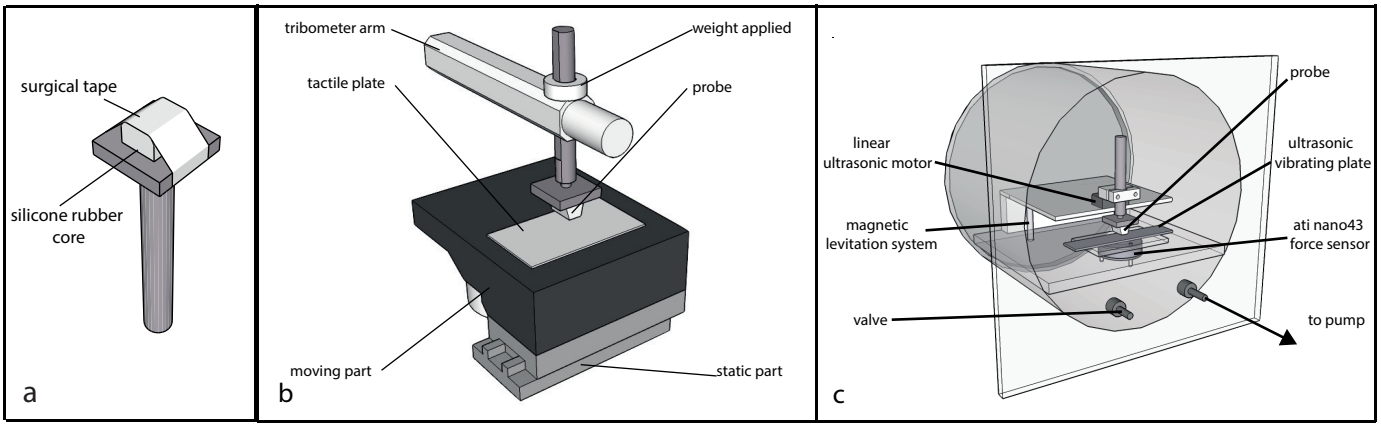

Fig. 1: Schematic diagram of (a) the artificial fingertip, (b) the tribometer for measuring the friction of artificial probes under ambient pressure, and (c) the pressure chamber for housing the tribometer and the developed low pressure tribometer.

Fig. 1(b). It was equipped with a vacuum pump (Piccolo, Thomas, Germany) and the inner pressure was measured by a manometer and regulated with a valve. It was necessary to implement a vibrational amplitude control system for the plate, which was similar to that described in [9], in order to ensure the consistency of the measurement conditions between the different atmospheric pressures. Without the control system, the reduction in the air damping on the resonator generated a significant change in the Q factor of the vibration system. This reduction, coupled with the mechanical noise induced by the friction measurements resulted in extremely unstable vibrational amplitudes of the plate. The closed-loop control implemented on the plate stabilised the vibration amplitude with a resolution of 50 nm during the friction measurements.

2.1.3 Measurement of the Velocity and Frequency Dependence

The tribometer described in section 2.1.1 was used to quantify the influence of the exploration velocity and vibrational frequency of the plate on the friction reduction. The plate employed for the pressure experiments was reused to measure the influence of the scanning velocity of the probe on the reduction of friction. Four different aluminium ultrasonically vibrating plates were designed by FE modelling (Salome-Mecha) to study the influence of the vibrational frequency on the reduction in friction. The plates have identical surfaces and employ the same vibrational mode but the thickness was varied in order to obtain different vibrational frequencies. Their dimensions are 41 x 76 mm with thicknesses of 1, 1.25, 1.6 and 2 mm and resonant frequencies of 36.6, 43.3, 53.7 and 66.1 kHz respectively. All the plates exhibited the same vibrational mode with a spatial wavelength of 16 mm (Fig. 2). A similar closed-loop control of the vibrational amplitude was implemented for all the plates to maintain stability of the amplitude under the range of measurement conditions investigated. A similar rough plastic film was attached to the plates in order to obtain a uniform surface roughness of 1.23 $\pm$ 0.03 µm Ra. During the measurement, the finger was supported by a 30 degrees finger holder and attached by double side tape on the finger nail. The vibration was measured by a piezoceramic on the plate used as a sensor contextually with the vibration of the skin through the Laser Vibrometer.

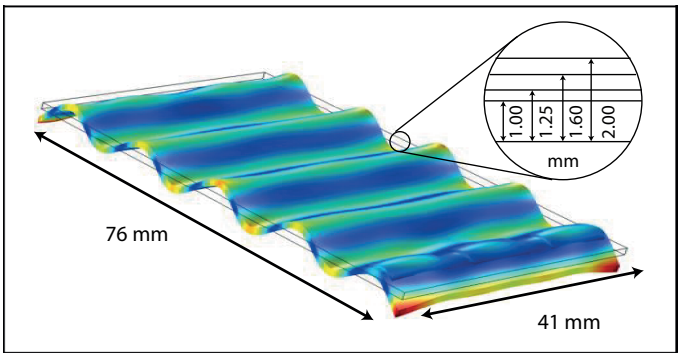

Fig. 2: Finite element representation of the vibrational mode of the aluminum plates developed for the frequency dependent study.

2.2 Real Finger Pad Friction Measurements

2.2.1 Passive Tribometer

Previous studies of the squeeze film effect have reported measurements of the friction between a plate and a finger pad in active touch [10]. In this configuration, the finger is voluntarily exploring the surface and thus the subject is responsible for the speed of exploration and the normal force adjustment. In order to precisely control these two parameters, a passive touch based tribometer was adapted (Longshore System Engineering, Cornwall, UK) (Fig. 3a). A beam with a bearing acting as a pivot to allow free rotation is displaced laterally with a reciprocating velocity controlled by a DC motor. There is a 2-axis strain gage sensor at one end of the beam below which the vibrating plate is attached. A counterweight on a screw thread at the other end of the beam allows it to be balanced. Weights are placed on the sensor assembly to vary the normal force that is applied to the finger. An arm support provides user comfort and ergonomic control with secure wrist and hand support to allow precise finger pad positioning. A wedge-support is provided to position the finger at an angle of 30° to the plate. The tangential and normal forces are measured using

TABLE 1: Summary of the participants for the *in vivo* friction measurements

Participant	p1	p2	p3	p4	p5	p6
Age	27	26	32	35	30	27
Gender	F	F	F	F	M	M

two strain gauge ADC interfaces with 16-bit precision and a sampling frequency of 100 kHz implemented on a NI ADC system. The force measurements, amplitude data and position of the beam were then stored on a Windows computer using Labview and re-sampled using Matlab. Windowing was done to extract only the forces while the finger pad was located in the central region of the moving plate; data from the borders of the plates were removed to reduce the noise in the dynamic friction imposed by the triangular displacement profile of the tribometer beam.

2.2.2 Vibrating Plate

The vibrating device is a steel plate with dimensions 120 x 22 x 2 mm, equipped with 15 piezoceramic actuators used as a driver and one as a sensor; the resonant frequency is 25.1 kHz with a stable maximum in the center. The relationship between the voltage applied to the ceramic transducer and the generated vibrational amplitude for the mode selected was calibrated by using an interferometric vibrometer (OV-5000, Polytech, Germany) (Fig. 3b). A closed-loop system was implemented to control the vibrational amplitude of the plate to ensure the stability of the acquired data for applied normal forces $\leq$ 2 N and vibrational amplitudes $\leq$ 2.5 µm. The mean roughness of the steel plate is 0.36 $\pm$ 0.03 µm Ra as characterised using a Surface Profiler (MicroXAM 100HR, KLA-Tencor, Belgium).

2.2.3 Experimental Protocol

Table 1 summarises the details of the participants for the *in vivo* friction measurements; all participants gave their informed consent. It should be noted that the measurements can be quite long and exhausting for a participant since completing a full 3D matrix for a range of velocities and loads takes a minimum of 5 h. To prevent any change in the finger pad characteristics and possible artefacts due to movements of the finger, the participants were only subjected to one parameter (velocity or normal force) for a given session. The finger to be studied was initially cleaned with a commercial soap and water and, after thorough rinsing with water, it was allowed to equilibrate for at least 10 min under ambient conditions of 16 °C and a relative humidity of 50%. The arm of the participant was positioned in the holder for the most comfortable position. The right hand index finger pad was supported by the wedge support at 30° to the horizontal and additionally adjusted by using a tape on the second phalange to prevent rotation of the finger under the high loads. Each session was initiated by automatic load calibration after which standard calibrated weights were placed on the sensor/ultrasonic plate assembly for applying the required normal force. The vibrational amplitude was increased by a staircase function in steps of 0.1 - 0.2 µm for every three full sliding cycles.

3 Experimental Results

3.1 Results for Artificial Fingertips

3.1.1 Probe Validation

Fig. 4(a) shows the frictional forces for the probe under a normal force of 0.25 N and at a vibrational amplitude of 1.35 µm relative to the corresponding values without vibration. It also shows published data for a human finger pad [2] and for an another probe called Tango plus [3], [11] that were both acquired under approximately similar conditions to those employed for the current probe. Tango plus has an external layer mimicking the *stratum corneum* and a porous inner structure exhibiting similar viscoelastic behaviour to that of the inner tissues of the fingertip. In all cases the ultrasonic vibration induced a reduction in friction by a factor of $\sim$ 4, thus demonstrating that the current probe is a suitable mimic for the human finger pad. This is confirmed by the results shown in Fig. 4(b) that compares the velocity and acceleration of the plate, probe and finger pad also under a normal force of 0.25 N and at a vibrational amplitude of 1.35 µm. In terms of the phase shift relative to the plate and the magnitudes, the results are similar.

3.1.2 Frictional Data at Reduced Pressure

The coefficient of friction of the probe at atmospheric and at a reduced pressure of 0.5 atm as a function of the vibrational amplitude is shown in Fig. 5 for a normal force of 0.78 N. The measurements were repeated 10 times and the RMSE is 0.002. The decrease in the coefficient of friction with increasing amplitude is similar within experimental uncertainty for both pressures. If the squeeze film effect was responsible for the reduction in friction at ambient pressure, a smaller attenuation would be expected in the reduced pressure environment; see Eq. (5).

3.1.3 Frictional Data as a Function of the Vibrational Frequency, Velocity and Normal Force

Plots of the relative coefficient of friction as a function of the vibrational amplitude for the different resonant frequencies of the aluminium plates are shown in Fig. 6. The data exhibit the expected reduction in μ' with increasing amplitude. For a given amplitude, the value of μ' decreases systematically with increasing frequency and, at an amplitude of 3 µm, the value at a frequency of 66.1 kHz is $\sim$ 40% of that at 36.6 kHz. Fig. 7 shows plots of the relative coefficient of friction as a function of the vibrational amplitude for exploration velocities in the range 25 - 100 mm/s and an applied normal force of 0.5 N. Again, the data exhibit the expected reduction in μ' with increasing amplitude. For a given vibrational amplitude, the value of μ' decreases systematically with decreasing exploration velocity and, at an amplitude of 3 µm, the reduction of the friction at a velocity of 25 mm/s is a factor of $\sim$ 4 greater than that at 100 mm/s. Fig. 8 shows that the relative coefficient of friction is independent of the applied normal force for the three values examined.

3.2 *In Vivo* Friction Results

Six participants (four female and two male, mean age 29.5 $\pm$ 3.5), who gave their informed consent in performing the experiment.

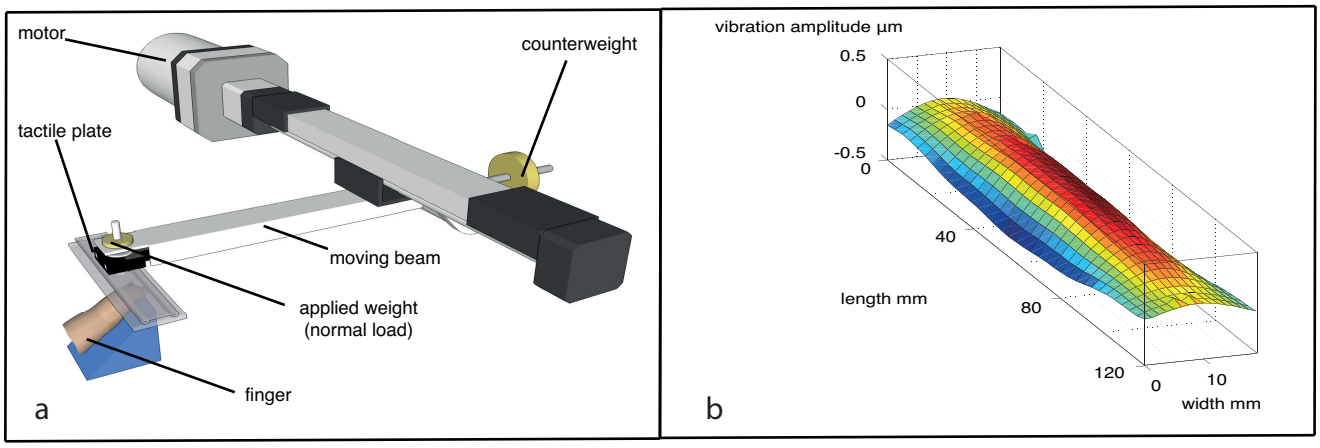

Fig. 3: (a) Schematic diagram of the reciprocating passive tribometer, (b) cartography of the vibrating steel plate as measured by an interferometric vibrometer.

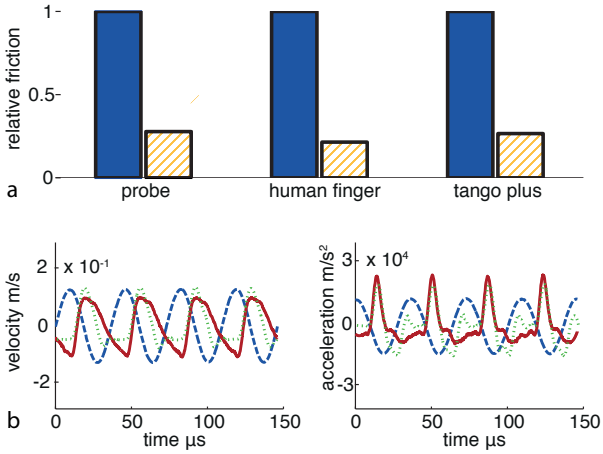

Fig. 4: (a) Comparison between the relative reduction in the friction of the current probe, a human fingertip [2] and the Tango plus probe [3], [11] due to ultrasonic vibration, where the filled and dashed bars correspond to vibration off and on respectively. (b) The velocity and acceleration of the ultrasonically vibrating plate (dashed blue line), probe (dotted green line) and finger pad (continuous red line) for a vibrational amplitude of 1.35 µm and applied normal force of 0.25 N.

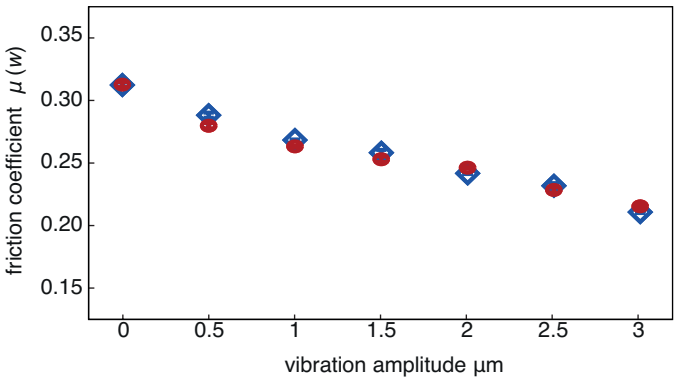

Fig. 5: The coefficient of friction of the probe as a function of the vibrational amplitude under atmospheric (blue diamonds) and reduced (red circles) pressure. A normal force of 0.78 N was applied during these tribometric measurements.

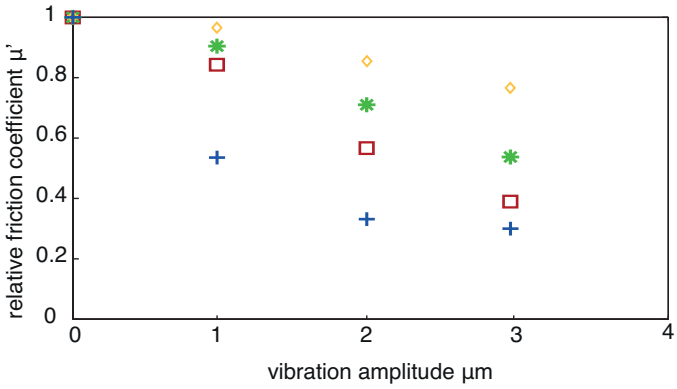

Fig. 6: The relative coefficient of friction for the probe sliding on an ultrasonic vibrating plate for an applied normal force of 1.0 N and an exploration velocity of 30 mm/s, and for vibrational frequencies of 36.6 (yellow diamonds), 43.3 (green stars) 53.7 (red squares) and 66.1 kHz (blue crosses).

3.2.1 *Frictional Load Index*

Fig. 9 shows a plot of the frictional force for a finger pad (p1) as a function of the applied normal force at an exploration velocity of 40 mm/s measured using the passive tribometer with the plate not being vibrated. Data for the 1st cycle and for the 10th cycle are shown in Fig. 9. These preliminary results confirm that the friction coefficient between the non-vibrated ultrasonic plate and the finger is essentially independent on the normal load.

3.2.2 *Influence of the Vibration*

Previously published *in vivo* data gathered with a passive tribometer are valuable for validating the modelling presented in part 1 [4], which is a main aim of the current

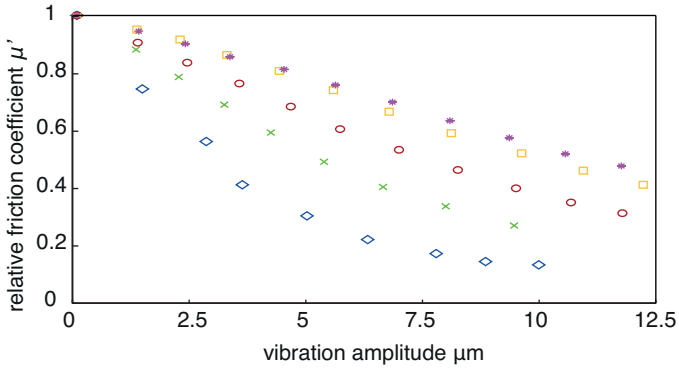

Fig. 7: The relative coefficient of friction for the probe sliding on an ultrasonic vibrating plate as a function of the vibrational amplitude for an applied normal force of 0.5 N and vibrational frequency of 25.1 kHz. The exploration velocities are 10 (blue diamonds), 25 (green crosses), 50 (red circles), 75 (yellow squares) and 100 mm/s (purple stars).

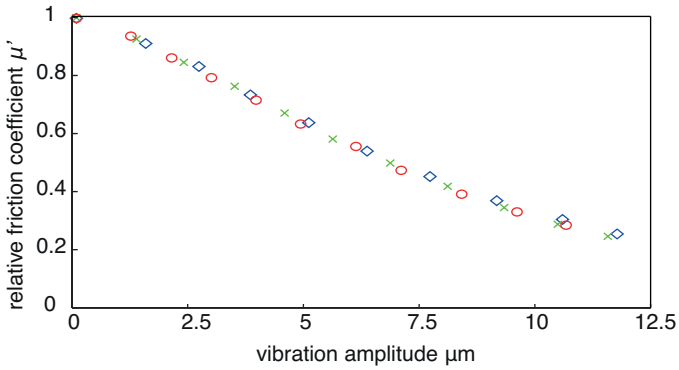

Fig. 8: The relative coefficient of friction for the probe sliding on an ultrasonic vibrating plate as a function of the vibrational amplitude for applied normal forces of 0.25 N (blue diamonds), 0.5N (green crosses), and 0.75 N (red circles), with an exploration velocity of 25 mm/s, and vibrational frequency of 25.1 kHz.

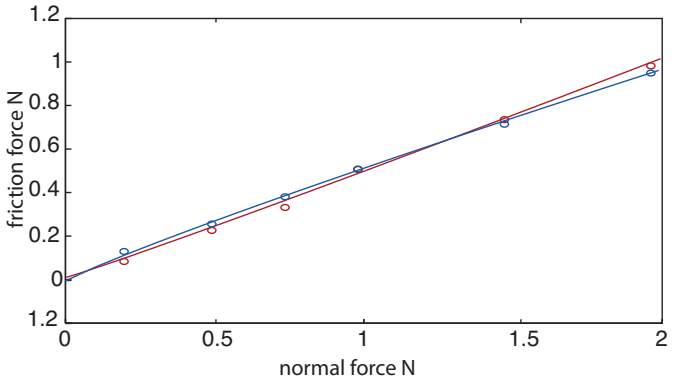

Fig. 9: The frictional force as a function of the applied normal force for a finger pad with an exploration velocity of 40 mm/s for the 1st exploration cycle (red) and the 10th cycle (blue). The lines are the best fit to (7).

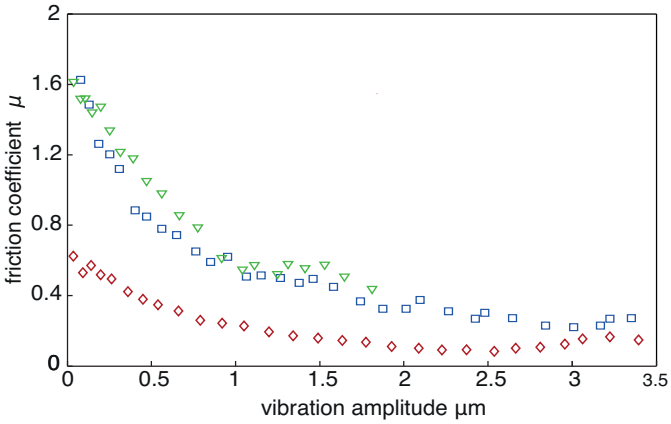

Fig. 10: Literature data [8] for the coefficient of friction as a function of vibrational amplitude at a frequency of 25.1 kHz and an exploration velocity of 17 mm/s for three different participants with applied normal forces of $\sim$ 0.1 N.

paper. Consequently, it will be included in this section for convenience. Fig. 10 shows such data [8] for the coefficient of friction as a function of the vibrational amplitude at a frequency of 25.1 kHz and an exploration velocity of 17 mm/s for three different participants and a similar applied normal force of $\sim$ 0.1 N. It exemplifies the wide variation in the absolute coefficients of friction for different participants.

Similar data measured in the current work are presented in Fig. 11(a) for one participant (p5) with an applied normal force of 0.5 N, and a vibrational frequency of 25.1 kHz for three exploration velocities of 20, 40 and 80 mm/s. The reduction in the friction is systematically greater with decreasing exploration velocity. Comparable trends for the dependency of the vibrational amplitude are evident in Fig. 11(b) from a normalization of the data shown in Fig 10, but this was for a single exploration velocity of 17 mm/s. An important point about Fig. 11(b) is that normalisation results in an approximate superposition of the data. The mean values of the relative coefficient of friction as a function of the vibrational amplitude for all participants are presented in Fig. 12. There is not a systematic dependence on the applied normal force for the range examined.

4 Discussion

On the basis of FE modelling, it was argued that the reduction in friction for ultrasonic haptic displays could be ascribed to a ratchet mechanism in which engagement induces lateral deformation of the fingerprint ridges, or the contacting surface in the case of artificial probes, until the frictional mobilisation criterion is satisfied [4]. Thus during any vibration cycle, the friction is either (i) zero when there is a loss of contact or (ii) less than the slip value. The model was evaluated in the current work by calculating the influence of the vibrational amplitude for a range of exploration velocities and normal forces for *in vivo* and probe frictional data.

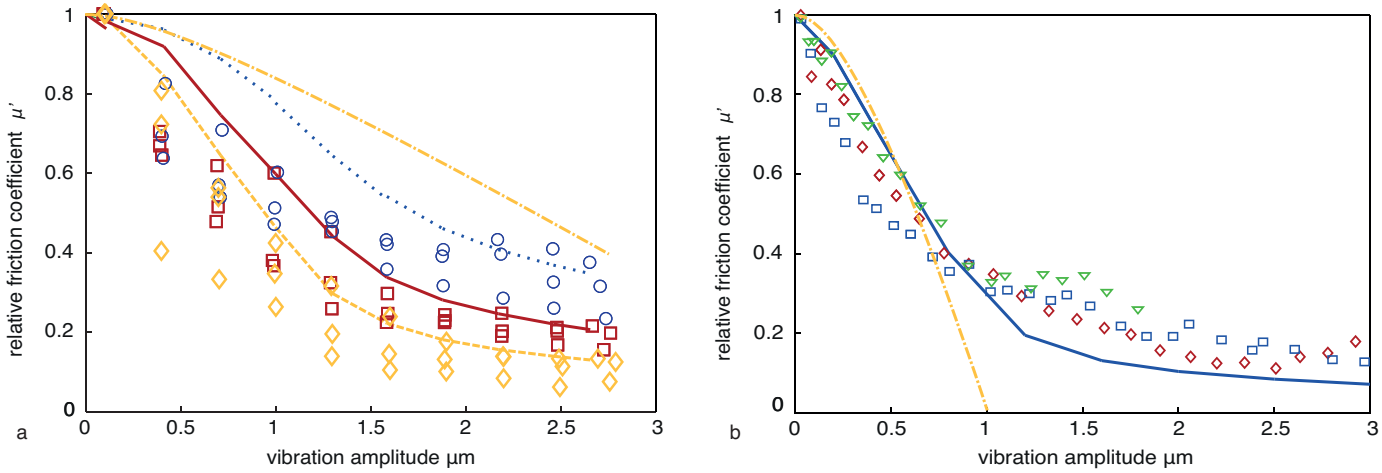

Fig. 11: (a) The relative coefficient of friction for p5 as a function of the vibrational amplitude at a frequency of 25.1 kHz, an applied normal force of 0.5 N and the following exploration velocities: 20 (yellow diamonds), 40 (red squares) and 80 (blue circles) mm/s. The dashed yellow line, red line, and blue dotted line are, respectively, the prediction of the FE model [4] of the friction reduction in the experimental condition. (b) Literature data for an applied normal force of 0.10N for three different subjects (red diamonds, blue squares, and green triangles), exploration velocity of 17 mm/s and the vibrational frequency of 25.1 kHz [8], compared with the FE model prediction (blue line) [4]. The yellow chain lines was calculated using the squeeze film model [6].

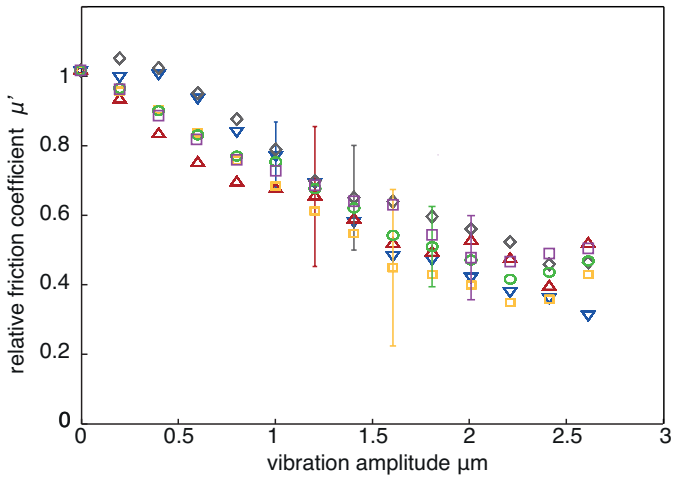

Fig. 12: Mean relative coefficient of friction for all participants (p1 - p6) as a function of the vibrational amplitude for the following applied normal forces: 0.2 (blue down triangle), 0.5 (red up triangle), 0.75 (grey diamonds), 1.0 (yellow squares, 1.5 (green circles), and 2 N (purple left triangles). The error bars indicate the mean standard deviation between the participants.

4.1 Mechanical Model Validation

4.1.1 *Velocity and Frequency Influence*

The calculated values of μ' with the FE model are compared with the experimental data in Fig. 11 and the trends in the numerical values are reasonably similar to those measured despite the model being relatively simple. The self-consistency of the FE results and the dimensionless group derived from the spring-slider model was demonstrated by showing that this group could be used to satisfactorily superimpose the numerical results applied to a finger pad [4]. However, at vibrational amplitudes smaller than ~ 1 μm the intermittent contact may be insufficiently developed for the friction not to be influenced by the Young's modulus of the *stratum corneum* and the applied normal force, depending on the vibrational frequency. This is the case for the reduced variables plot of the *in vivo* data given in Fig. 13. There is reasonable data superposition for vibration amplitudes > 1 μm and these data were fitted to the exponential function (2) with $\Psi^* = 4.69 \pm 0.32$ as shown in the figure. This value of Ψ^* is greater than that (2.38 ± 0.21) for the FE analysis of a finger pad, but it reflects the greater scatter of *in vivo* measurements of ultrasonic displays and, in particular, the small range of the dimensionless group that could be fitted. In comparison, using the probe, it is possible to achieve data superposition for a range of vibrational frequencies, and exploration velocities as well as vibrational amplitudes (Fig. 14) since the minimum vibrational amplitude is 1 μm. In this case, the value of is 0.70 ± 0.04.

It is of interest that the boundary condition assumption of $\mu = 0$ when $\Psi = 0$ in the derivation of Eq. (2) seems to satisfy the experimental data rather than a finite value of μ at $\Psi = 0$. This suggests that the performance of ultrasonic displays could be improved further by increasing the vibrational frequency to values that are greater than those examined in the current work, due to the dependence of Ψ on this variable.

4.1.2 *Influence of the Applied Normal Force*

Fig. 8 and the fit reported in Fig. 14 show that for the artificial fingertip there is no influence on μ' of the applied normal force, and consequently for the value of Ψ^*. However, as discussed previously, *in vivo* data are considerably more scattered and less reproducible as exemplified in Fig. 15 for two of the participants and a range of applied normal forces. A possible contributory factor is that the finger pads exhibited a wide range of Young's moduli so that not all

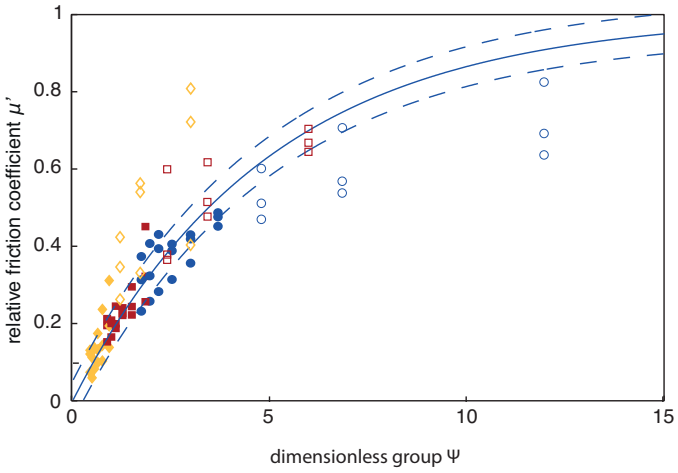

Fig. 13: Relative friction for participant p5 with an exploration velocity of 20 (yellow diamonds), 40 (red squares) and 80 mm/s (blue circles) as a function of the dimensionless group; the data are taken from Fig. 11(a). The full line is the best fits of the filled points to Eq. (2) and the value of Ψ^* is 4.69 $\pm$ 0.32; the unfilled points correspond to $w < 1\,\mu$m and were not included in the fit, as the dimensionless group is not relevant for small amplitude of vibration
. The dashed lines show the RMSE variation of the fit.

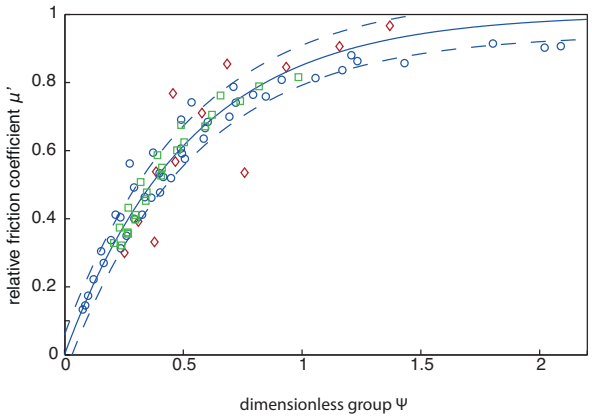

Fig. 14: The relative coefficient of friction as a function of the dimensionless group for the probe sliding on an ultrasonic vibrating plate with a range of vibrational frequencies (red diamonds), exploration velocities (blue circles) and applied normal forces (green squares) the data are taken from Figs 6, 7 and 8 respectively. The full lines are the best fits to Eq. (2) and the value of Ψ^* is 0.70 $\pm$ 0.04; the dashed lines correspond to the RMSE variation.

the data corresponded to the intermittent contact being sufficiently well developed. In such cases, the dimensionless group approach becomes inapplicable at smaller vibrational amplitudes. However, by taking mean values of the data for all participants (Fig. 12) and fitting to the exponential function, mean values of Ψ^* as a function of the applied normal force were obtained (Fig. 16). The figure shows the best fit to a linear relationship with a slope of -0.094 with 95% confidence bounds of -0.49 and 0.30 and an intercept of 1.80 with 95% confidence bounds of 1.34 and 2.27. Thus it may be concluded from these data that Ψ^* is not a strong function of the applied normal force and that the mean value of Ψ^* is reasonably consistent with that of the numerical data for which $\Psi^* = 2.38 \pm 0.21$ [4].

The FE model employed a Coulombic boundary condition:

$$F_l = \mu_0 F_{reac} \tag{6}$$

where F_l is the lateral force and F_{reac} is the normal reaction force of the vibrating plate. However, a finger pad exhibits non-Coulombic friction against smooth surfaces [12], [13]:

$$F_l = k_f F_{reac}^n \tag{7}$$

where k_f is the friction factor and n is the frictional load index with $2/3 \leq n \leq 1$. Consequently, Eq. (1) could be generalised as follows:

$$\Psi = \frac{U F_{reac}^n}{k_f w f \mu_0 (1+\nu)} \tag{8}$$

where k_{f0} is the intrinsic value of k_f. The data in Fig. 9 were fitted to Eq. (7) with $F_{reac} = F_n$ since the plate was in a static state, with k_f = 0.49 $\pm$ 0.02 and n =1.05 $\pm$ 0.08 for the 1st cycle and k_f = 0.52 $\pm$ 0.01 and n = 0.91 $\pm$ 0.05 for the 10th cycle. The dependence of the friction on the applied normal force may be understood because the friction of human skin is described by the adhesion mechanism [12]. That the value of n is approximately unity probably arises because the stainless steel plate used for the *in vivo* friction measurements is not optically smooth and it is known that topographically rough surfaces exhibit such Coulombic behavior [13].

In principle, the dimensionless group should be modified according to Eq. (8) but the current data strongly suggest that the *in vivo* and the artificial fingertip friction modulation is not a function of the applied normal force. Thus Eq. (1) is the better descriptor of the phenomenon for both *in vivo* and probe measurements. This is probably a consequence of the friction modulation being primarily governed by the deformation of the fingerprint ridges and the extent to which there is a loss in contact rather than being dominated by slip for which the adhesion mechanism would apply.

4.2 Squeeze Film Effect

The values of μ' calculated using the squeeze film model [6] are also shown in Fig. 11. The experimental data fit less closely and the model cannot account for the friction being a function of the exploration velocity. Moreover, these findings are consistent with the observation that the friction is not influenced by a reduced ambient pressure in the case of the artificial probe (Fig. 5). The interplay between the frictional ratchet mechanism demonstrated in this paper and the recent measurements suggesting a role of the squeeze film effect [14] is outside of the scope of the current work, and will be the subject of future investigations. Indeed, an initial study of the contribution of the squeeze film effect to the attenuation of friction was performed by Vezzoli et al. [15]. The result obtained in this study, which dealt with a real finger in reduced pressure, was a partial decrease in friction reduction as a function of the pressure. This behavior may suggest a combination of both effects. However,

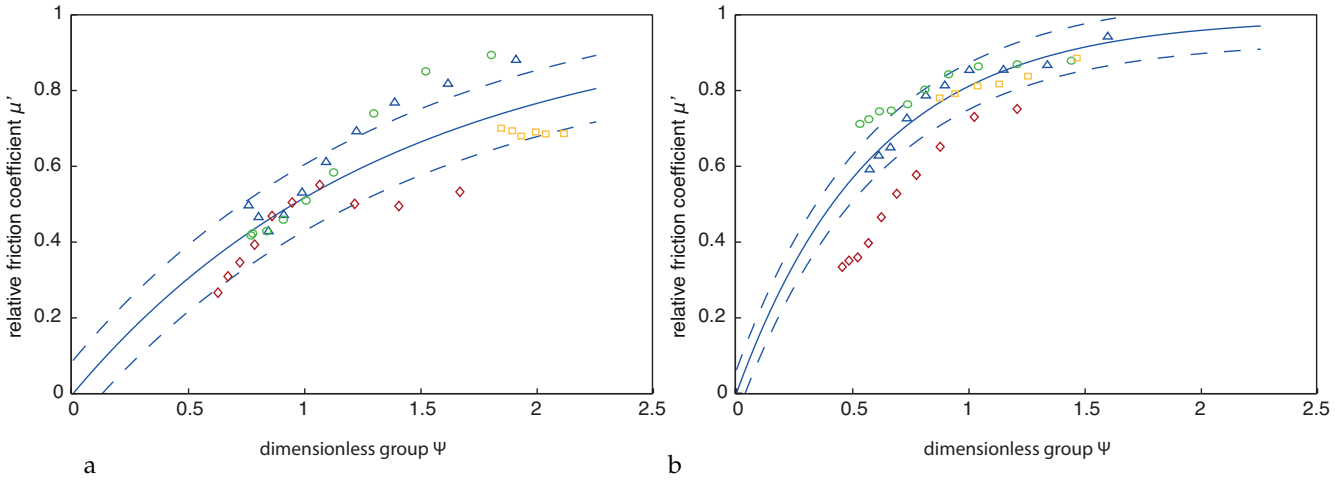

Fig. 15: The relative coefficient of friction as a function of the dimensionless group measured for two participants with an exploration velocity of 40 mm/s and a range of normal forces. (a) p2: 0.75 (red diamonds), 1 (blue triangle), 1.5 (green circles) and 2 N (yellow squares). (b) p3: 0.2 (red diamonds), 0.75 (blue triangle), 1 (green circle), and 2 N (yellow squares). The full lines are the best fits to Eq. (2) and values of Ψ^* equal to 1.89 ± 0.18 and 0.78 ± 0.046 respectively; the dashed lines correspond to the standard deviation of the fit to the exponential function (2).

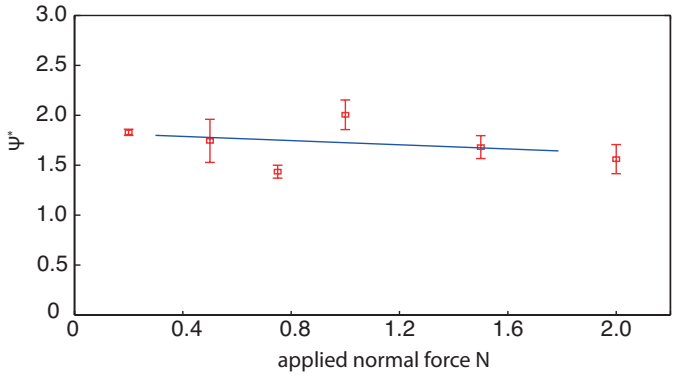

Fig. 16: The characteristic value of the dimensionless group as a function of the applied normal force calculated by fitting Eq. (2) to the data in Fig. 12. The line is the best linear fit to the data.

it was clear that the more refined methodology reported here is necessary to avoid complications due to the possible influence of the reduced pressure on the mechanical and frictional properties of the skin.

5 Conclusion

The current experimental data are consistent with the FE model developed in part 1 [4] and also the data superposition scheme derived in that work. Thus, the proposed ratchet mechanism is a satisfactory explanation for the friction modulation of ultrasonic displays. In particular, the friction modulation depends on the exploration velocity and is independent of the applied normal force and, in the case of the current probe, independent on the ambient air pressure. On the basis of the current work, it is not possible to quantify the relative contribution of squeeze film levitation. Data reduction using an exponential function of a dimensionless group shows a reasonable description of experimental data, provided that the intermittent contact is sufficiently well developed. This requires that the vibrational amplitude must be > 1 μm for the range of frequencies examined here. Another important point confirmed by this work is the influence of the vibrational velocity on the reduction of friction, not the simple vibrational amplitude (fw).

Acknowledgments

The Authors acknowledge FP7 Marie Curie Initial Training Network PROTOTOUCH (grant agreement No. 317100) for funding, and the IRCICA laboratory for hosting.

References

[1] M. Biet, G. Casiez, F. Giraud, and B. Lemaire-Semail, "Discrimination of virtual square gratings by dynamic touch on friction based tactile displays," in *Symposium on Haptic interfaces for virtual environment and teleoperator systems*, 2008, pp. 41–48.

[2] X. Dai, J. Colgate, and M. Peshkin, "LateralPaD: A surface-haptic device that produces lateral forces on a bare finger," in *2012 IEEE Haptics Symposium (HAPTICS)*, Mar. 2012, pp. 7–14.

[3] R. Fenton Friesen, M. Wiertlewski, and J. E. Colgate, "The role of damping in ultrasonic friction reduction," *IEEE - Haptic Symposium 2016*, pp. 167–172.

[4] E. Vezzoli, Z. Vidrih, V. Giamundo, B. Lemaire-Semail, F. Giraud, T. Rodic, D. Peric, and M. Adams, "Friction reduction through ultrasonic vibration: Part 1: Modelling intermittent contact and friction reduction," *Submitted to IEEE Transaction on Haptics*, 2016.

[5] T. Watanabe and S. Fukui, "A method for controlling tactile sensation of surface roughness using ultrasonic vibration," in *IEEE International Conference on Robotics and Automation, Proceedings*, vol. 1, May 1995, pp. 1134–1139 vol.1.

[6] M. Biet, F. Giraud, and B. Lemaire-Semail, "Squeeze film effect for the design of an ultrasonic tactile plate," *IEEE Transactions on Ultrasonics, Ferroelectrics, and Frequency Control*, vol. 54, no. 12, pp. 2678–2688, Dec. 2007.

[7] C. Winter, "Friction feedback actuators using squeeze film effect," Ph.D. dissertation, Ecole Polytechnique Federale de Lausanne, 2014.

[8] T. Sednaoui, E. Vezzoli, B. M. Dzidek, B. Lemaire-Semail, C. Chiappaz, and M. Adams, "Experimental evaluation of friction reduction in ultrasonic devices," in *IEEE - World Haptics Conference 2015*, 2015, pp. 37–42.
[9] W. Ben Messaoud, B. Lemaire-Semail, M.-A. Bueno, M. Amberg, and F. Giraud, "Closed-loop control for squeeze film effect in tactile ttimulator," *Actuator 2014*.
[10] L. Winfield, J. Glassmire, J. Colgate, and M. Peshkin, "T-pad: Tactile pattern display through variable friction reduction," in *EuroHaptics Conference and Symposium on Haptic Interfaces for Virtual Environment and Teleoperator Systems. World Haptics 2007. Second Joint*, 2007, pp. 421–426.
[11] R. Fenton Friesen, M. Wiertlewski, M. A. Peshkin, and J. E. Colgate, "Bioinspired artificial fingertips that exhibit friction reduction when subjected to transverse ultrasonic vibrations," *IEEE - World Haptics Conference 2015*.
[12] M. J. Adams, S. A. Johnson, P. Lefèvre, V. Lévesque, V. Hayward, T. André, and J.-L. Thonnard, "Finger pad friction and its role in grip and touch," *Journal of The Royal Society Interface*, vol. 10, no. 80, 2012.
[13] B. M. Dzidek, M. Adams, Z. Zhang, S. Johnson, S. Bochereau, and V. Hayward, "Role of occlusion in non-Coulombic slip of the finger pad," in *Haptics: Neuroscience, Devices, Modeling, and Applications*, ser. Lecture Notes in Computer Science, M. Auvray and C. Duriez, Eds. Springer Berlin Heidelberg, Jan. 2014, pp. 109–116.
[14] M. Wiertlewski, R. Fenton Friesen, and J. E. Colgate, "Partial squeeze film levitation modulates fingertip friction," *Proceedings of the National Academy of Sciences*, vol. 113, no. 33, pp. 9210–9215, 2016. [Online]. Available: http://www.pnas.org/content/113/33/9210.abstract
[15] E. Vezzoli, W. Ben Messaoud, F. Giraud, and B. Lemaire-Semail, "Pressure dependence of friction modulation in ultrasonic devices," *World Haptics Conference (WHC)*, 2015.

Thomas Sednaoui Sednaoui got a double MS degree in aerospace engineering from IPSA (Paris, France) and SAU University (Shenyang, China) in 2010. He worked at the European Space Agency (ESA) - Telerobotic & Haptic Lab to develop exoskeletons haptic system for teleoperation for ISS Experiment. From October 2013 he is employed by STMicroelectronics and doing his PhD Thesis with the ITN Prototouch Project. His research focuses on the understanding and industrialisation of ultrasonic devices.

Eric Vezzoli got his MS degree in Physics Engineering from the Politecnico of Milan (Italy) in 2013. From September 2013 he is research assistant at L2EP-IRCICA Laboratory working on his PhD Thesis with the ITN Prototouch Project. His domain of research are tactile stimulation principle modelling, tactile display designing and tactile perception.

Brygida Dzidek Studied Materials Science Engineering from the University of Silesia (Poland). She gained research experience working in Swiss Federal Laboratories for Materials Science and Technology (EMPA) developing new biomaterials and electro-ceramic composites. From September 2013 she is a Research Fellow in the School of Chemical Engineering at Birmingham University carrying out her work within the EU funded ITN Prototouch.

Betty Lemaire-Semail received the Ph.D. degree in 1990 from the University of Paris XI, Orsay. From 1990 to 1998, she was an assistant professor at the Ecole Centrale of Lille and she is now a professor at the University Lille 1. Her main field of interest now deals with the modeling and control of piezoelectric actuators for positioning and force feedback applications.

Cedrik Chappaz Cedrick Chappaz obtained his PhD degree of Physics from Universit de Besanon in 2003. He held various positions inside R&D department from STMicroelectronics, semiconductor company. Since 2015, he is CEO of HAP2U, a company delivering ultrasonic solutions for touch interfaces.

Michael Adams was awarded a PhD in molecular acoustics from the University of Essex, UK andis Professor of Product Engineering and Manufacturing in the School of Chemical Engineering at the University of Birmingham, UK since 2004 and was previously a Senior Scientist with Unilever R&D. He is a Fellow of the UK Royal Academy of Engineering. He was the recipient of the Donald Julius Groen Prize (IMechE) for outstanding achievements in interfacial engineering. His research interests include the friction of human skin and applications to tactile sensors and displays.

Chapter Three

Part 3: Role of fingerprint mechanics and non-Coulombic friction in ultrasonic devices.

Eric Vezzoli[1], Thomas Sednaoui[2], Brygida Dzidek[3], Cedrick Chappaz[2], Michael Adams[3], Betty Lemaire-Semail[1]

[1] L2EP-IRCICA Laboratory, University of Lille 1, Lille, France

[2] L2EP-IRCICA and STMicroelectronics, Crolles F38920, France

[3] School of Chemical Engineering, University of Birmingham, Birmingham B15 2TT, UK

Authors' contributions

TS, EV and BD designed and coordinated the study and drafted the manuscript; BD, TS and EV performed the experiments and conducted the data analysis; MJA, BLS and CC participated in the statistical analysis. All authors made substantial contributions to the critical revision of the submitted manuscript.

Role of Fingerprint Mechanics and non-Coulombic Friction in Ultrasonic Devices

Conference Paper · June 2015

DOI: 10.1109/WHC.2015.7177689

CITATIONS
6

READS
65

6 authors, including:

Eric Vezzoli
GoTouchVR
18 PUBLICATIONS **39** CITATIONS
SEE PROFILE

Brygida Dzidek
University of Birmingham
5 PUBLICATIONS **19** CITATIONS
SEE PROFILE

Thomas Sednaoui
STMicroelectronics
6 PUBLICATIONS **18** CITATIONS
SEE PROFILE

Michael J Adams
University of Birmingham
58 PUBLICATIONS **1,093** CITATIONS
SEE PROFILE

Role of Fingerprint Mechanics and non-Coulombic Friction in Ultrasonic Devices *

Eric Vezzoli, Brygida Dzidek, Thomas Sednaoui, Frédéric Giraud, *Member, IEEE,*
Michael Adams, and Betty Lemaire-Semail, *Member, IEEE*

***Abstract*— Ultrasonic vibration of a plate can be used to modulate the friction of a finger pad sliding on a surface. This modulation can modify the user perception of the touched object and induce the perception of textured materials. In the current paper, an elastic model of finger print ridges is developed. A friction reduction phenomenon based on non-Coulombic friction is evaluated based on this model. Then, a comparison with experimental data is carried out to assess the validity of the proposed model and analysis.**

I. Introduction

Current touch based user interfaces lack natural or at least credible haptic feedback, for example, when interacting with a virtual keyboard, which was one of the main issues during the initial commercialization of smartphones. Haptic interaction is still limited to the vibration of the whole device, but is ineffective in recreating the sensation expected from an image on the screen. Few approaches have shown a realistic potential for coupling with the flat capacitive position sensing displays that are employed in consumer devices. One involves the use of a lateral vibrating surface to simulate the vibrotaction signal of the fingertip induced by sliding over a real texture [1]. Another is based on the modulation of the friction between a sliding finger and the active surface. The possibility of tracking the position of a finger led to the generation of a spatio-temporal relationship that is useful for simulating texture [2]. Stimulating the whole fingertip area in the same manner led to the classification of this approach as global stimulation. Electrovibration and ultrasonic vibration are the two leading technologies for coupling with capacitive touch screens. The former is based on the polarization of the finger pad with a high voltage supplied plate covered with an insulator [3]–[5], the resulting attractive force results in an increased friction while interacting with the display. The latter involves out-of-plane ultrasonic vibration to attenuate the friction between the contacting finger pad and the display. The generation of a squeeze film effect between a vibrating plate and the finger pad was the first mechanistic interpretation [6], [7]. It relied on a simplified model of the interaction between two smooth rigid surfaces because of the enormous complexity of a real finger pad-display interaction e.g. the large range of Knudsen numbers involved and the viscoelastic deformation of a finger pad. There is evidence that squeeze flow is an important contributory factor [8] but an analysis of the mechanical and tribological interactions between a finger pad and an ultrasonic vibrating plate has never been performed. This is essential because the coefficients of friction associated with such devices can be > 0.1, which is greater than that which would be expected by an effective acoustic levitation mechanism (< 0.01); intermittent finger pad contacts have been confirmed recently [9]. The aim of the current work is to introduce a first order mechanical model of the finger pad that is applicable to the ultrasonic domain. Firstly, The mechanical interplay between the proposed model with a lateral vibrating ultrasonic plate is evaluated and a psychophysical assessment is proposed to assess the relevance of the approach. Secondly, the interaction with a normal ultrasonic vibrating plate is analyzed and the reduction in the friction with a smooth surface is estimated.

II. Finger Pad Tribology

Provided that a finger pad is sufficiently moist, particularly due to occlusion of moisture secreted from the sweat pores in the finger print ridges when in contact with a smooth impermeable surface such as glass, the friction may be described by stochastic molecular theories that have been developed for elastomers [10]. Friction arises from the intermittent extension and rupture of molecular junctions at the sliding interface, which involves dangling macromolecular chains; such bonds are continually pinning and depinning due to thermal activation. A characteristic of elastomers is that they exhibit aging such that the adhesion to a rigid substrate increases with the dwell time. This arises because molecular rearrangements occur at the interface and the associated relaxation times are coupled to those for pinning. Thus disruption of the pinning process will result in a reduction of the friction. Frictional aging for finger pads is an extreme example that occurs over tens of seconds due to the plasticization of the asperities on the finger pad ridges by the secreted moisture, which results in an increase in the contact area [11]. It is reasonable to suppose that this is accompanied by aging associated with the formation of molecular bonds.

* This work was funded by the European Union under the FP7 programs FP7-PEOPLE-317100 PROTOTOUCH.

E. Vezzoli, F. Giraud and B. Lemaire-Semail are with L2EP-IRCICA Laboratory, University of Lille 1, Lille, France, 59650 (phone: +33 362531632; e-mail: eric.vezzoli@ed.univ-lille1.fr, frederic.giraud@polytech-lille.fr, betty.semail@polytech-lille.fr).

B. Dzidek and M. Adams are at the School of Chemical Engineering, University of Birmingham, Edgbasto, B152TT, United Kingdom (e-mail: b.m.dzidek@bham.ac.uk, m.j.adams@bham.ac.uk).

T. Sednaoui is with L2EP-IRCICA and STMicroelectronics, Crolles F38920, France (e-mail: thomas.sednaoui@st.com).

III. Lateral Ultrasonic Vibrations

A. Introduction

In this section, the influence of lateral vibration on a finger pad under a small tangential load, which is less than that required for slip, is considered. It is proposed that the friction is reduced by micro-slip due to the disruption of the molecular bond network. Such slip requires the elastic retractive force induced in the finger pad by the periodic displacement to be greater than the frictional force. It is probable that, at low vibrational frequencies, this displacement will be completely accommodated by the gross deformation of the finger pad. However, the finger pad is viscoelastic so that the stiffness increases with frequency [12]; at sufficiently high frequencies it will be assumed that (a) the response is entirely elastic and (b) the finger pad is sufficiently rigid that the deformation is localized to the finger print ridges.

B. Bed of springs approximation

The elastic response of a finger pad will be modelled as a bed of springs as shown schematically in Fig. 1. The springs may be treated as finger print ridges for current purposes.

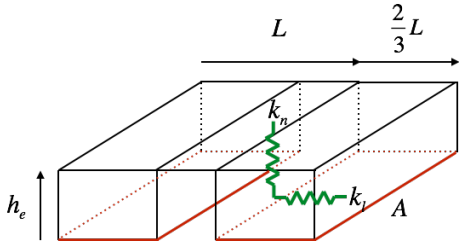

Figure 1: Bed of springs model.

The normal stiffness, k_n, is defined by:

$$k_n = \frac{E_e A}{h_e} \tag{1}$$

where E_e is the Young modulus of the *stratum corneum*, A is the contact area between the plate and the ridges and h_e is the undeformed height of the ridges. The tangential stiffness, k_l, is defined by:

$$k_l = \frac{G_e A}{h_e} \quad \text{and} \quad G_e = \frac{E_e}{2(1+\nu)} \tag{2}$$

where G_e is the shear modulus and ν is the Poisson modulus of the ridges. The dependence of A on the normal force, F_n, is assumed to be:

$$A = k(F_n)^{\frac{2}{3}} \tag{3}$$

where k is equal to $138.1\ \mathrm{mm^2/N^{\frac{2}{3}}}$ (this value is the result of a best fit to the experimental data reported in [13]).

TABLE I

Parameters Value

	Parameter	Value
i	E_e	1 MPa
ii	ν	0.4
iii	h_e	150 µm
iv	ρ	900 Kg/m^3

The other parameters considered in the analysis are given in table 1. Thus, the value of k_l could be calculated from (2) using that of A obtained from (3).

C. Modelling slip

The criteria for stick and slip are given by the following expressions:

$$k_l \Delta x_{max} \le \mu_s F_n \qquad \text{No slip} \tag{4}$$

$$k_l \Delta x_{max} > \mu_d F_n \qquad \text{Slip}$$

where Δx_{max} is the maximum displacement of the springs induced by the lateral vibrating plate, μ_s is the static coefficient of friction and F_n is the applied normal force across the bed of springs. If the slip condition is satisfied, there is relative displacement when $k_l \Delta x > \mu_s F_n$ until the relative velocity between the finger pad and the plate is zero, $V = 0$, Fig. 2. In the represented case, μ_s is 1, the dynamic coefficient of friction μ_d is 0.7, and the applied normal force is 0.5 N. The calculation ignores the offset tangential preload force, which could not be measured in the current work. If it is greater than the force induced by the periodic displacement, then no slip will occur in the direction of the offset force and slip will be enhanced in the other direction, so that the model will correspond to a lower bound solution. In Fig 2, the case for an ultrasonic harmonic vibration of 20 kHz of 5 µm for an applied force of 0.5 N is represented.

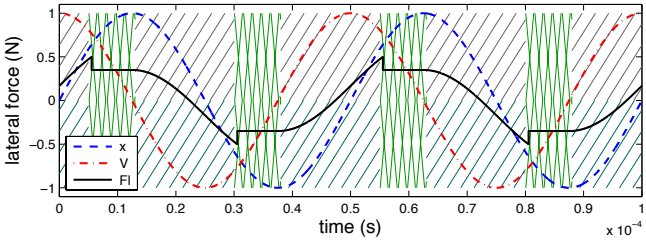

Figure 2: Steady state lateral sliding where x is the normalized position of the plate, V is the normalized speed of the plate and F_l is the lateral force experienced by the finger. In the gray shaded area, the relative motion between the ridges and the plate is zero. In the green crossed area the finger is sliding on the plate.

A glide threshold is defined as the minimum amplitude of vibration necessary to induce a transition from stick to slip as represented in Fig. 2:

$$\Delta x_t = \frac{\mu_s F_n}{k_l} \tag{5}$$

where Δx_t is the critical threshold displacement. The contact area between the finger pad and the plate is dependent on the

applied normal force (3) and this dependence influences the value of k_l (2). It is possible to compute the dependence of the threshold displacement on the applied normal force by solving (4) for small time steps to calculate the associated lateral displacements, δx, with the limit defined by (5) as shown in Fig. 3a.

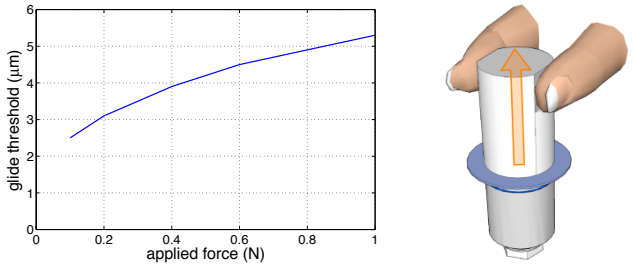

(a) (b)

Figure 3: Glide threshold as a function of the applied force (a) and experimental setup for psychophysical evaluation (b).

D. Psychophysical validation

1) Experimental setup

In order to validate the model, it is necessary to evaluate the induced tactile response of a lateral vibrating plate. A Langevin actuator (FBL28302SSF-FC, Fuji Ceramics Corporation, Japan) was employed with a closed-loop vibration amplitude stabilization system to ensure the stability of the vibration amplitude during the experiment. The employed actuator has a resonance frequency of 27.83 kHz at ambient temperature. The control of the piezoelectric actuator was implemented with piezoceramic sensor glued on the body. A DSP (EZDSPF2812, Texas Instrument, USA) were programmed do obtain the desired behavior of the device. The actuator has two parallel surfaces at the top of the device (2x1.4 cm^2) on both sides for making contact with the finger pad, Fig 3b.

2) Methododolgy and results

Four participants (male, age between 26 and 41) were asked to describe their tactile perception while holding the actuator as in Fig. 3b for vibrational amplitudes of 0, 2 and 4 μm after imposing a small tangential force on the vibrator that was insufficient to induce gross slip. All participants gave their informed consent to perform the experiment. They were equipped with a headset to cancel the influence of environmental noise and they were asked to close their eyes during the experiments. The frequency of the stimulation was the resonance of the actuator at 27.83 kHz. The amplitudes of vibration were changed randomly and the participants reported their corresponding tactile evaluation. None of the participants could identify a difference between the 2 μm amplitude and the static condition. However, all reported a sensation of slip for an amplitude of 4 μm with comments such as "it felt more slippy." This amplitude corresponds to the glide threshold for an applied normal force of about 0.4 N, which is typical of the values used in touch [13].

IV. Normal Vibrations

A. Introduction

In this section, the interaction of the proposed model with a normal vibrating plate is proposed, and the friction reduction arising from the interaction with a smooth surface is estimated. It has been shown that an ultrasonic vibrating plate in the normal direction can induce intermittent contact with a finger pad for vibrational amplitudes of a few micrometres [9]. This attach/detach phenomenon could lead to a friction reduction during the sliding motion of the finger due to the influence on the interfacial molecular bonding interactions in addition to the development of a gaseous squeeze film. Here, the loading/unloading cycle of a finger pad again will be represented by a bed of equivalent elastic springs to investigate the mechanism in more detail. A key factor is that the detachment will lead to rupture of the interfacial bonds and thus finite time is required for repinning. It is assumed that the viscoelastic retardation time of the finger pad is infinitely long during the unloading cycle of an out-of-plane imposed vibration compared to the reciprocal frequency of the vibration. The finger print ridges are much stiffer than the finger pad and also it is assumed that they will behave elastically during unloading.

B. Bed of springs model

Following a compression cycle of a continuous out-of-plane vibration, the springs will unload and detachment will require the vibration amplitude to be greater than the unloaded length of the spring. The critical amplitude to induce detachment, W_c, is given by the following expression for the current model:

$$W_c = \Delta z_n = \frac{F_n}{k_n} \tag{6}$$

where Δz_n is the compression induced by the normal load and k_n was calculated from (1). The dependence of the necessary vibrational amplitude to induce detachment of the fingertip as a function of the applied force in the range relevant to touch is reported in Fig 4. The analysis is valid for frequencies greater than 20 kHz.

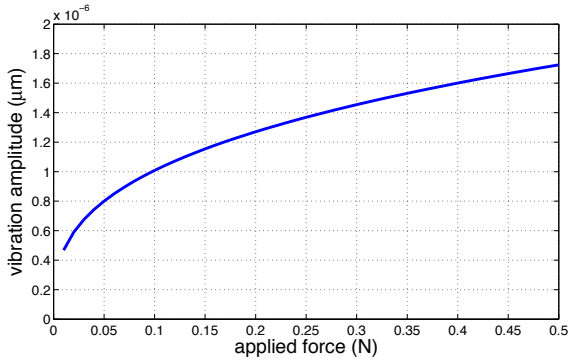

Figure 4: Detach condition of the fingerprint in function of the applied force: as an example, for 0.15 N applied a vibration amplitude of 1.2 μm are required to induce detachment.

C. *Non- Coulombic friction*

In the previous section, it was shown that detachment was possible for a range of normal vibrational amplitudes that are compatible with those commonly employed in ultrasonic devices. Assuming that there is not frictional aging, then it is possible to calculate the minimum effect on the periodic frictional force by taking account of the fact that the coefficient of friction decreases with increasing normal force for smooth surfaces [11]; this analysis is relevant for the possible application of the principle to the screen of smartphone and tablets. Finally, a comparison with experimental data will be made to examine the significance of the phenomenon.

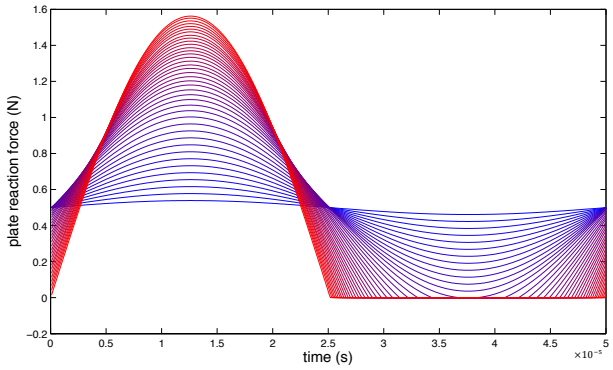

Figure 5: Plate reaction force as a function of the time over a vibration cycle for different vibrational amplitudes. The amplitude of vibration varies from 0.1 µm (blue) to 8 µm (red). During the detachment of the springs from the plate, the plate reaction force is zero.

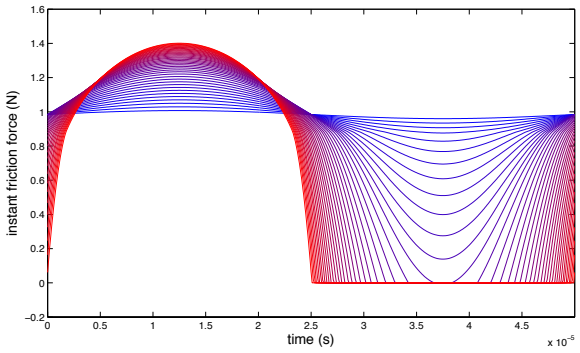

Figure 6: Instantaneous frictional force as a function of the time over a vibration cycle for different vibrational amplitudes. The amplitude of vibration varies from 0.1 µm (blue) to 8 µm (red). During the detachment of the springs from the plate, the frictional force is zero.

At equilibrium, the integral of the imposed force from the the bed of springs must be equal to the total reaction force of the plate over a vibration cycle:

$$\int_{cycle} F_{reac} dt = F_n T \tag{7}$$

where F_{reac} is the normal reaction force of the plate in contact with the springs and T is the vibrational period of the plate. The vibration of the plate is described by $\phi \sin(2\pi f t)$, where ϕ is the vibrational amplitude and f is the frequency. In this case, the frequency is 20 kHz leading to a period of 50 µs. With this relationship it is possible to compute the instantaneous compressive force, F_{reac}, of the springs induced by the vibrating plate; the case shown in Fig. 5 is for an applied normal force of 0.5 N. The corresponding frictional force, $\mu_d F_{reac}$, is plotted in Fig. 6. It may be seen that the contact is frictionless for an increasing proportion of the unloading cycle as the amplitude of vibration increases.

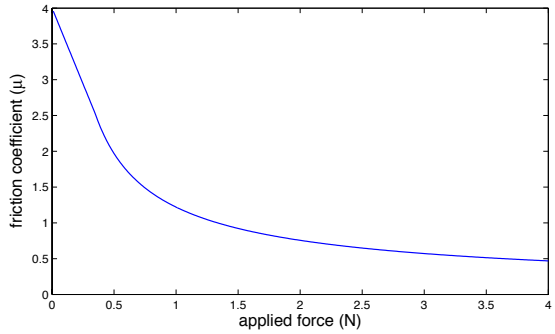

Figure 7: Coefficient of friction between a finger pad and a smooth surface as a function of the applied normal force [11].

The radial contact pressure profile for a finger pad in contact with a smooth flat plate is not uniform as assumed above but can be approximated by the Hertzian function:

$$P(r) = \frac{3}{2}\frac{F_n}{\pi b^2}\sqrt{1 - \frac{r^2}{b^2}} \tag{8}$$

where b is the radius of contact and r is the radial coordinate with an origin at the center of contact. From a knowledge of $P(r)$, it is possible to integrate the reaction force across the contact over the cycle period and hence compute the mean normal force as a function of time. The frictional force can then be calculated from the following integral:

$$F_l = \int_0^b \mu_d(F_{reac}) P(r)\, \pi^2 dr \tag{9}$$

where μ_d is a function of the normal force as given in Fig. 7. Fig. 8 shows that the calculated value of the relative coefficient of friction, $F_l(\phi)/F_l(0)$, decreases with increasing vibration amplitude.

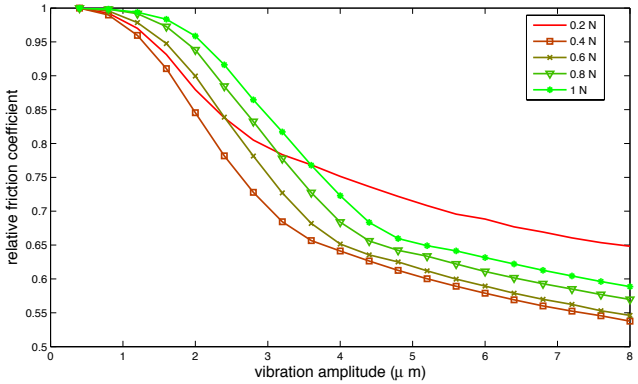

Figure 8: Relative coefficient of friction as a function of the vibrational amplitude induced by the non-linearity of the coefficient of friction.

D. *Experimental comparison*

It was possible to compare the simulated friction reduction recovered by this method with experimental data taken from [14] to highlight the compatibility of the effect with the general results observed for ultrasonic devices. In that work, the friction reduction induced by the normal ultrasonic vibrating device has been measured with a tribometer for different index fingers and for different loads applied. Fig. 9 shows a comparison of the reduction in the coefficient of friction measured for three fingers with an applied normal force of 0.35 N for different vibrational amplitudes. The model predicts the trend of decreasing friction with increasing amplitude as observed experimentally.

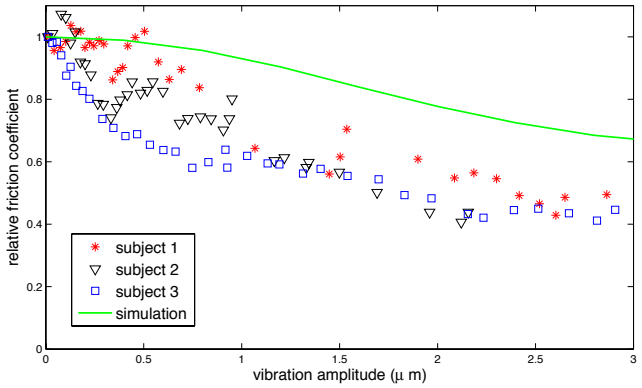

Figure 9: Experimental comparison between the modeled phenomena and experimental results taken from [14] for normal vibration; the considered frequency was 25 kHz.

V. Discussion

The proposed elastic model is a considerable simplification of the real system, but nevertheless can explain part of the behavior of a finger pad sliding over an ultrasonic vibrating plate. The reduction in friction has been used for the creation of different tactile stimulators [15], [16], but the underlying mechanisms are still unresolved. The squeeze film effect has been shown to be a contributory factor [9] but the behavior of the friction modulation is not in complete agreement with the analysis proposed in [6], which suggests that there are other concomitant contributions. The currently proposed elastic model of the fingerprint ridges is consistent with a psychophysical assessment of the influence of lateral ultrasonic vibrations. In particular, it is clear that ultrasonic perturbation frequencies are essential to induce a sufficiently stiff response of the finger pad and also cause micro-slip in a temporal domain that is at least comparable to the times required to thermally reactivate a molecular junction. Published values of such times are sparse but it is interesting that, for thin molecular layers in aqueous media, repinning times are ~ 200 μs [17], which is comparable to the period (50 μs) of the vibrational frequency (20 kHz).

In the case of normal vibrations, the results of the model are consistent with the trends observed experimentally [9]. Taking account of the non-linearity of the coefficient of friction was an important factor in the model. Again, high frequencies are a prerequisite for ensuring that the gross retardation time of the finger pad is much longer than the cycle time of the vibration. While the reduction in friction calculated with the current model was based on the separation time between a finger pad and a virtual vibrating plate, ultrasonic frequencies will induce a synergistic effect of ensuring that the disrupted molecular junction network remains at least partially disrupted even during contact. This would result in a further reduction in the coefficient as well as a possible contribution from a squeeze flow effect. It is also possible that an additional effect could be attributed to a reduction in the occlusion arising from the secreted moisture from the sweat pores (*deocclusion*). Essentially, the intermittent loss of contact could allow some moisture to diffuse from the contact region and hence result in asperity hardening compared with a continuous intimate contact

Simple models of the type described in the current work are useful in order to establish key principles for formulating models that are more complete. The non-linear viscoelastic behavior of the finger pad is particularly relevant since it controls the gross temporal response of the finger pad. In addition, it is important to consider the details of the contact mechanics because detachment involves radial crack propagation in which an annulus of failure grows from the periphery of a contact [13]. Consequently, different mechanisms may dominate across the contact region e.g. the squeeze flow mechanism may be localized at the periphery of the contact.

VI. Conclusions

A simple model of the interaction of a finger pad with a plate vibrating at ultrasonic frequencies, which is based on representing the finger print ridges as elastic springs, captures some of the critical factors that govern the performance of vibrational haptic displays. In particular, it is concluded that ultrasonic frequencies are essential for ensuring that the finger pad is sufficiently stiff to cause periodic contact separation for out-of-plane vibrations. More work is required to establish the relative contributions of this mechanism, squeeze flow and deocclusion. For both normal and lateral vibrations, it also necessary to consider the disruption of the network of molecular junctions that are responsible for friction.

VII. Acknowledgements

The authors would like to thank Sofiane Ghenna for the useful assistance with the piezoelectric actuator.

References

[1] M. Wiertlewski, J. Lozada, and V. Hayward, "The Spatial Spectrum of Tangential Skin Displacement Can Encode Tactual Texture," IEEE Trans. Robot. vol. 27, no. 3, pp. 461–472, Jun. 2011.

[2] M. Biet, G. Casiez, F. Giraud, and B. Lemaire-Semail, "Discrimination of Virtual Square Gratings by Dynamic Touch on Friction Based Tactile Displays," in *symposium on Haptic interfaces for virtual environment and teleoperator systems, 2008.* pp. 41–48.

[3] E. Vezzoli, M. Amberg, F. Giraud, and B. Lemaire-Semail, “Electrovibration Modeling Analysis,” in Haptics: Neuroscience, Devices, Modeling, and Applications, M. Auvray and C. Duriez, Eds. Springer Berlin Heidelberg, 2014, pp. 369–376.
[4] O. Bau, I. Poupyrev, A. Israr, and C. Harrison, “TeslaTouch: Electrovibration for Touch Surfaces,” in Proceedings of the 23rd Annual ACM Symposium on User Interface Software and Technology, New York, USA, 2010, pp. 283–292.
[5] K. A. Kaczmarek, K. Nammi, A. K. Agarwal, M. E. Tyler, S. J. Haase, and D. J. Beebe, “Polarity Effect in Electrovibration for Tactile Display,” IEEE Trans. Biomed. Eng., vol. 53, no. 10, pp. 2047–2054, 2006.
[6] M. Biet, F. Giraud, and B. Lemaire-Semail, “Squeeze film effect for the design of an ultrasonic tactile plate,” IEEE Trans. Ultrason. Ferroelectr. Freq. Control, vol. 54, no. 12, pp. 2678–2688, 2007.
[7] T. Watanabe and S. Fukui, “A method for controlling tactile sensation of surface roughness using ultrasonic vibration,” in, 1995 IEEE International Conference on Robotics and Automation. Proceedings, 1995, vol. 1, pp. 1134–1139 vol.1.
[8] W. Ben Messaoud, E. Vezzoli, F. Giraud, and B. Lemaire-Semail, “Pressure dependence of friction modulation in ultrasonic devices,” proposed in World Haptics Conference (WHC), 2015.
[9] X. Dai, J. E. Colgate, and M. A. Peshkin, “LateralPaD: A surface-haptic device that produces lateral forces on a bare finger,” in 2012 IEEE Haptics Symposium (HAPTICS), pp. 7–14.
[10] A. N. Gent, G. R. Hamed, and W. J. Hung, “Adhesion of elastomers: Dwell time effects,” J. Adhes., vol. 79, no. 4, pp. 315–325, Apr. 2003.
[11] B. Dzidek, M. Adams, Z. Zhang, S. Johnson, S. Bochereau, and V. Hayward, “Role of Occlusion in Non-Coulombic Slip of the Finger Pad,” in Haptics: Neuroscience, Devices, Modeling, and Applications, M. Auvray and C. Duriez, Eds. Springer Berlin Heidelberg, 2014, pp. 109–116.
[12] M. Wiertlewski and V. Hayward, “Mechanical behavior of the fingertip in the range of frequencies and displacements relevant to touch,” J. Biomech., vol. 45, no. 11, pp. 1869–1874, 2012.
[13] M. J. Adams, S. A. Johnson, P. Lefèvre, V. Lévesque, V. Hayward, T. André, and J.-L. Thonnard, “Finger pad friction and its role in grip and touch,” J. R. Soc. Interface, vol. 10, no. 80, p. 20120467, 2013.
[14] T. Sednaoui, E. Vezzoli, B. M. Dzidek, B. Lemaire-Semail, C. Chiappaz, and M. Adams, “Experimental evaluation of friction reduction in ultrasonic devices,” proposed in World Haptics Conference (WHC), 2015.
[15] M. Amberg, F. Giraud, B. Semail, P. Olivo, G. Casiez, and N. Roussel, “STIMTAC: A Tactile Input Device with Programmable Friction,” in Proceedings of the 24th Annual ACM Symposium Adjunct on User Interface Software and Technology, New York, NY, USA, 2011, pp. 7–8.
[16] L. Winfield, J. Glassmire, J. E. Colgate, and M. Peshkin, “T-PaD: Tactile Pattern Display through Variable Friction Reduction,” in s. World Haptics Conference (WHC), 2007, pp. 421–426.
[17] C. Drummond, J. Israelachvili, and P. Richetti, “Friction between two weakly adhering boundary lubricated surfaces in water,” Phys. Rev. E, vol. 67, no. 6, p. 066110, 2003.

Chapter Three

Part 4: Characterizing and imaging gross and real finger contacts under dynamic loading.

Séréna Bochereau[1],Brygida Dzidek[2], Michael Adams[2] ,Vincent Hayward[1]

[1] Sorbonne Universités, UPMC Univ Paris 06, UMR 7222, ISIR, F-75005, Paris, France.

[2] School of Chemical Engineering, University of Birmingham, Birmingham B15 2TT, UK.

Authors' contributions

SB and VH designed and coordinated the study and drafted the manuscript; BMD and SB performed the experiments and conducted the data analysis; MJA and VH participated in the analysis. All authors made substantial contributions to the critical revision of the submitted manuscript.

Characterizing and imaging gross and real finger contacts under dynamic loading

Séréna Bochereau, Brygida Dzidek, Michael Adams, and Vincent Hayward, *Fellow, IEEE*

Abstract—We describe an instrument intended to study finger contacts under tangential dynamic loading. This type of loading is relevant to the natural conditions when touch is used to discriminate and identify the properties of the surfaces of objects — it is also crucial during object manipulation. The system comprises a high performance tribometer able to accurately record *in vivo* the components of the interfacial forces when a finger interacts with arbitrary surfaces which is combined with a high-speed, high-definition imaging apparatus. Broadband skin excitation reproducing the dynamic contact loads previously identified can be effected while imaging the contact through a transparent window, thus closely approximating the condition when the skin interacts with a non-transparent surface during sliding. As a preliminary example of the type of phenomenon that can be identified with this apparatus, we show that traction in the range from 10 to 1000 Hz tends to decrease faster with excitation frequency for dry fingers than for moist fingers.

Index Terms—fingerprint imaging, bio-tribology, dynamic loading, tactile stimulation

1 Introduction

For almost a century it has been observed that our tactile system mostly extracts information about the substance and the surface details of objects during the sliding movements of the fingers [1], [2], [3], [4]. Unless a finger contact is nearly perfectly lubricated, the slip of a finger against most surfaces elicits complex oscillations. Steady sliding may occasionally be induced by lubrication from surfactants in aqueous solutions [5], [6], something that happens when we clean dishes with soapy water and experience difficulties feeling them. The more common case of the dry or moderately wet surfaces, however, is invariably associated with slip-induced oscillations.

These perceptually significant mechanical oscillations arise even if the counter-surfaces have roughnesses down to nanometer scales [7]. They are evident for asperities at micrometer scales [8], [9] and higher [10]. These observations justify the need to develop methods to characterise finger contacts under dynamic loading conditions, since such dynamic contacts are the rule rather than the exception during the tactile interaction with objects.

Since the observations of Gibson regarding human perceptual behaviour [11], it has been widely recognised that the information available from statically loading fingers and hands with objects has little perceptual value. There are three main types of informative finger contacts: when a finger interacts with an object causing a quasi-static evolution of its mechanical state, when a finger collides with a surface, and during sliding on a surface or at the onset of slip [12]. Only the latter two cases qualify as dynamic contacts.

The apparatus that was developed in the current work specifically addresses the study of dynamics contacts. The evolution of these contacts can be divided into epochs [13], [14], [15], [16], [7] which typically can be identified through two approaches. A first approach is through the bulk measurement of frictional forces. Such measurements require special instruments owing to the need to obtain a reliable response over a large frequency range, to viz., 500 Hz. A second approach is to image the contact of the finger through a transparent surface. While the bulk frictional response of a finger to movement is relatively easy to obtain in the quasi-static case, the evaluation of the mechanical consequences of the friction associated with a dynamic finger is more difficult. Thus far such characterisation was either obtained indirectly, either acoustically [17], through acceleration signals [18], [19], [20], remote velocimetry [10], or directly by imaging through transparent surfaces.

When a person explores a surface, skin tribology depends crucially on the spontaneous motor programs that are called upon for each type of surface and perceptual task. For example, seeking to detect a small asperity on a smooth surface, such as a micro-crack, will involve a very low tonic output, but the identification of the essence of a wood from its grain might evoke much greater activation. Replacing a complex surface with which the skin interacts by a rigid surface that oscillates in a complex manner, [21], is arguably a reasonable approximation to sliding on a complex surface. Consider that the propagation of mechanical waves in the skin is of the order of $10\,\mathrm{m\,s^{-1}}$, [22], which at 10 Hz corresponds to a wavelength of 1 m. At 1 kHz, the wavelength re-

S. Bochereau and V. Hayward are with Sorbonne Universités, UPMC Univ Paris 06, Institut des Systèmes Intelligents et de Robotique, Paris, France, Email: vincent.hayward@isir.upmc.fr.
B. Dzidek and M. Adams are with the school of Chemical Engineering, University of Birmingham, Birmingham, UK
Email: m.j.adams@bham.ac.uk

duces to 10 mm but at such frequencies viscous forces dominate, [23], and the skin may then be considered a rigid solid. It can be further observed through behavioural studies that the tangential component of the interaction force with an object is particularly rich in information concerning the texture roughness and shape of the surface topographical features making up the texture [24].

From the above observations we constructed an apparatus that can excite the skin tangentially with arbitrarily complex displacements in a wide frequency range, while simultaneously imaging the contact at high spatial and temporal resolutions. The apparatus can also measure the tribology of a finger sliding on arbitrary natural surfaces and can further ascertain that interfacial forces, which arise during exploration and during testing, are indeed equivalent. We present preliminary results and discuss their implications. Before doing so, we briefly review relevant contact imaging and tribological measurement techniques.

2 Related Work

2.1 Imaging finger contacts

A prism-based Frustrated Total Internal Reflection principle (FTIR), see Fig. 1, was adopted by Levesque and Hayward to image finger contacts with flat, raised, or indented surfaces [25]. This technique can produce high contrast images of the intimate contact of a finger with a transparent surface. It was possible to image the temporal evolution of the skin strain patterns in the contact region area during rotation and lateral movements. By examining changes in the triangulation of tracked skin features, they found that patterns of skin compression and expansion resulted from a combination of gross movements and surface features.

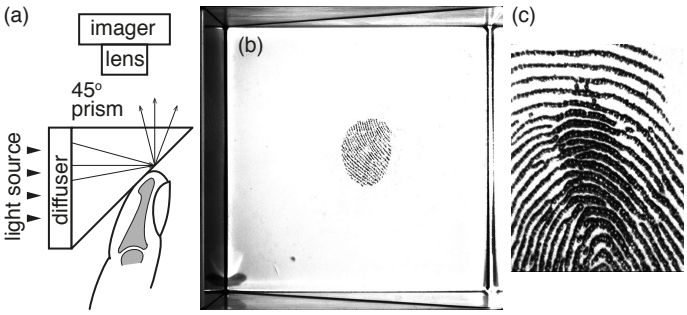

Fig. 1: (a) Prism-based Frustrated Total Internal Reflection principle. With a correctly designed diffuser, light entering the prism is completely reflected, yielding a bright background. Any object in intimate contact with the face of the prism at distances smaller than the wavelength of the light disrupts reflection locally. (b) High contrast images of the 'real' contact since objects distant from the surface by more than a few tens of nm will leave reflected light intact. (c) Transitions from sticking to sliding, see [26], can be directly observed since sliding ridges exhibit smaller contacts areas than sticking ridges.

Using the same device, André et al. found that the skin hydration level reduced the tendency of a contact to slip, irrespective of the variations of the coefficient of friction [15]. Delhaye et al., employing a similar technique, but with coaxial illumination to facilitate the movement of the counter-surface, observed the contact area evolution during the stick to slip transition in distal, proximal, radial and ulnar directions. This study examined the differences in the stick ratio and the contact area displacement with time or tangential force using an optical flow algorithm [27]. Coaxial illumination, however, produces lower contrast images than prism-based frustrated reflection since the background inter-ridge surfaces reflect significant light, but it has the advantage of giving images that do not required aspect-ratio correction.

Another very popular approach to take advantage of the Frustrated Total Internal Reflection principle is in a direct manner [28, Sec. 12.3], as shown in Fig. 2(a). Here, light is injected in a slab of glass acting as a light trap, giving a dark background when no object is in contact with it. When there is an intimate contact, reflection is also frustrated, but here some of the light escaping from the contact scatters and diffuses inside the finger tissues. Another portion escapes the trap, giving rise to an intensity graded image on a black background Fig. 2(b). Some of this light also reflects from the surfaces that are in close vicinity. In the image shown in Fig. 2(b), the bright spots visible inside the sweat ducts are probably the result of specular reflections of this light against menisci of exuding sweat, see Fig. 2(c). Wiertlewski et al. recently took advantage of this technique for imaging finger contacts at ultrasonic frequencies [29], which to our knowledge is the first example of *in vivo* finger contact imaging under dynamic loading, albeit in the normal direction.

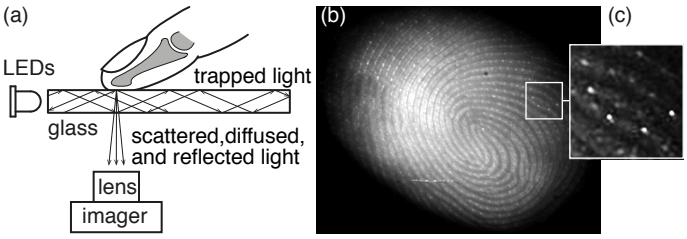

Fig. 2: (a) Imaging finger contacts using frustrated total reflection to scatter light at the points of contact. Illumination can be conveniently provided by LED devices. (b) The resulting image combines scattered, tissue-diffused, and reflected light. (c) Contrast enhanced area of detail shows specularities from sweat menisci.

Lastly, using direct illumination and image processing techniques to compensate for low contrast, Tada and Kanade showed that as the indentation depth/normal force increases, a large overall area is created, and that the stick region disappears faster as speed increases [30].

2.2 Finger Tribometry Against Natural Textures

Several tribometers exist that are capable of measuring finger tribology *in vivo* [31], [32], [33], [34], [35]. Some of

these devices are capable of measuring the interaction of a bare finger with a wide range of natural textures [36], [21], [37]. The particular design adopted herein, Fig. 3., was developed by Wiertlweski et al. [38] and adapted by Platkiewicz et al. to record natural textures [39]. Recently, Janko et al. described a high performance tribometer that was employed to identify a range of physical effects arising from the nonlinear nature of friction [40].

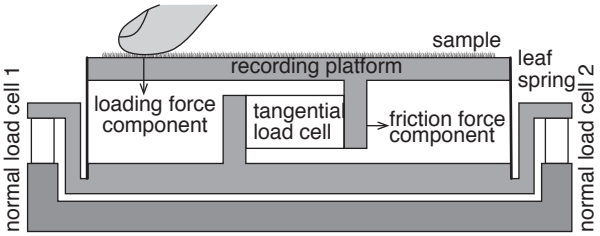

Fig. 3: Tribometer measuring tangential and normal components independently.

The present design features a very high ratio of interfacial forces component separation to ensure that normal loading and frictional forces are accurately measured. The leaf springs transmitting normal loads to the load cells have the feature of being 1000 times stiffer in the normal direction than in the tangential direction.

3 Apparatus

3.1 Requirements

The main challenge was to achieve force sensing with sufficient bandwidth, at least up to 500 Hz but ideally up to 1 kHz, in order to cover the temporal frequencies associated with scanning textures [41], [42]. In practice, this requirement reduces down to eliminating any sharply undamped modes from the mechanical structure at frequencies in the desired operating band that would be difficult to compensate by inverse filtering.

In terms of skin excitation, the requirements involved ensuring a stable and robust signal causality relationship between a transducer and a finger over a wide frequency band. One approach, the isotonic approach, is to arrange for the transducer to have a mechanical impedance that is much smaller than that of the finger and to measure displacements resulting from a known applied force. Such an approach is possible, [43], but difficult to implement here owing to the mass of the plate used to image the finger contact. The converse approach, the isometric approach, which is adopted here, is to arrange for the transducer to have an impedance that dominates that of the finger and to measure the force resulting from its displacement.

3.2 Design and Construction

The present tribometer design was optimised by constructing it from three single-block mechanical parts connecting the load sensors, achieving high rigidity. The sample holder platform was designed to be light and rigid. It was machined out of a single block of grade 2017 aluminium as depicted by Fig 4.

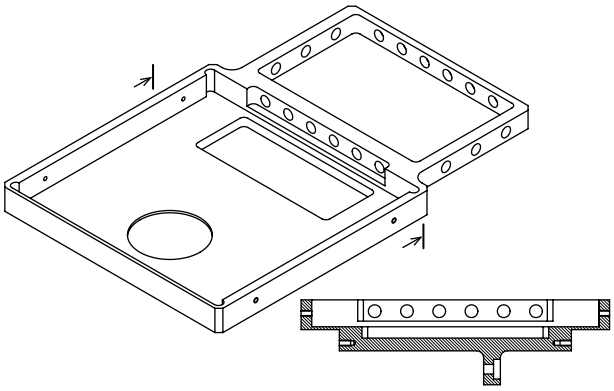

Fig. 4: Sample holder platform.

The lateral frame supported the skin excitation transducer, which was connected to it by a set of compliant leaf springs. The transducer was actuated by a contactless electrodynamic voice-coil motor (Model NCC01-07-001-1R, H2W, Santa Clarita, CA). It is represented schematically in Fig. 5. The plate in contact with the finger serves as a transparent imaging window. The imaging system is described in the next section.

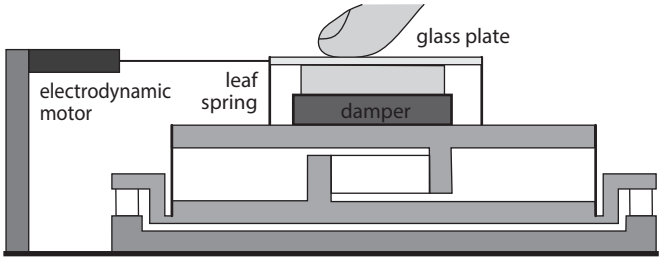

Fig. 5: Reproduction set-up with the sensors to mesure a finger-vibrating glass interaction.

The modal response of the sample holder platform was evaluated using an impact hammer to excite the structure (Low impact hammer type 086E80, PCB Piezotronics). The results revealed that the response was satisfactory with a first peak at 550 Hz due to the platform's cantilevered design, see Fig. 6. The tribometer's performance was reported in [7].

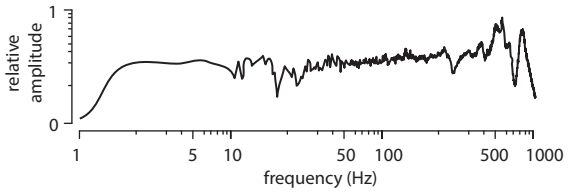

Fig. 6: Mechanical impulse response of the platform over 20 tests.

We adopted the guideline that the stiffness of the plate suspension and the damping coefficient should be of the same order as that of a fingertip while the moving mass

should be many times greater in order to achieve the required signal causality. This way, any force applied by the motor to the plate will be converted into an acceleration in a simple manner. In the lateral-medial direction, the mean bulk elasticity of human fingers is known to be about $1.0\,\mathrm{N\,mm^{-1}}$ and the damping coefficient of the order of $1.0\,\mathrm{N\,s\,mm^{-1}}$ [44]. These target figures were thus adopted. As a result of the mechanical properties of the finger, the amplitudes of the bulk oscillations during exploration can reach one or two millimetres, thus the transducer was designed to achieve these values when oscillating at different frequencies.

The springs were made from copper beryllium beams that were cut to give the required stiffness. The frame holding the moving glass plate was machined from magnesium for rigidity and low mass. To achieve the required damping, we designed a Foucault-current damper of a design similar to that described in [45]. The armature was made of two aluminium plates that moved without contact between pairs of magnets, as seen in Fig. 7.

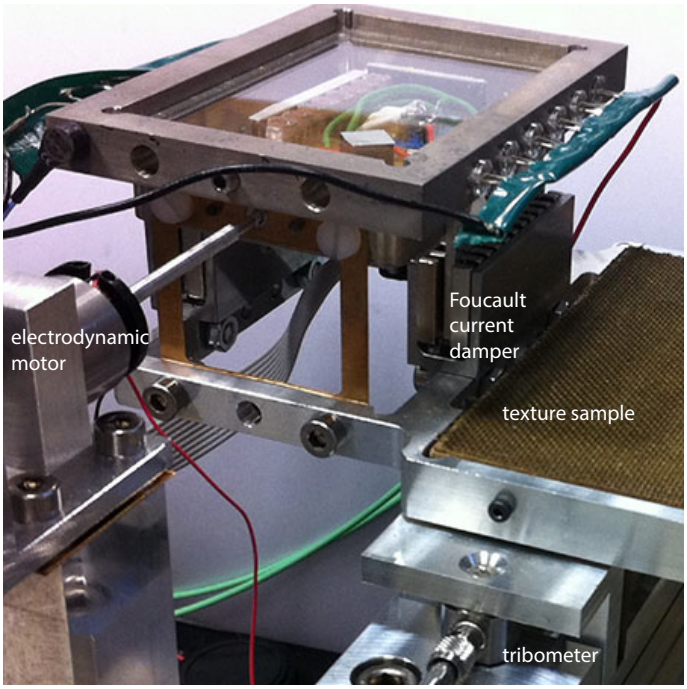

Fig. 7: Transducer with transparent platform mounted on the tribometer alongside the texture sample.

The damping viscosity obtained is a function of several parameters [45]. The size, spacing, and number of magnets are important ones. We employed twelve pairs positioned every 2 mm using plastic spacers on either side of the moving plate. The material with which the armature was made was non-alloyed aluminium (99% pure) to maximise conductivity and minimise mass. The air gap between the magnet and the armature was set to 0.1 mm. The magnets were $15 \times 3.5 \times 2$ mm and made of Neodymium (NdFeB) with nickel coating giving a flux density 1.4 T.

3.3 Identification

Sending a step impulse to the motor, Fig. 8, allowed us to identify the parameters of the system by minimising $|\hat{f}(t) - f(t)|$ where $\hat{f}(t)$ and $f(t)$ are the model and the measured ground reaction forces respectively. Table 1 lists the identified parameters.

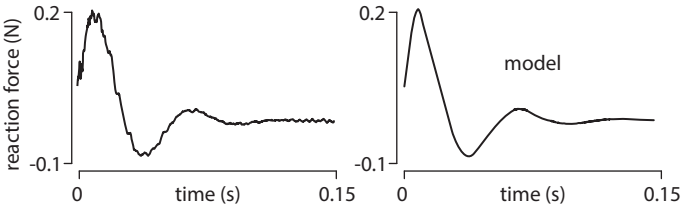

Fig. 8: Damped response to a step function.

TABLE 1: Transducer parameters.

mass m	81 g
resonance frequency F_0	17 Hz
spring constant k	0.93 N/mm
damping ratio ξ	0.35

3.4 Interfacial force measurement during excitation

From the system's free body diagram, Fig. 5, the forces acting on the plate were: the force of elasticity, f_k, the force of viscosity, f_b, the interfacial force of finger friction, f_d, and the force of the actuators, f_a, giving $-m\ddot{x} = f_k + f_b + f_\mathrm{d} + f_\mathrm{a}$. However, the reaction force sensed by the tribometer's lateral sensor is, $f_\mathrm{s} = f_k + f_b$, thus if the acceleration of the plate, $\ddot{x}$, is measured, then the interfacial force of the finger friction can be evaluated from $f_\mathrm{d} = -m\ddot{x} - f_\mathrm{s} - f_a$, where all the terms are known and where m is the only parameter to be precisely determined.

4 Imaging Apparatus

A high-speed camera (Model Mikrotron MotionBLITZ EoSens mini2) was employed to image a fingerpad contact under dynamic loading in the two modes described earlier. To achieve high spatial resolution in addition to the high temporal resolution, it was fitted with a Navitar 6000 zoom having a 12 mm fine focus augmented with a telescopic adapter and a 0.75x lens attachement. This set-up allowed focus from a whole fingertip contact down to just five fingerprint ridges at high resolution. Obtaining a sufficient level of illumination was a challenge in order to serve the needs of the two total internal reflection methods that were available, together or separately.

4.1 Prism-based Frustrated Total Internal Reflection

A right-angle prism was positioned below the vibrating glass plate using a 3-axis micro-positioner, and adjusted to leave a 0.1 mm gap between the prism and the glass plate. Index-matching immersion oil was then used to fill

the gap and the oil was retained there by capillarity, thus realising a continuous, yet deformable, optical milieu, see Fig. 9. A bright cold light source (KL 2500 LED, Schott, Germany) was employed for illumination. An opal diffuser ensured that the light was transmitted onto the camera by illuminating the prism volume without being reflected back by the smooth air-glass interface and without escaping the prism from internal surfaces.

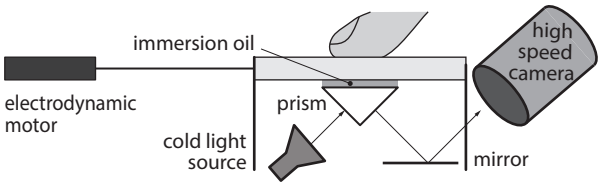

Fig. 9: Dynamically loaded fingertip imaged though prism-based Frustrated Total Internal Reflection set-up.

The prism was immobile, did not add mass to the the moving parts and allowed for high-speed imaging. In this mode, the natural damping introduced by the liquid interfaces eliminated the need for Foucault-current damping. With this technique, images at high spatial resolution and high temporal resolution could be obtained. One example of an image acquired in a static condition is shown in Fig. 10.

Fig. 10: Occluded real finger contact imaged under static conditions at 24 Hz frame rate showing the degree of detail that can be obtained at 2 N and 2 s of contact time.

Contrast was sufficient to enable excitation at imaging frequencies as high as 1 kHz. One example can be seen in Fig. 11 where a 'real' contact area could easily be imaged at such high frequencies[1].

4.2 Direct Illumination Total Internal Reflection

Green coloured light was transmitted into the glass plate by a set of laterally-placed light emitting diodes (LED), creating total internal reflection, and allowing for the fingerprint in contact with the plate to be visible. To increase light incidence, the four edges of the glass plate were polished to an optical quality finish. The green coloured light minimised the fraction of light diffused by the skin tissue, which acted as a filter for the complementary colour.

1. The literature also refers frequently to the notion of 'true' contact. Here the terms 'real' and 'true' are considered to be equivalent.

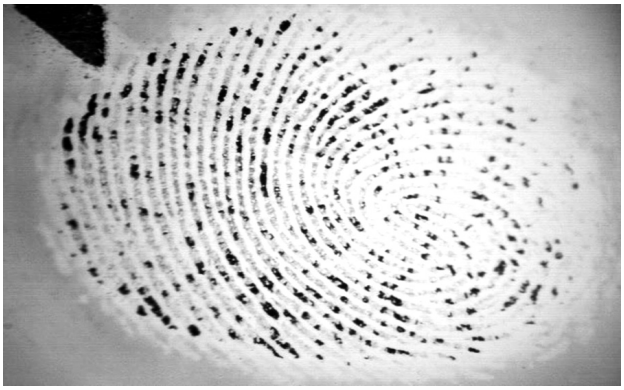

Fig. 11: Real finger contact area under static conditions at a 1 kHz frame rate after 2 s of contact time and for a 2 N normal load.

The frame was designed to house twelve green LEDs (HLMP-CM1A-560DD, Avago, 59 000 mcd each) with 15° dispertion giving 36 lm of illumination in total. They shone through 2 mm diaphragmes to guide as much light as possible into the 2 mm-thick glass plate to reduce the reflections on the edges of the glass that could escape the light trap, see Fig. 12. Optionally to increase the light intensity even further, we also used a cold light source (KL 2500 LED, Schott, Germany) with a green filter transmitting the light into the glass frame. With this configuration, it was possible to reach 100 Hz image sampling capability.

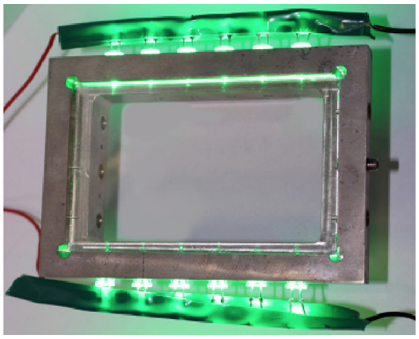

Fig. 12: Illuminated vibrating plate.

A 45° angle mirror was used to enhance the optical stability of the set-up and facilitate the horizontal camera mounting, see Fig. 13. The light path from the green LEDs around the set up was frustrated until light reflected off a fingerprint ridge in contact with the glass.

Figure 14 illustrates the type of image that can be obtained with this method. It is a combination of light arising from the real contact, light reflected by the fingerpad surface, and light diffused in the tissue. This image should be contrasted with that seen in Fig. 11 as they each deliver very different types of information.

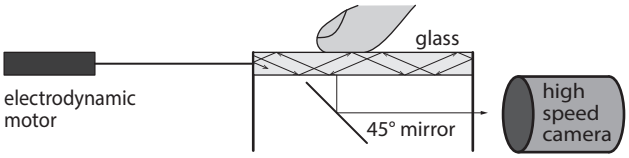

Fig. 13: Direct Frustrated Total Internal Reflection set-up.

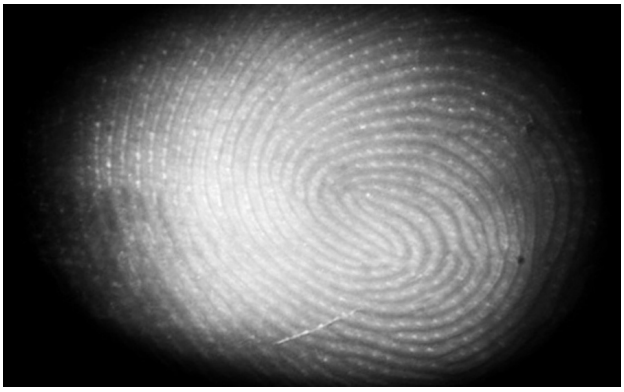

Fig. 14: Fingerpad image mode at 100 Hz for 2 N normal load.

5 Preliminary Bio-Tribology Measurements

In this section we show some examples of the stimulation and characterisation capabilities of the apparatus described previously. It is made evident without elaborative quantitatification that the establishment of the real contact area by a finger is a multifactorial phenomenon. For brevity, the physics behind these observations will be discussed in future publications.

5.1 Real Contact Area Dynamics during Static Loading

The imaging apparatus was able to precisely visualise the way in which the real contact area evolves with occlusion time and with applied load, see [26] and [35], for a definition of these terms. Briefly, occlusion occurs when a fingerpad is in contact with a smooth impermeable surface so that the secretion of moisture from the sweat pores in the fingerprint ridges is trapped at the interface and is absorbed by the *stratum corneum*. The ridges and their surface topographical features become more compliant over a period of tens of seconds due to the plasticisation by the moisture and hence the real area of contact increases with the time of contact until an asymptotic value is reached.

A static test was performed while the real finger contact area was imaged in a time-lapsed manner using the prism-based FTIR method, (1, 1.5, 3, 5, 8, and 20 s). A flat glass prism was pressed down onto the fingerpad in order to induce total internal reflection, with the applied load gradually increased until the required maximum value is achieved. We observed this phenomenon previously using a different apparatus configuration [35]. Before a set of measurements, the index finger was washed with commercial soap, rinsed with distilled water and allowed to dry for 10 min until an equilibrated clean skin state was achieved. The result can be seen in Fig. 15.

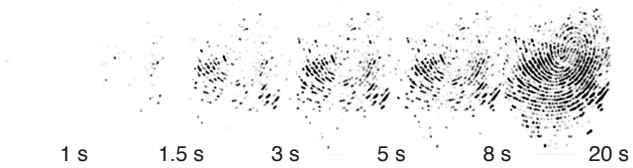

Fig. 15: Time-lapse real contact imaging as the normal load increases according to the time dependent normal loading indicated by Fig. 16.

It can be observed how the real contact area increases gradually owing to occlusion dynamics while the gross contact area reaches its ultimate value very rapidly, see Fig. 16. This phenomenon wad discussed and analysed elsewhere in greater detail where the methods are also described [46].

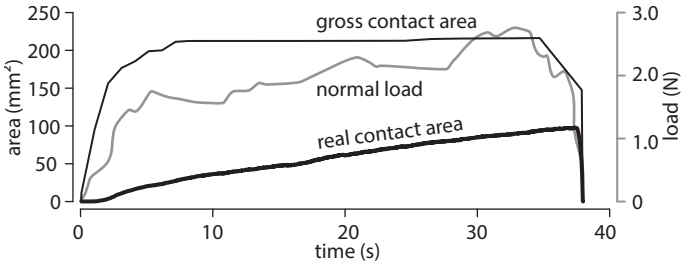

Fig. 16: Result of the analysis of the images of Fig. 15.

5.2 Real Contact Area Under Dynamic Conditions

Exploring textures always corresponds to dynamic contacts since fingertips constantly make and break multiple contacts as the skin ridges interact with the relatively moving asperities. It is these rapid mechanical fluctuations that contain the texture perceptual information.

During steady sliding, the resulting broadband, complex oscillations that can be readily observed and converted to the frequency domain and thus viewed as a sum of a large number of sinusoidal signals. It is thus informative to investigate how dynamic contacts behave as a function of frequency. The formation of the real contact area as the origin of friction between a fingertip and a surface is a multifactorial phenomenon. To investigate these factors, dynamic tests were performed where the participant pressed a finger on the glass plate, and then maintained it at around 1 N while the plate was vibrated at different frequencies. Absence of slip between the fingerpad and the glass plate could be visually ascertained. The same fingerpad skin state preparation was carried out for the dynamic conditions as for the static ones. Figure 17 illustrates the complex influcence of the different factor that were varied: tangential loading rate, contact duration, and skin hydration.

Several trends can be observed by simple inspection. Skin hydration has a significant impact at the onset of a

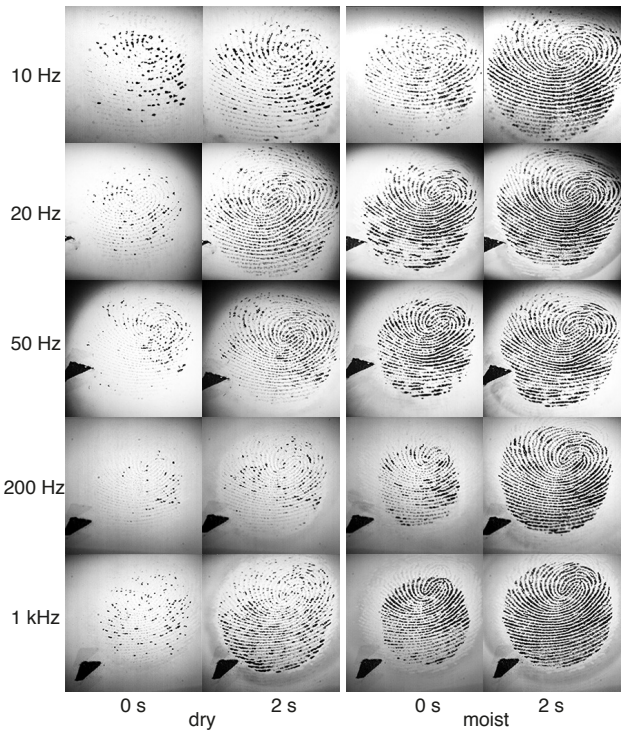

Fig. 17: Real contact imaging as a function of tangential loading rate, contact duration, and skin hydration.

contact and during its evolution, as can be observed by comparing images (row pairs) taken for the same loading conditions but at different times after contact onset. Dry and moist refer to different natural states of the finger; the clean index finger of one of the authors was dabbed with a dry or moist tissue before each measurement to induce the appropriate state. The effects of dynamic lateral loading are also different according to normal loading rate as can be seen by inspection of the columns of Fig. 17.

Notably, a moist finger tended to become less sensitive to loading rate than a dry finger. Another trend is that dynamic normal loading does not seem to disrupt the occlusion process and hence the increase in the real area of contact with time. Since finger hydration could not be controlled with accuracy, monotonicity is not always present in the images sequences taken under different conditions. Taking advantage of the simultaneous tribological measurement, we could nevertheless conduct a preliminary quantification of the creation of traction for different hydration states under dynamic loading.

Figure 18 reports the resulting traction measured under the above conditions and at frequencies of 10, 20, 50, 100, 200, 500, and 1000 Hz. Recall that traction, or interfacial shear stress, is defined as the force per unit of real contact area [26]. In this preliminary analysis we averaged the tangential traction force component and the real contact area over three trials per condition of duration 2.0 s. The normal load was (0.94 ± 0.60) N for the dry condition and (0.75 ± 0.30) N for the moist condition. To minimise the estimation error of the real contact area due to the variations in the initial moisture contents, the value employed in the analysis was based on the difference between the final and initial values.

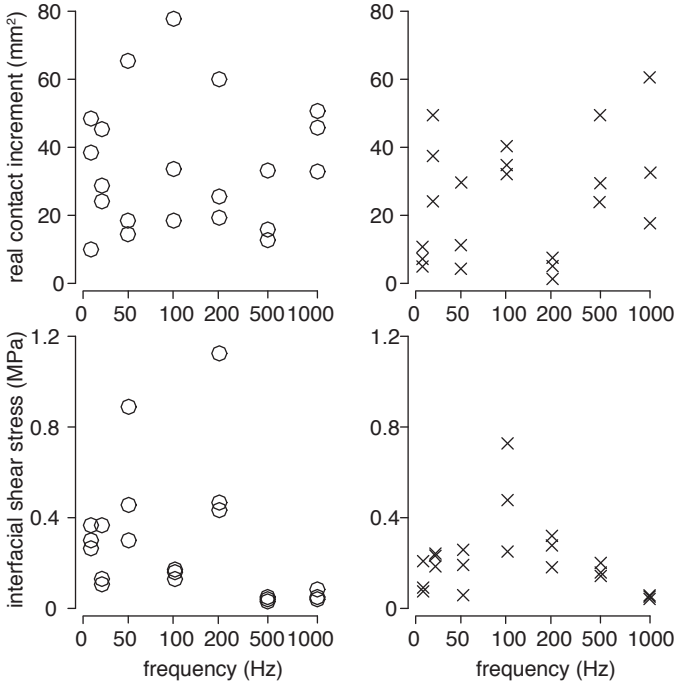

Fig. 18: Real contact growth over 2 s and interfacial shear stress as a function of tangential loading frequency (∘ dry, × moist).

It can be observed that while the formation of the real contact area is relatively insensitive to loading rate, shear stress tends to decrease with this parameter. This effect is less pronounced for moist fingers than for dry fingers. A possible explanation for this phenomenon can be found in the acceleration of the occlusion mechanism at the low frequencies. Thus the effect is weaker at higher frequencies for dry fingers since moisture results in a contact with a significant initial occlusion [46]. Note that the estimation of interfacial shear stress accounted only for the increment of real contact area over a period of two seconds. The observation that the growth of real contact area for dry fingers is more sensitive to the effect of time — and here to loading rate — than it is for moist fingers may contribute to explaining the previously observed phenomenon that the dryness of fingers may not necessarily impact significantly the coefficient of friction but rather the propensity of a finger contact to fail rapidly under load [15].

5.3 Images obtained with direct FTIR

Images taken under direct FTIR were acquired in conditions similar to that of the previous section but for lower frequencies and longer durations owing to the limitations of this approach in obtaining contrasted images. Unlike those of Fig. 17, the frames shown in Fig. 19 were heavily processed to compensate for the lack of illumination dynamics by normalising them to the darkest and brightest pixels. This means that the

images obtained at the onset of a contact have very few brightness levels.

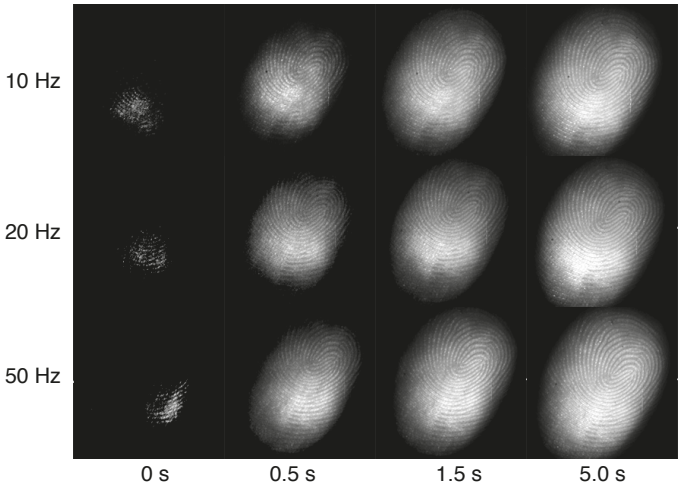

Fig. 19: Images acquired using direct FTIR.

The comparison of the images in Fig. 17 and in Fig. 19 strongly corroborates the assumption adopted in [29] that the brightness level strongly correlates with friction, which is turn is correlated with the real contact area. In effect its real contact is likely to increase the portion of light being scattered while the other contributors to brighness, diffusion and reflection, would remain by and large unchanged. On the other hand, the notion that brightness correlates with the mean contact pressure is not well supported by the present results since correlating brightness, and hence real contact, with gross pressure would depend on an analysis of the contact mechanics at the ridge length-scale and more importantly at the asperity length-scale [46].

6 Conclusion

We described an apparatus capable of recording the dynamics of finger interaction with natural textures and to excite fingers with the same dynamics but with the added benefit of imaging with high spatial and temporal resolutions the evolution of both the gross behaviour of the finger through direct FTIR as well as the microscopic details of the real contact area. This will allow us to gain information of how a fingerpad deforms under load while sliding on otherwise non-transparent materials.

The apparatus enables a wide range of studies related to physical underpinning of tactile material discrimination and identification in perceptual tasks. It could also lead to a better understanding of the grip regulation mechanisms on arbitrary surfaces.

Standardised loading patterns such as sharp transients or step loadings can also be examined in order to visualise the transient phenomena that most certainly take place during natural discriminative or prehensile behaviours. The role of the fingerprint in tactile perception may also potentially be clarified since our newly introduced technique will allow us to investigate the behaviour of ridges at frequencies that are relevant to natural conditions. Future work may also involve evaluating the effects of dynamic loading on fingertip ridge deformation.

Acknowledgment

This work was supported by the FP7 Marie Curie Initial Training Network PROTOTOUCH, (No. 317100) and the European Research Council (FP7) ERC Advanced Grant (PATCH) to V.H. (No. 247300). The authors would like to thank Ramakanth Singal, Bernard Javot, and Rafał Pijewski for engineering assistance, Stephen Sinclair for help with the signal acquisition software, and Simon Johnson for invaluable advice regarding the imaging apparatus.

References

[1] L. E. Krueger, "Tactual perception in historical perspective: David Katz's world of touch," in *Tactual Perception; A Sourcebook*, W. Schiff and E. Foulke, Eds. Cambridge University Press, 1982, pp. 1–55.

[2] S. J. Lederman and R. L. Klatzky, "Extracting object properties through haptic exploration," *Acta Psychologica*, vol. 84, no. 1, pp. 29–40, 1993.

[3] M. Hollins, R. Faldowski, S. Rao, and F. Young, "Perceptual dimensions of tactile surface texture: A multidimensional scaling analysis," *Perception and Psychophysics*, vol. 54, no. 6, pp. 697–705, 1993.

[4] M. Hollins and S. J. Bensmaïa, "The coding of roughness," *Canadian Journal of Experimental Psychology/Revue canadienne de psychologie experimentale*, vol. 61, no. 3, pp. 184–195, 2007.

[5] S. C. Richards and A. D. Roberts, "Boundary lubrication of rubber by aqueous surfactant," *Journal of Physics D: Applied Physics*, vol. 25, no. 1A, p. A76, 1992.

[6] W. H. Briscoe, S. Titmuss, F. Tiberg, R. K. Thomas, D. J. McGillivray, and J. Klein, "Boundary lubrication under water," *Nature*, vol. 444, no. 7116, pp. 191–194, 2006.

[7] D. Gueorguiev, S. Bochereau, A. Mouraux, V. Hayward, and J.-L. Thonnard, "Touch uses frictional cues to discriminate flat materials." *Scientific reports*, vol. 6, p. 25553, 2016.

[8] M. Wiertlewski, C. Hudin, and V. Hayward, "On the 1/f noise and non-integer harmonic decay of the interaction of a finger sliding on flat and sinusoidal surfaces," in *Proceedings of World Haptics Conference*, 2011, pp. 25–30.

[9] E. Wandersman, R. Candelier, G. Debrégeas, and A. Prévost., "Texture-induced modulations of friction force: the fingerprint effect." *Physical Review Letters*, vol. 107, no. 16, p. 64301, 2011.

[10] L. R. Manfredi, H. P. Saal, K. J. Brown, M. C. Zielinski, J. F. Dammann, V. S. Polashock, and S. J. Bensmaia, "Natural scenes in tactile texture," *Journal of neurophysiology*, vol. 111, no. 9, pp. 1792–1802, 2014.

[11] J. J. Gibson, "Observations on active touch," *Psychological Review*, vol. 69, pp. 477–491, 1962.

[12] V. Hayward, "Is there a plenhaptic function?" *Philosophical Transactions of the Royal Society B*, vol. 366, no. 1581, pp. 3115–3122, 2011.

[13] E. R. Serina, C. D. Mote Jr., and D. Rempel, "Force response of the fingertip pulp to repeated compression - effects of loading rate, loading angle and anthropometry," *Journal of Biomechanics*, vol. 30, pp. 1035–1040, 1997.

[14] D. T. V. Pawluk and R. D. Howe, "Dynamic lumped element response of the human fingerpad," *Journal of Biomechanical Engineering*, vol. 121, no. 2, pp. 178–183, 1999.

[15] T. André, V. Levésque, V. Hayward, P. Lefèvre, and J.-L. Thonnard, "Effect of skin hydration on the dynamics of fingertip gripping contact." *The Journal of the Royal Society Interface*, vol. 8, no. 2, pp. 1574–1583, 2011.

[16] A. V. Terekhov and V. Hayward, "Minimal adhesion surfaces in tangentially loaded digital contacts," *Journal of Biomechanics*, vol. 44, no. 13, pp. 2508–2510, 2011.

[17] F. Martinot, P. Plenacoste, and C. Chaillou, "Haptic sounds and vibrations of human fingerprints," in *International Conference on Sensing Technology*, 2005, pp. 615–620.
[18] T. Iwamoto and H. Shinoda, "Finger ring tactile interface based on propagating elastic waves on human fingers," in *Proceedings of World Haptics*, 2007, pp. 145–150.
[19] Y. Tanaka, Y. Horita, A. Sano, , and H. Fujimoto, "Tactile sensing utilizing human tactile perception," in *World Haptics Conference (WHC)*, 2011, pp. 621–626.
[20] Y. Shao, V. Hayward, and Y. Visell, "Spatial patterns of cutaneous vibration during whole-hand haptic interactions," *Proceedings of the National Academy of Sciences*, vol. 113, no. 15, pp. 4188–4193, 2016.
[21] M. Wiertlewski, J. Lozada, and V. Hayward, "The spatial spectrum of tangential skin displacement can encode tactual texture," *IEEE Trans Robot*, vol. 27, no. 3, pp. 461–472, 2011.
[22] R. O. Potts, E. M. Buras, and D. A. Chrisman, "Changes with age in the moisture content of human skin," *Journal of investigative dermatology*, vol. 82, no. 1, pp. 97–100, 1984.
[23] Q. Wang and V. Hayward, "Biomechanically optimized distributed tactile transducer based on lateral skin deformation," *International Journal of Robotics Research*, vol. 29, no. 4, pp. 323–335, 2010.
[24] A. M. Smith, C. E. Chapman, M. Deslandes, J. S. Langlais, and M. P. Thibodeau, "Role of friction and tangential force variation in the subjective scaling of tactile roughness," *Experimental Brain Research*, vol. 144, no. 2, pp. 211–223, 2002.
[25] V. Levesque and V. Hayward, "Experimental evidence of lateral skin strain during tactile exploration." in *Proceedings of Eurohaptics*, 2003, pp. 261–275.
[26] M. J. Adams, S. A. Johnson, P. Lefèvre, V. Lévesque, V. Hayward, T. André, and J.-L. Thonnard, "Finger pad friction and its role in grip and touch." *Journal of The Royal Society Interface*, vol. 10, no. 80, p. 20120467, 2013.
[27] B. Delhaye, P. Lefevre, and J.-L. Thonnard, "Dynamics of fingertip contact during the onset of tangential slip," *Journal of the Royal Society Interface*, vol. 11, no. 100, p. 20140698, 2014.
[28] R. Ehrlich, *Why toast lands jelly-side down: Zen and the art of physics demonstrations*. Princeton University Press, 1997.
[29] M. Wiertlewski, R. F. Friesen, and J. E. Colgate, "Partial squeeze film levitation modulates fingertip friction," *Proceedings of the National Academy of Sciences*, vol. 113, no. 33, pp. 9210–9215, 2016.
[30] M. Tada and T. Kanade, "An imaging system of incipient slip for modelling how human perceives slip of a fingertip," in *Annual International Conference of the IEEE Engineering in Medicine and Biology Society*, 2004, pp. 2045–2048.
[31] S. Pasumarty, S. Johnson, S. Watson, and M. J. Adams, "Friction of the human finger pad: Influence of moisture, occlusion and velocity," *Tribology Letters*, vol. 44, no. 2, pp. 117–137, 2011.
[32] F. Massi, E. Vittecoq, E. Chatelet, A. Saulot, and Y. Berthier, "Design of a tribometer for investigating tactile perception," *Proceedings of the Institution of Mechanical Engineers, Part J: Journal of Engineering Tribology*, vol. January, 2014.
[33] S. Derler and L.-C. Gerhardt, "Tribology of skin: Review and analysis of experimental results for the friction coefficient of human skin," *Tribology Letters*, vol. 45, no. 1, pp. 1–27, 2012.
[34] M. Adams, B. Briscoe, and S. Johnson, "Friction and lubrication of the human skin." *Tribology Letters*, vol. 26, no. 3, pp. 239–253, 2007.
[35] B. Dzidek, M. Adams, Z. Zhang, S. Johnson, S. Bochereau, and V. Hayward, "Role of occlusion in non-coulombic slip of the finger pad," in *Haptics: Neuroscience, Devices, Modeling, and Applications, Part-I*, 2014, pp. 109–116.
[36] A. H. F. Martinot and M. C. C. Biet, "Mechanical responses of the fingerpad and distal phalanx to friction of a grooved surface: Effect of the contact angle." *IEEE transactions in Haptics*, pp. 297–300, 2006.
[37] T. A. Fishel and G. E. Loeb., "Bayesian exploration for intelligent identication of textures." *Frontiers in Neurorobotics*, vol. 6, pp. 17 603–17 611, 2012.
[38] M. Wiertlewski, S. Endo, A. M. Wing, and V. Hayward, "Slip-induced vibration influences the grip reflex: A pilot study," in *World Haptics Conference (WHC)*, 2013, pp. 627–632.
[39] J. Platkiewicz, J. Mansutti, A. Bordegoni, and V. Hayward, "Recording device for natural haptic textures felt with the bare fingertip." in *Haptics: Neuroscience, Devices, Modeling, and Applications, Part-I*, 2014, pp. 521–528.
[40] M. Janko, R. Primerano, and Y. Visell, "On frictional forces between the finger and a textured surface during active touch." *IEEE Transactions on Haptics*, vol. 9, no. 2, pp. 221–232, 2015.
[41] A. W. Goodwin and J. W. Morley, "Sinusoidal movement of a grating across the monkey's fingerpad: Representation of grating and movement features in afferent fiber responses," *Journal of Neuroscience*, vol. 7, no. 7, p. 2168, 1987.
[42] G. Campion and V. Hayward, "Fundamental limits in the rendering of virtual haptic textures," in *Proceedings of the First Joint Eurohaptics Conference and Symposium on Haptic Interfaces for Virtual Environment and Teleoperator Systems*, 2005, pp. 263–270.
[43] M. Wiertlewski and V. Hayward, "Transducer for mechanical impedance testing over a wide frequency range through active feedback," *Review of Scientific Instruments*, vol. 83, no. 2, p. 025001, 2012.
[44] ——, "Mechanical behavior of the fingertip in the range of frequencies and displacements relevant to touch," *J Biomech*, vol. 45, no. 11, pp. 1869–1874, 2012.
[45] A. Mohand-Ousaid, G. Millet, S. Regnier, S. Haliyo, and V. Hayward, "Haptic interface transparency achieved through viscous coupling," *International Journal of Robotics Research*, vol. 31, no. 3, pp. 319–329, 2012.
[46] B. Dzidek, S. Bochereau, M. Adams, V. Hayward, and S. Johnson., "Frictional dynamics of finger pads are governed by four length-scales and two time-scales." in *Proceedings of the Haptic Symposium.*, 2016, pp. 161–166.

Séréna Bochereau received an MEng in Materials Science from the University of Oxford in 2013. She is currently a Marie Curie PhD Fellow at the Institut des Systemes Intelligents et de Robotique at Universit Pierre et Marie Curie, Paris. Her current research include physical invariants in tactile perception and the reproduction of natural textures.

Brygida Dzidek received her Master Degree in Material Science Engineering at University of Silesia in Poland. Specialised in smart biomaterials systems. The objectives of her PhD research are experimental and analytical analysis of tribological interaction of the finger pad and tactile displays.

Mike Adams (FREng, FIChemE, FInstP, FRSC) joined the University of Birmingham School of Chemical Engineering in 2004 as Professor of Product Engineering and Manufacture from Unilever R&D where he was a Senior Scientist with responsibilities for materials science and product processing. In 1999, he was awarded the Donald Julius Groen Prize by the Institution of Mechanical Engineers for outstanding achievements in the tribology of complex materials and in 2016 he was awarded the Tribology Trust Silver Medal for outstanding and sustained contributions to the science and technology of Tribology. He has published over 200 scientific papers and co-edited four books on Tribology in Particulate Technology, Theoretical and Computational Methods in Tribology, Solid-Solid Interactions and Dynamics of Complex Fluids. His research interests include the tribology of skin and the finger pad. He has coordinated a number of EU projects on tactile sensors and haptic displays.

Vincent Hayward (M'84-SM'04-FIEEE'08), Dr-Ing degree in 1981 from the University de Paris XI. He was a postdoctoral fellow then a visiting assistant professor in 1982 at Purdue University, and joined CNRS, France, as Chargé de Recherches in 1983. In 1989, he joined the Department of Electrical and Computer Engineering at McGill University as an assistant, associate, and then a full professor in 2006. He is now professor at the Université Pierre et Marie Curie. He has published more than 250 articles in journals and conferences, co-founded spin-off companies and received best paper and research awards. He was on the editorial boards of the IEEE Transactions on Robotics, the ACM Transaction on Applied Perception, and the IEEE Transactions on Haptics.

General discussion and future questions

This thesis investigated the tribological interactions of the human finger pad with different reference surfaces (RSs) and tactile displays (TDs). In the wide range of analyses of mechanical properties of the finger pad, an attempt has been made to explain the nature of the interactions based on critical material parameters, environmental influences and experimental data. More specifically the objectives of this thesis were:

- ✓ Fingerpad tribology of selected RSs and TDs – data appropriate for formulating and validating FEA simulations.
- ✓ Fingerpad tribology of existing, optimised and novel TDs – identified tribological mechanisms and performance.

In Part 1 of the first Chapter, the development an analytical elastic contact model, based on a geometrical simplification of the finger pad and its deformation behaviour with smooth surface is described. It was shown that the secant modulus of the finger pad is linearly proportional to the load, which leads to expressions for the gross and ridge contact areas as a function of load. The model proposed in the publication proved to be consistent with experimental contact area data, obtained both directly from ink print images and indirectly from friction measurements of a finger pad. The Young modulus of the ridges calculated from the experimental data using the analytical model was considerably less than the wide range of reported values of *stratum corneum* using mechanical measurements at high water activities. Nevertheless, the findings were consistent with reported values obtained directly using dynamic optical coherence elastography. This highlights the difficulty of measuring and interpreting the Young modulus by using mechanical measurements. The model, however, was limited to the fully occluded state, where it is reasonable to assume that the

fingerprint ridges make complete contact with the surface owing to the plasticization induced by the secretion of moisture as sweat. In the initial and partially occluded states, it will be necessary to account for the influence of the topography of the ridge surfaces that may not have been completely flattened owing to the limited plasticization.

Part 2 of Chapter 1 describes the quasi-static component of the kinetic friction as a function of the occlusion time. The friction factor and load index were used, in order to define the relationship between the friction coefficient and the load exerted by the finger. It was shown that for smooth surfaces, the occlusion time dependent load index provides a sensitive measure of the transition, from a multiple asperity Coulombic contact, to one that is non-Coulombic. This phenomenon is due to the finger print ridges developing an intimate contact with the counter surface. Rough surfaces appear to be indifferent to occlusion as evidenced by the insensitivity of the coefficient of friction to the sliding time. This phenomenon may also play an important role in our ability to detect slip, which is crucial in grip function.

The results represented an important precursor to understanding the much more complex dynamic behaviour elicited by the finger pad in haptic experiments during the further research. Moreover, they provide a basis for elucidating the complex evolution of a finger pad contact when tangentially loaded, and could therefore be used for modelling contact mechanics. In the future, such finding might have a positive impact the virtual reality (VR) technology.

Research questions following from Chapter One:

- The influence of occlusion on the friction and compression studies was limited to only one subject and three different surfaces; another larger study has concluded that occlusion has a major effect on the variability for different subjects [Derler, S. et.al, 2014]. Is there a way to classify the moisture secretion during *in-vivo* experiments? If

the phenomenon appears to be following first order kinetics, is there a common maximum moisture saturation level?

- The surface topography of the finger ridges was simplified in the model, which is reasonably satisfactory for the occluded state when such features are probably flattened. Is it possible to model the contact area, and hence the friction, when a finger pad is not fully occluded?
- Can any other model be proposed in order to discriminate the relevance of the bone? More particularly, could finite element models support the assumptions made about strain hardening in describing the compression of a finger pad?
- The proposed model was only evaluated for two angles of inclination of the finger. Does the model remain valid for all such angles?

The presented work in Chapter 2 has shown that four characteristic length scales, rather than just two as previously assumed, are required to describe the contact mechanics of the finger pad. Classification included the area of contact associated with the gross finger geometry, the ridges, the junctions, and the asperities on the junctions. In addition, there were two characteristic times described, respectively associated with the growth rates of the junctions and of the real contact areas. These length and time scales play a key role and important factor in understanding how the Archardian-Hertzian transition drives both the large increase of friction and the reduction of the areal load index during persisting finger contacts with impermeable surfaces.

The author's findings demonstrate that the growth of the contact area results from a two-step mechanism, with some correlation between the steps. These findings imply that multiple asperity contact might play a key role in vibration-based tactile stimulation devices. The rendering of tactile sensation could be more realistic if the contact area and pressure distribution of the finger experiencing the device was measured to adapt to the stimuli in real

time against varying ambient or physiological conditions. Such corrective actions would be feasible since a few seconds are required for full plasticisation and for the formation of intimate contacts.

Texture appreciation and shape discrimination also rely on frictional dynamics since they can be expected to depend on the microscopic features of finger pads. Tactile interactions involving relatively short times scales are more easily accomplished if the friction is small. However, precision tasks and object gripping *per se* generally require long dwell times and are facilitated by the relatively high friction induced by the plasticisation of the asperities according to the degree of roughness and permeability of the counter-surfaces.

Finger parameters such rigidity and moisture level can be extremely variable among different subjects. The measurements and models described are limited to only one or two subjects. Such a restricted number arose from the novelty of the experiments as well as the perspective of the study. The focus of this study was to distinguish and characterise the general phenomena that should be representative of any subject. Clearly there will be large variations between different subject groups depending, for example, on age, gender and racial background. In particular, subjects will exhibit a wide range of skin moisture levels and indeed, this was observed for a single subject during a single day. Nevertheless, the fundamental physics should be invariant across subjects even though, for example, there will be a large range of finger pad friction values.

The proposed classification is novel and needs to be explored further. Many factors of the intermittent contact can be precisely measured; nevertheless, there are still a few examples that do not follow the expected kinetics. Some examples in Part 2 (Chapter 2) clearly suggest the appearance of the extreme situations, where characteristic time cannot be described. Thus, there is a need for an additional correlation for e.g. moisture offset level classifier.

Research questions following from Chapter Two:

- Can the moisture level of the finger pad be classified using grey scale image analysis?
- Is it possible to characterise the pressure distribution by FTIR?
- How can the topographical features be correlated with the contact area of a finger pad?

Chapter 3 combines the most significant implementations of the author's models to describe the experimental data. This chapter contains the results of collaborative work with project partners, for which common knowledge and previous experience assisted in the understanding and improvement of existing tactile solutions.

The research was performed in various laboratories and with various equipment due to the nature of the various collaborations. Most of the frictional data presents in the analysis was measured using three tribometers (at Unilever Port Sunlight, University of Birmingham and University of Lille), however the simplicity of this type of equipment, precise pre-calibration and the strict protocols for each experiment, eliminated potential uncertainties in the data. Moreover, several experiments were repeated in the different locations to increase the range of studies as well as confirming reproducibility.

Part 1 opens the discussion of the mechanical interaction between a finger pad and a flat ultrasonically vibrating surface. The experimental data were analysed and compared with a squeeze film model of ultrasonic lubrication, which is one of most important technologies in the next generation of the tactile devices. The mismatches between the model and measurements were highlighted; most importantly the friction does not reduce to zero with increasing vibration amplitude as predicted. An empirical model based on the friction coefficient measurements was proposed and a general trend of the friction reduction was described. The analysis published in Part 1 was a precursory experiment within the

collaboration. Since theoretical models were not proven to be correct by empirical data, new extended experiments were conducted. The set of parameters was extended and the number of participants increased. The results were presented in Part 2 of this publication. The measurements were consistent with the finite element model developed in Part 1 of this publication and a data superposition scheme derived in that work. The proposed ratchet mechanism explained the friction modulation of ultrasonic displays. It was concluded that the friction modulation depends on the exploration velocity and is independent of the applied normal force either and the ambient air pressure. Based on these results, it was not possible to quantify the relative contribution of squeeze film levitation.

Data reduction using an exponential function of a dimensionless group showed a reasonable description of the experimental data, provided that the intermittent contact is sufficiently well developed. These findings were broadly discussed and compared. Its impact on the design of future ultrasonic haptic devices will be very significant.

In Part 3 of Chapter 3 a simple model, of the interaction of a finger pad with a plate vibrating at ultrasonic frequencies. It was based on representing the finger print ridges as elastic springs, which captures some of the critical factors that govern the performance of vibrational haptic displays. It was concluded that a critical minimum ultrasonic frequency was essential for ensuring that a finger pad is sufficiently stiff to cause periodic contact separation for out-of-plane vibrations.

The correlation of the two most important parameters (coefficient of the friction and amplitude of the vibration) that govern the performance of ultrasonic devices has been discussed. However, more work is required to establish the relative contributions of other possible mechanisms such as squeeze flow deocclusion. This would require more extensive and advanced measurements.

Part 4 of Chapter 3 described an apparatus capable of recording the dynamics of finger pad interactions with natural textures. Moreover, the setup allows also to excite fingers with the same dynamics as the natural textures but with the additional benefit of imaging with high spatial and temporal resolutions of the details of the real contact area.

A pioneer setup allows gaining information of how a finger pad deforms under load while sliding on otherwise non-transparent materials. The apparatus enables a wide range of studies related to the physical underpinning of tactile material discrimination and identification in perceptual tasks. It could also lead to a better understanding of the grip regulation mechanisms on arbitrary surfaces.

Standardised loading patterns such as sharp transients or step loadings can also be examined in order to visualise the transient phenomena that most certainly take place during natural discriminative or prehensile behaviours. The role of the fingerprint in tactile perception may also potentially be clarified since our newly introduced technique will allow us to investigate the behaviour of ridges at frequencies that are relevant to natural conditions. Future work may also involve evaluating the effects of dynamic loading on fingertip ridge deformation.

Such a wide range of new possibilities for exploration combined with image processing protocols should be valuable for future researchers. The advanced technology should allow texture and shape reproduction to become more realistic and assist in psychophysical of texture recognition.

Research questions following from Chapter Two Chapter Three:

- In addition to ultrasonic vibration and electrovibration, is there another way to influence the frictional modulation on a flat surface?

- How is friction modulation affected by contact area evolution? Is there a way to monitor and control this parameter?
- Is friction reduction stick-slip dependent?
- Is it possible to predict the inter-dependence of moisture level, sliding velocity and vibrational amplitude?

The thesis combines 8 independent publications, creating a single comprehensive study of the contact properties and behaviour of finger pads. However, the author appreciates that that there are many others potential methods to perform the proposed experiments. The methodological and analytical choices were based on authors current knowledge and problem understanding. Nevertheless, the statistical relevance and significance of the experimental results is supported by the work being published in refereed scientific journals and the resulting citations of these papers.